LBL--26091

DE89 002492

ELECTRONIC BEHAVIOR OF HIGHLY CORRELATED METALS*

Ariel Reich

Department of Physics,
University of California, Berkeley, CA 94720

and

Materials and Chemical Sciences Division,
Lawrence Berkeley Laboratory, Berkeley, CA 94720

October 1988

---

*This work was supported by the Director, Office of Energy Research, Office of Basic Energy Sciences, Materials Sciences Division of the U. S. Department of Energy under Contract No. DE-AC03-76SF00098.

Electronic Behavior of Highly Correlated Metals

Ariel Reich

ABSTRACT

This thesis addresses the question of the strongly interacting many-body problem: that is, systems where the interparticle correlations are so strong as to defy perturbative approaches. These subtle correlations occur in narrow band materials, such as the lanthanides and actinides, wherein the *f*-electrons are so localized that a variety of new phenomena, including intermediate-valence and heavy-fermionic behavior, may occur. As well, one has the alloying problem, where local interactions are paramount in determining the overall behavior. The technique employed in dealing with these systems is the Small Cluster method, wherein the full many-body Hamiltonian for a small grouping of atoms, coupled with periodic boundary conditions, is solved exactly. This is tantamount to solving a bulk crystal at the high points of symmetry in the Brillouin Zone. The mathematical overhead is further reduced by employing the full space group and spin symmetries. By its very nature, the Small Cluster method is well able to handle short-range interactions, as well as the combinatorial complexity of the many-body problem, on an equal footing. The nature of long-range order and phase transition behavior can not be incorporated, but sometimes clues as to their origin can be discerned. The calculations presented include: a two-band Anderson model for an intermediate-valence system, wherein photoemission and fluctuation behavior is examined; a single-band Hubbard model for a ternary alloy system, such as copper-silver-gold; and a Hubbard model for a heavy-fermion system, wherein Fermi surface, transport, magnetic and superconducting properties are discussed.

To my father,
who did not live to the see this day;
and, my mother,
who might not have always understood,
but was always supportive.

Acknowledgments

I wish to acknowledge the contribution and encouragement of the following people: Daryl Chrzan, Changfeng Chen, Cesar Proetto, Erik Sowa, Randy Victora, as well as the rest of the solid-state theory group at Berkeley, the staff and students at the Nordisk Institut for Teoretisk Atomphysik (NORDITA) and the H.C. Ørsted Institut in Copenhagen for their gracious hospitality during my year in Denmark, and last, but not least, I wish to express my enormous debt of gratitude to my thesis advisor, Leo Falicov, for his invaluable guidance and friendship throughout these graduate years.

Table of Contents

Chapter I. Introduction to Highly-Correlated Electronic Systems

I. Introduction

There was a saying, something to the effect that "You cannot change one thing in the Universe without affecting every other." This is the statement of the many-body problem – a problem at the heart of modern physics – to take into account, in some consistent manner, the intricate correlation between the particles in a system. This notion pervades every scale of the quantum world, from condensed matter, to nuclear, to particle physics.

In terms of the low-energy excitations of a many-body system, one may speak of *quasiparticles* and *collective excitations*. When the interactions act to merely dress the particles, with effective masses, charges, etc., then one is talking about quasiparticle excitations. When particles respond in concert, as for example in a plasma oscillation, then one is referring to a collective excitation.

One of the surprising aspects of many-body physics is that initially strong interactions acting between the particles of a system sometimes can be renormalized as weak residual interactions acting upon quasiparticles. An example is Coulomb screening in a solid. Therein, a negatively charged electron repels others until the positively charged shell built up around the electron effectively screens out its charge. This screened entity then interacts quite weakly with other such quasiparticles, and may act in concert to build up collective excitations: plasmons.

The notion of quasiparticles is thus an inherently perturbative notion. Systems where perturbation theory applies are therefore referred to as "normal". However, as Pines[1] states quite clearly: "It would seem that nature does not believe in power-series expansions in the many-body problem." In the case of superconductivity, at the temperature where perturbation theory breaks down, one sees the instability to Cooper pair formation, *i.e.* a

phase transition takes place. Any approach based on normal one-electron states is doomed to failure unless carried to all orders simultaneously. In this new superconducting phase, however, one may speak of the quasiparticles as electrons with long-range order whose energies are modified from the non-interacting case by a gap energy. The collective excitations correspond to excitons, formed by pairs of quasiparticles, and almost unmodified plasmons.

There are, of course, the "abnormal" systems where many-body effects are non-perturbatively strong, and it is incumbent on the physicist to seek new tools with which to describe the related phenomena. This thesis deals with one method in particular, the Small-Cluster Method.

The purpose of this chapter is: (i) to survey the physical properties of the heavily-interacting systems under study, (ii) to give an account of other theoretical methods, employed in dealing with these systems, (iii) to give an exposition into the workings of the Small-Cluster approach, and (iv) to summarize the nature of the various calculations reported in this thesis.

II. Physical systems with large many-body correlations

Most condensed-matter systems do not present very strong correlation effects, luckily so that modern physics can avail itself of very powerful methods, such as the *ab initio* pseudopotential approach, to describe a wide variety of physical systems. Simple metals, compounds, and especially semiconductors are all finding adequate description through the band-structure picture, with each band corresponding to a set of quasiparticle excitations.

There are regions of the periodic table that still elude such approaches. Most notably, there are the lanthanides and actinides, at the bottom of the table, whose occupation of the *f*-levels represents the extreme limit of electron localization and correlation. There is also the metallic alloys, which represent the two-headed problem of configurational statistics, and electronic band structure.

A. Heavy-Fermion and Intermediate-Valence Behavior

The phenomena of heavy fermions and intermediate valence are related and should be considered as part of a spectrum of behavior, which ranges in one extreme from the almost-completely uncorrelated *s*-band metals, such as the alkalis, to *p*-band materials such as semiconductors, to the increasingly narrow-band transition metals, until finally arriving at the lanthanides and actinides, where the 4*f* and 5*f* electrons come into play (see Fig. 1).

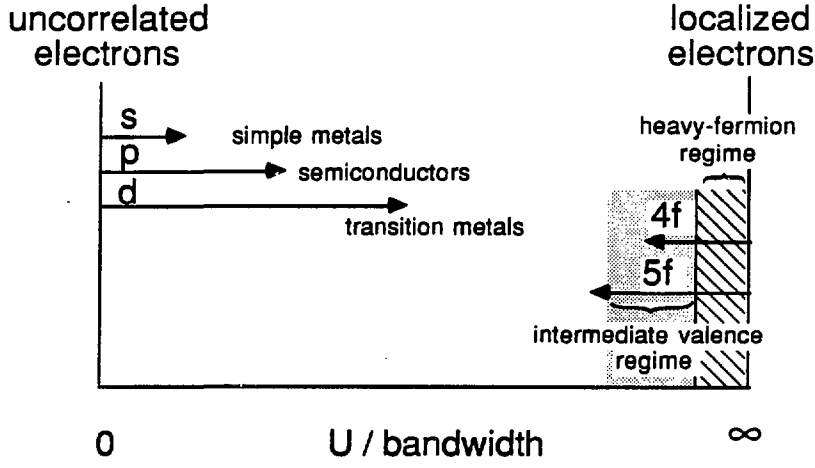

FIG. 1. Following Fulde *et. al.*[2], the spectrum of metal behavior is presented as a function of the intra-orbital Coulomb repulsion U, for various band metals. This diagram does not include the factor of band occupancy: heavy-fermionic behavior resulting from near-half filling of the *f*-band, intermediate valence occurring at lower fillings with the *f*-electrons hybridizing strongly with the conduction band.

As one could easily guess, one of the chief determining factors of this spectrum is the occupation of orbitals of higher and higher shells, and larger angular momentum. In the *d*- and *f*-band metals, the filling of these multiply-degenerate levels compete quite closely with an outer *s*-orbital. In the crystal lattice, this outer *s*-orbital overlaps the most with adjacent atoms and forms the widest bands, while the *d*- and *f*-bands are each narrower in

turn, and are mostly due to hybridization with the *s*-band. There is another feature to this localization, and that is the increase in electron-electron correlation. As two electrons in the same orbital would spend much time close together, they would exact a large Coulomb repulsion penalty, U. The many-body interactions thus become quite strong, resulting in many new subtle effects coming into play. One may therefore classify electrons as being itinerant (easy to hop from atom to atom), such as the *d*-band electrons in the transition metals, or localized, as for solid molecular oxygen. In the rare earths, one may have a coexistence of both extremes.

The itinerant electrons of the *d*-band transition metal series may interact to form paramagnetic (normal), ferromagnetic and antiferromagnetic structures[3]. The latter case, as occurs in chromium, is perceived as being the result of band structure and Fermi surface effects, which results in a spin-density-wave instability, with the separating of part of the Fermi surface and a lowering of the overall energy. As for the other metals, there is an intra-site exchange interaction favoring the parallel alignment of spins, the so-called Hund's rule, competing with the assignment of energies according to the band dispersion. The first effect is to favor ferromagnetic order, the second paramagnetic. It is in iron, nickel and cobalt where ferromagnetism wins out. Place nickel with oxygen in nickel oxide, however, and the resulting structure is antiferromagnetic. Here, Hund's rule assures the strong local moment on the nickels remain, but the presence of the paramagnetic oxygen between the nickels prevents electronic exchange in anything but an antiparallel configuration. Thus, the system is insulating with a residual, band-structure induced, antiferromagnetic interaction.

One sees the large Coulomb repulsion from a magnetic ion leading to an interaction which is ferromagnetic in some instances, antiferromagnetic in others. In the free-electron model, a similar phenomenon occurs and it is known as the Ruderman-Kittel-Kasuya-Yosida (RKKY) interaction. It is the result of a second derivative singularity in the magnetic susceptibility of the free-electron gas, and is oscillatory with period $2k_F$ (thus alternately ferro- and antiferromagnetic), and decreases asymptotically with distance as $1/r^3$. The idea of the magnetic *f*-electrons interacting indirectly through the almost-free conduction electrons is the mechanism for making elements such as gadolinium indirect

ferromagnets. It also leads to complicated spin arrangements in other rare-earth elements.

The intermediate-valence systems, such as cerium, represent a competition between two *f*-orbital configurations, all others inaccessible due to the large Coulomb repulsion in these localized orbitals. The *f*-electrons participate only indirectly, through hybridization, in the conduction process. In the heavy-fermion materials, such as UBe_{13}, this *f*–electron transport is somewhat less difficult, the large band masses resulting in a large electrical resistance and heat capacity, and the residual antiferromagnetic interactions yield susceptibilities far larger than ordinary metals. The large scaling differences between heavy-fermion, intermediate-valence and conventional metals is demonstrated in Table I.

Table I. Experimental evidence[4] attesting to the qualitative difference between heavy-fermion, intermediate-valence and conventional metals.

	Heavy-Fermion Materials			Intermediate Valence	Conventional	
	super conductor	magnet	normal			
	UPt_3	U_2Zn_{17}	$CeAl_3$	Ce	Pd	Ag
Specific Heat coefficient $\gamma(0)$ mJ/mole-K^2	450	400	1600	12.8	9.4	0.6
Magnetic Susceptibility $\chi(0)$ memu/mole	7	12	40	2.4	0.8	–
Room-Temperature Resisitivity μ-ohm-cm	150	110	170	77	20	2

There have been a variety of simple models introduced to shed light on the competition between band structure and correlation effects. This simplification is necessitated by the enormous combinatorial difficulties presented by full, rather than mean-field averageable, many-body interactions. Kondo[5] modeled dilute magnetic alloys by coupling a conduction

band with a sole magnetic impurity. In this way, the spin compensation of the conduction electrons near the magnetic ion could be described. Straightforward as this model may seem, it took the advent of renormalization group techniques to account exactly for the transition to Kondo behavior. At the other extreme, Hubbard[6] proposed a single-band model with on-site Coulomb repulsion, a model whose rich magnetic structure and metal-insulator transition behavior seems to belie its simple form. In order to answer the question of the interplay of the *s* and *d* bands (or for that matter, *s* and *f*) Anderson[7] proposed a two-band model, with which questions of moment formation, magnetic quenching and charge fluctuations can be addressed.

B. Alloy Behavior

The problem of predicting alloy properties between unlike metals has been a daunting task for condensed-matter physicists. Depending on concentration and temperature conditions, one may find solid solutions, component segregation, ordering of compounds, structural transformations, etc. (See Figure. 2). One may pursue the problem by one of two tacks: a classical statistical approach or quantum mechanical one. Either limit has proven satisfactory in some physical situations; but a fully predictive theory where both statistical and band structure considerations come into play still eludes physicists.

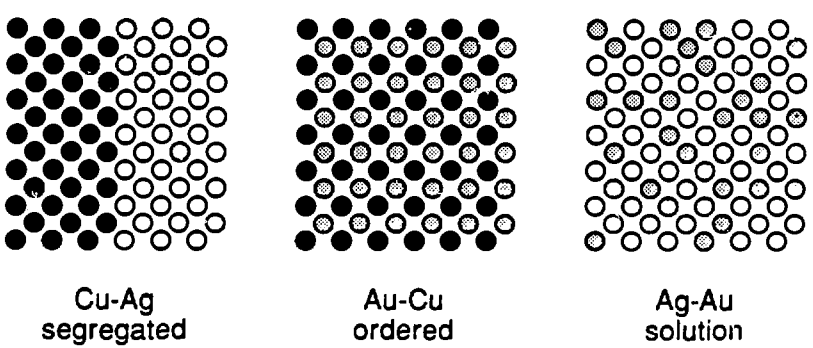

FIG. 2. An example of the rich structure of alloy systems. The three metals copper, silver and gold are so much alike, yet as alloys, Cu-Ag segregates almost completely, Au-Cu orders in specific ratios, and Ag-Au forms the almost prototypical solid solution.

In the former, one creates a phenomenological theory where all the quantum mechanics is embodied into effective pair-pair interactions (or even higher order groupings) and then classical statistical mechanics calculations yield the configurational entropy.

In the simplest example, following Kittel and Kroemer[8] , one ascribes binding energies between nearest-neighbor atoms of types A-A, B-B and A-B binding energies u_{AA}, u_{BB} and u_{AB}, respectively. In a crystal structure with p nearest neighbors, and x the concentration of element B, it can easily be shown that the mixing energy, u_M, obeys:

$$u_M = \frac{1}{2} p x (1-x)[u_{AB} - \frac{1}{2}(u_{AA} + u_{BB})] . \quad (2.1)$$

The mixing entropy per atom is:

$$\sigma_M = -[(1-x)\log(1-x) + x \log x] . \quad (2.2)$$

The free energy of mixing can be expressed as $f_M = u_M - \tau\sigma_M$ with τ the reduced temperature. A system is said to *segregate* in a composition range where the free energy has negative curvature, since the system would find segregating into a linear combination of various constituents outside of this range more energetically favorable. This region is known as a *solubility gap*. Bearing this in mind, one can establish an upper limit for the onset of the gap at a temperature of:

$$\tau_M = \frac{1}{4} p [u_{AB} - \frac{1}{2}(u_{AA} + u_{BB})] , \quad (2.3)$$

which aptly demonstrates the competition between binding like and unlike species.

A variety of approaches have been proposed to handle alloy behavior[9]. They proceed from two tacks: local or band pictures. In the local picture, where short-range interactions can be best handled, one has the cluster-variation method[10,11] (CVM), wherein one can extend the above model to include second-nearest neighbor interactions, effective three-atom (ring) interactions, and even four-atom (tetrahedron or square) interactions. By virtue of all the adjustable parameters involved, they are set to fit best the experimental phase diagrams.

The other limit is to consider the alloy amenable to band description. The question at

hand is which quantity, relevant to the pure metals, must be suitably averaged. In the virtual crystal approximation, one assumes the overall potential to be the weighted average of the pure metal constituents. In the Coherent Potential Approximation (CPA) introduced by Soven and by Velicky *et.al.*[12], wherein the self-consistent band energies are acquired by assuming all atoms scatter independently, an averaging of the pure metal Green's functions.

In the limit of very dilute alloys, one can appeal to perturbation theory to treat the impurity atom as a perturbing potential, whose effects are screened quite effectively past a distance of one lattice unit[13]. The other extreme, taken up by Terakura *et. al.*,[14] is to perform *ab initio* Local Density Approximation (LDA) calculations on a few selected ordered compounds, compare the relative energies of formation, and extract effective "forces" from them.

There have been attempts to connect the band-structure and cluster expansions[15,16], an example being the Cluster-Bethe lattice approach. The Bethe lattice, which is coupled here to a central cluster whose configuration is varied, forms a branching ringless tree, which though unrealistic, provides an easily handled continuum and represents some extension over no band structure at all.

The Small Cluster approach, described below, offers a compromise between statistical averaging and band structure, offering a little of both.

III. Survey of theoretical approaches to many-body systems

The fermion many-body problem is very much a problem onto its own and has occupied a lot of the literature[1]. Perturbation expansions, based on Feynman diagrams and Green's function approaches, are usually straightforward to carry out, though the question of convergence can be quite difficult to answer.

For example, consider a Hamiltonian $H = H_0 + V$, where H_0 is the one-electron part and the interaction, V, is bilinear in the fermion fields. The one-particle Green's function, $G(\mathbf{k},t)$, being the probablility that a quasiparticle, at time t, will have wavevector $\mathbf{k}$, can be shown[17] to obey:

$$G(\mathbf{k},t) = -i \frac{\langle \Phi_o | T(c_{\mathbf{k}}(t) c^{\dagger}_{\mathbf{k}}(0) S) | \Phi_o \rangle}{\langle \Phi_o | S | \Phi_o \rangle} \tag{3.1}$$

where $|\Phi_o\rangle$ is the ground state of H_0, T is the Wick time-ordering operator, and the S-matrix is given by:

$$S = \sum_n \frac{(-1)^n}{n} \int_{-\infty}^{\infty} \cdots \int_{-\infty}^{\infty} dt_1 \cdots dt_n \; T \{V(t_1) V(t_2) \cdots V(t_n)\}, \tag{3.2}$$

This of course assumes that there is no symmetry cross-over from the non-interacting to the interacting ground state, and that the series converges. One can see that only in the regime where (3.2) can be expanded unambiguously does the quasiparticle picture have meaning. Beyond that, one must resort to different approaches.

Without the conventional tools in hand, some theorists have sought to exploit various properties of these heavily-interacting systems. For the actinides and lanthanides, the large multiplicity of the *f*-orbitals has encouraged some to examine $1/N$ expansions[18], where N is the number of orbitals per site. That is to say, seven orbitals is "close enough" to an infinite number of degrees of freedom that one can expand about the infinitely degenerate state, an analytically soluble limit.

With the very large Coulomb energies effectively forbidding double occupation within a site for the heavy-fermion materials, a new statistics is suggested which is even more restrictive than fermionic. With this in mind, Coleman[19] and others have pursued the *slave-boson* approach, wherein a fictitious boson is introduced to satisfy the book-keeping of single electron occupancy, and together, the bosons and electrons can yield to conventional field-theoretic approaches. The problem is that subsequent application of mean-field theory to the bosonic degrees of freedom can lead to nonsensical results.

A similar tack is the projection process first proposed by Gutzwiller[20], which is to take the non-interacting many-body wave function, that is to say, the product of one-electron functions up to the Fermi level, and then project out any part containing doubly-occupied

sites.

Others have elected to run simulations on small clusters of atoms. This includes the present author, and the details of the method are the subject of the next section. There is however, in addition to the exact diagonalization approach, a Monte Carlo technique first introduced by Scalapino *et al.*[21,22]. They use the well-known Metropolis algorithm[23] to evaluate numerically the action integral within the field-theoretic context. Hirsch[24] was able to refine the technique for the Hubbard model, by mapping the d-dimensional fermion quantum problem onto a $(d + 1)$-dimensional Ising problem, whose updating procedures in a Monte Carlo scheme are much more well-defined.

III. Small Cluster approach

The small cluster approach proceeds from the premise that working with a crystal of N-atoms, with periodic boundary conditions imposed, is equivalent to solving a bulk crystal, sampled at N points of the Brillouin Zone. If this mini-crystal preserves the full symmetry of the lattice environment, then the sampled points will be points of high symmetry. The cluster hierarchy in the face-centered-cubic (fcc) structure is illustrated in Figure 4. One can see the logical progression, as more and more atoms are added, to eventually saturate the entire Brillouin Zone, starting at the points of high symmetry and working inwards.

In the context of the many-body problem, the advantage is quite clear. In order to treat electron-electron interactions non-perturbatively, one must take into account each n-electron configuration explicitly, a problem whose scope grows exponentially with n. Without a statistical approach, such a problem becomes intractable for all but small n.

The advantage of this sampling technique is fully realized when examining physical features that depend on the high-symmetry points of the crystal, as is often the case for electron band edges. Also, the small cluster size can model short-range interactions quite effectively. Conversely, long-range phenomena, and in particular phase-transition behavior, can not be modeled, but the underlying mechanisms can sometimes be discerned.

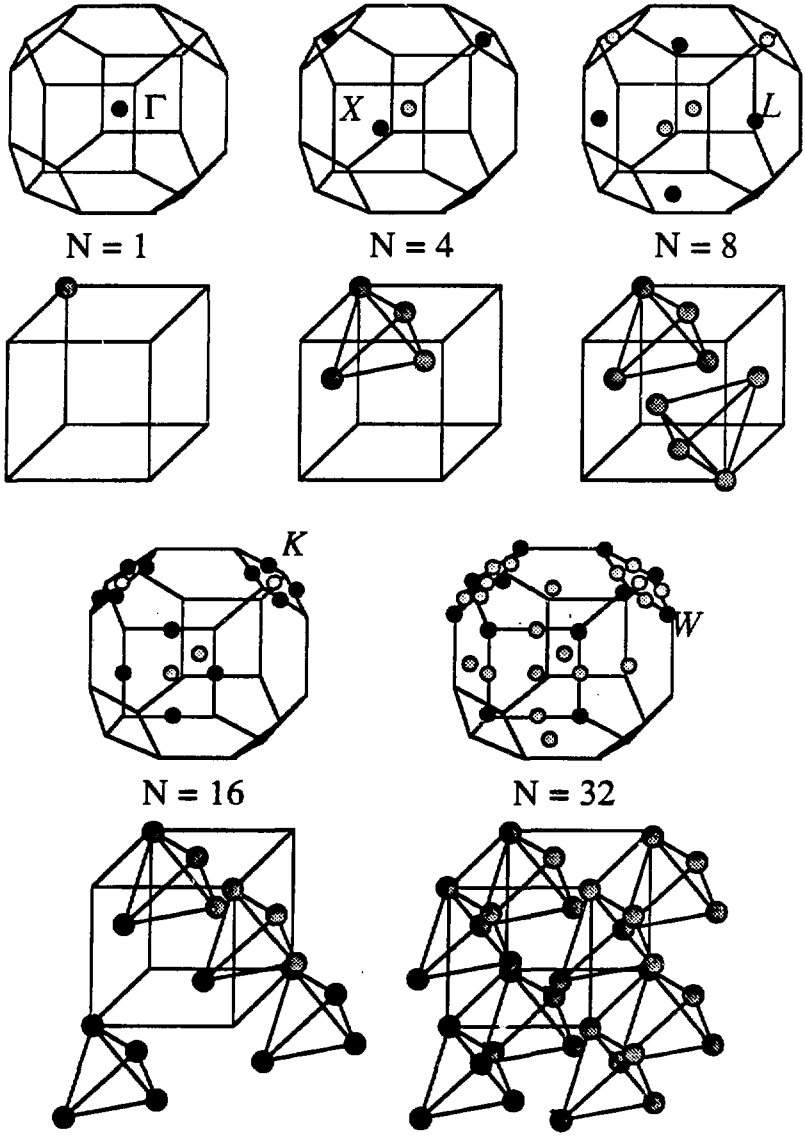

FIG. 4. The Small-Cluster approach hiearchy for the fcc (face-centered-cubic structure). Maintaining cubic symmetry imposes the requirements that the possible cluster sizes are N = 1, 4, 8, 16, 32... atoms, which corresponds to an equivalent number of points in the Brillouin Zone. Notice that the 8-atom and 16-atom clusters have inreconcilable k-vector samplings, *i.e.* one is not the subset of the other.

Although the solution of simple two-atom clusters formed the work of Falicov[25] and Harris in 1969, and Lin[26] and Falicov in 1980, the method really came into its own in 1984 with the solution of a four-atom tetrahedral-cluster model by Falicov[27] and Victora. This work is notable in its full utilization of group theory to factorize the Hamiltonian matrix into smaller Jordan blocks corresponding to the different irreducible representations of the underlying space group. Since then a whole series of works have been published[28], covering such diverse behavior in metals as photoemission, magnetism, thermodynamics, valence fluctuations, superconductivity, phonon processes, etc.

A. Space group symmetry

Each crystal environment presents a set of symmetry operations which leaves it invariant. These operations include the identity element, operational inverses, exhibit associativity, in other words, have all the properties of a group. While this is not meant to a treatise on group theory, and while the author strongly recommends acquaintance with texts such as Falicov[29] or Tinkham[30], a few concepts should be elaborated here.

In solid state physics the space group contains operations which involve both point and translational operations. The point operations consist of the various rotations and reflections the crystal admits about a given basis point. The periodicity of the lattice is revealed by its translation group. A space group is called *symmorphic* if it consists only of point operations taken about a basis point. Non-symmorphic groups, which are not considered in this thesis, include operations such as screw axes and glide planes which do not fall into the previous categories.

A Hamiltonian which purports to describe a system with a given group symmetry, must itself preserve the symmetry of that system. Therefore, wave functions following one particular representation of that group can only mix with wave functions of that same representation.

A familiar example from atomic physics are the spherical harmonics, Y_{lm}, which follow the representations of the full rotation group, *i.e. s, p, d, f,* etc., corresponding to

l = 0,1,2,3, etc. Group theory says that only functions with the same (l,m) can mix, and imposing a Coulomb potential yields radial eigenfunctions, which are the Laguerre polynomials in the hydrogen atom.

1. A Four-site fcc crystal example

A case more in line with the work in this thesis is to illustrate the results of Falicov and Victora[13] wherein they solved a four-atom tetrahedral cluster Hubbard model. Using the second-quantization notation where $c_{i\sigma}$ ($c^{\dagger}_{i\sigma}$) represents the destruction (creation) of an electron on site i, and spin σ, the following Hamiltonian was imposed:

$$H = H_t + H_U \tag{3.1}$$

where

$$H_t = -t \sum_{<ij>\sigma} c^{\dagger}_{i\sigma} c_{j\sigma} \tag{3.2}$$

is the nearest-neighbor hopping, with hopping integral t, and

$$H_U = U \sum_i c^{\dagger}_{i\uparrow} c_{i\uparrow} c^{\dagger}_{i\downarrow} c_{i\downarrow} \tag{3.3}$$

is the on-site electron-electron Coulomb repulsion of strength U.

The nature of the relevant space group and its representations is presented in Chapter II, Section III. The salient feature here is that this problem can be mapped isomorphically onto the problem of solving an isolated tetrahedral molecule, which is governed by the Tetrahedral group, T_d. The group has five irreducible representations: Γ_1, Γ_2, Γ_3, Γ_4, and Γ_5 and consists of 24 operations: the identity (E), 3 two-fold rotations (C_2), 8 three-fold rotations (C_3), 6 reflections (σ) and 6 improper four-fold rotations (S_4), which are written in cycle notation in Table II.

Table II. The action of the T_d group operations on the four-atom cluster.

E	C_3		σ	S_4
(1)(2)(3)(4)	(234)	(124)	(12)	(1324)
C_2	(243)	(142)	(13)	(1423)
(12)(34)	(134)	(123)	(14)	(1342)
(13)(24)	(143)	(132)	(23)	(1243)
(14)(23)			(24)	(1234)
			(34)	(1432)

With this table, and the character table (Chapter 2, Section III, Table I) one can immediately write the (unnormalized) projection operator for the Γ_5 representation, say:

$$\sum_R P_R(\Gamma_5) = 1-(12)(34)-(13)(24)-(14)(23) -(12)-(13)-(14)-(23)-(24)-(34) +(1324)+(1423)+(1342)+(1243)+(1234)+(1432) \quad (3.4)$$

From (3.4) it is immediately straightforward to isolate the states for, say, four electrons following the Γ_5 representation. Starting from some simple four-electon states such as:

$$c_{1\uparrow}^\dagger\ c_{1\downarrow}^\dagger\ c_{2\uparrow}^\dagger\ c_{3\uparrow}^\dagger\ ,\quad c_{1\uparrow}^\dagger\ c_{2\downarrow}^\dagger\ c_{3\uparrow}^\dagger\ c_{4\uparrow}^\dagger \quad \text{and} \quad c_{1\uparrow}^\dagger\ c_{1\downarrow}^\dagger\ c_{2\uparrow}^\dagger\ c_{4\uparrow}^\dagger \quad (3.5)$$

one can form a basis for the ${}^3\Gamma_5$ (spin triplet) representation by projection thus:

$$|\Psi_1> \propto \sum_R P_R(\Gamma_5)\, c_{1\uparrow}^\dagger c_{1\downarrow}^\dagger c_{2\uparrow}^\dagger c_{3\uparrow}^\dagger$$

$$\propto \left(c_{1\uparrow}^\dagger c_{1\downarrow}^\dagger c_{2\uparrow}^\dagger c_{3\uparrow}^\dagger + c_{4\uparrow}^\dagger c_{4\downarrow}^\dagger c_{3\uparrow}^\dagger c_{2\uparrow}^\dagger - c_{3\uparrow}^\dagger c_{3\downarrow}^\dagger c_{4\uparrow}^\dagger c_{1\uparrow}^\dagger - c_{2\uparrow}^\dagger c_{2\downarrow}^\dagger c_{1\uparrow}^\dagger c_{4\uparrow}^\dagger\right)$$

$$= \frac{1}{2}\left(c_{1\uparrow}^\dagger c_{1\downarrow}^\dagger c_{2\uparrow}^\dagger c_{3\uparrow}^\dagger + c_{4\uparrow}^\dagger c_{4\downarrow}^\dagger c_{3\uparrow}^\dagger c_{2\uparrow}^\dagger - c_{3\uparrow}^\dagger c_{3\downarrow}^\dagger c_{4\uparrow}^\dagger c_{1\uparrow}^\dagger - c_{2\uparrow}^\dagger c_{2\downarrow}^\dagger c_{1\uparrow}^\dagger c_{4\uparrow}^\dagger\right)$$

(3.6)

$$|\Psi_2> \propto \sum_R P_R(\Gamma_5)\, c^\dagger_{1\uparrow} c^\dagger_{2\downarrow} c^\dagger_{3\uparrow} c^\dagger_{4\uparrow}$$

$$= \frac{1}{2}\left(c^\dagger_{1\uparrow} c^\dagger_{2\downarrow} c^\dagger_{3\uparrow} c^\dagger_{4\uparrow} + c^\dagger_{4\uparrow} c^\dagger_{3\downarrow} c^\dagger_{2\uparrow} c^\dagger_{1\uparrow} - c^\dagger_{3\uparrow} c^\dagger_{4\downarrow} c^\dagger_{1\uparrow} c^\dagger_{2\uparrow} - c^\dagger_{2\uparrow} c^\dagger_{1\downarrow} c^\dagger_{4\uparrow} c^\dagger_{3\uparrow} \right)$$

(3.7)

$$|\Psi_3> \propto \sum_R P_R(\Gamma_5)\, c^\dagger_{1\uparrow} c^\dagger_{1\downarrow} c^\dagger_{2\uparrow} c^\dagger_{4\uparrow}$$

$$= \frac{1}{\sqrt{8}}\Big(c^\dagger_{1\uparrow} c^\dagger_{1\downarrow} c^\dagger_{2\uparrow} c^\dagger_{4\uparrow} + c^\dagger_{4\uparrow} c^\dagger_{4\downarrow} c^\dagger_{3\uparrow} c^\dagger_{1\uparrow} - c^\dagger_{3\uparrow} c^\dagger_{3\downarrow} c^\dagger_{4\uparrow} c^\dagger_{2\uparrow} - c^\dagger_{2\uparrow} c^\dagger_{2\downarrow} c^\dagger_{1\uparrow} c^\dagger_{3\uparrow}$$

$$- c^\dagger_{1\uparrow} c^\dagger_{1\downarrow} c^\dagger_{3\uparrow} c^\dagger_{4\uparrow} - c^\dagger_{4\uparrow} c^\dagger_{4\downarrow} c^\dagger_{2\uparrow} c^\dagger_{1\uparrow} + c^\dagger_{3\uparrow} c^\dagger_{3\downarrow} c^\dagger_{1\uparrow} c^\dagger_{2\uparrow} + c^\dagger_{2\uparrow} c^\dagger_{2\downarrow} c^\dagger_{4\uparrow} c^\dagger_{3\uparrow} \Big)$$

(3.8)

(It is implicit that the creation operators are acting upon the vacuum, $|0>$.) Applying the Hamiltonian (3.1)–(3.3), one can therefore show the following relations hold:

$$H\,|\Psi_1> = -2\sqrt{2}\,t\;|\Psi_3> + U\,|\Psi_1> \qquad (3.9)$$

$$H\,|\Psi_2> = 2\sqrt{2}\,t\;|\Psi_3> \qquad (3.10)$$

$$H\,|\Psi_3> = -2\sqrt{2}t\;|\Psi_1> + 2\sqrt{2}\,t\;|\Psi_2> + U\,|\Psi_3> \qquad (3.11)$$

which, by solution of the secular equation, yields the energies as roots of the cubic:

$$E^3 - 2U E^2 + E\,(U^2 - 16t^2) + 8t^2 U = 0 \qquad (3.12)$$

B. Spin symmetry

In this thesis, all models considered are of a basis of singly degenerate, spherically symmetric orbitals, *i.e.* *s*-orbital like. Thus, the angular momentum of the many-body wavefunctions are pure spin, with no orbital angular momentum coming to play.

It is rather straightforward to arrange to isolate states with a given z-projection of angular momentum, i.e. separating the wavefunction according to the different values of $n_\uparrow - n_\downarrow = 2\,J_z$. To exploit the full spin symmetry, a bootstrap process is employed.

Denoting the angular eigenvectors for one spin 1/2 particle as

$$|\frac{1}{2},\frac{1}{2}> = |+> \quad , \quad |\frac{1}{2},\frac{-1}{2}> = |-> \ , \tag{3.12}$$

it is straightforward to show[31] that additional particles can be added on in the following manner:

$$|S+\frac{1}{2},S+\frac{1}{2}> = |S,S> \otimes |+>$$

$$|S-\frac{1}{2},S-\frac{1}{2}> = \sqrt{\frac{2S}{2S+1}}\,|S,S> \otimes |-> - \frac{1}{\sqrt{2S+1}}\,|S,S-1> \otimes |+> \tag{3.13}$$

where $|J,J_z>$ refers to a state with total angular momentum J, and z-projection J_z.

Table III. The number of representations of a given spin for 1-8 spin 1/2 particles.

N \ S	0	1/2	2	3/2	2	5/2	3	7/2	4
1		1							
2	1		1						
3		2		1					
4	2		3		1				
5		5		4		1			
6	5		9		5		1		
7		14		14		6		1	
8	14		28		20		7		1

As one can see from equation (3.13), a state of spin J = S for N particles gives rise to states of spin J = S - 1/2, S + 1/2 for N+1 particles. This procedure results in a multiplicity of angular eigenvectors as prescribed in Table III. With the multiplicities roughly doubling with each additional particle, one sees that this method becomes quite cumbersome for all but a small number of particles.

IV. Summary of Thesis

In Chapter 2, an exact solution of a four-site tetrahedral crystal model, the smallest face-centered cubic crystal, is presented in the case of an intermediate-valence system. The model consists of: (a) one extended orbital and one localized orbital per atom; (b) an interatomic transfer term between extended orbitals; (c) an interatomic hybridization between the localized and extended orbitals; (d) strong intra-atomic Coulomb repulsion between opposite-spin localized states; and (e) intermediate-strength intra-atomic Coulomb repulsion between the localized and extended states. These competing effects are examined as they manifest themselves in the intermediate-valence, photoemission, inverse photoemission and thermodynamic properties.

In Chapter 3, an exact solution of a four-site tetrahedral crystal model with periodic boundary conditions, the smallest face-centered cubic crystal, is presented in the case of binary and ternary alloy systems. The model consists of (a) a single s orbital per site with nearest-neighbor-only hopping (b) a Coulomb repulsion between electrons on the same site; and (c) a single electron per atom. The model, which represents Cu, Ag, Au, and their alloys, shows all the segregational, solutional, and compound-forming tendencies of the real systems. Such characteristics are absent in non interacting independent-electron approaches. Calculations demonstrate extreme sensitivity to the input one-electron parameters, with minor differences resulting in widely different alloying properties.

In Chapter 4, an exact solution of an eight-site crystal model with periodic boundary conditions, a small face-centered cubic crystal, is presented for the case of a heavy-fermion system. The model consists of: (a) a single, fully symmetric orbital per site, with nearest-neighbor and second nearest-neighbor hopping; (b) an infinite Coulomb repulsion between electrons on the same site; (c) antiferromagnetic superexchange interactions; and (d) a nearly-half-filled band (7/8 electron per site). Application of group-theoretical techniques yields a set of energies which are at most (analytic) solutions of quadratic equations. Depending on the sign of the nearest-neighbor hopping parameter the ground state exhibits either a huge accidental degeneracy (the heavy-fermion case), or simple, uniform, saturated

itinerant ferromagnetism. The model is, at once, easy to handle and yet rich in structure. Fermi surface, spin-wave, and electron transport properties are investigated, and consequences for real systems discussed.

In Chapter 5, the model of the previous chapter is further explored. Band fillings near half-filling (six, seven and eight electrons per cluster) are examined. Superconducting and antiferromagnetic correlations are studied and compared with the predictions of the non-interacting limit. The suitability of various approximations (the so-called BCS and Gutzwiller ground-state wave functions) are quantitatively estimated.

VI. References

[1]D. Pines, *Many-Body Problem*, (Benjamin, New York, 1961).

[2]P. Fulde, J. Keller and G. Zwicknagl, in *Solid State Physics*, edited by H. Ehrenreich and D. Turnbull, (Academic Press, New York, 1988) Vol. 41, p.1.

[3]W.A. Harrison, *Electronic Structure and Properties of Solids*, (W.H. Freeman, San Francisco, 1980), p. 520.

[4]P.A. Lee, T.M. Rice, J.W. Serene, L.J. Sham and J.W. Wilkins, in *Comments on Condensed Matter Physics*, (Gordon and Breach, Great Britain, 1986), Vol. XII, No.3, p.99; *American Institute of Physics Handbook*, 2nd ed., edited by D.E. Gray (McGraw-Hill, New York,1963); D.C. Koskimaki and K.A. Gschneider, Jr., Phys. Rev. B. **11**, 4463, (1975).

[5]J. Kondo, Progr. Theoret. Phys. (Kyoto) **32**, 37 (1964).

[6]J. Hubbard, Proc. R. Soc. London, Ser A **276**, 238 (1963).

[7]P.W. Anderson, Phys. Rev. **124**, 41 (1961).

[8]C. Kittel and H. Kroemer, *Thermal Physics*, 2nd ed. (Freeman, San Francisco, 1980) pp. 318-9.

[9]For a review, see W. Ehrenreich, *Solid State Physics*, edited by H. Ehrenreich, F. Seitz and D. Turnbull (Academic Press, New York, 1976) Vol. 31, p.149.

[10]R. Kikuchi and D. de Fontaine, Natl. Bur. Stand. (U.S.) Spec. Publ. No. 496, (U.S. GPO, Washington D.C. 1978), pp. 967 and 999.

[11]J. M. Sanchez, D. de Fontaine and W. Teitler, Phys. Rev. **26**, 1465 (1982).

[12]P. Soven, Phys. Rev. **156**, 809 (1967); B. Velicky, S. Kirkpatrick, H. Ehrenreich, Phys. Rev. **175**, 745 (1968).

[13]C. Kittel, *Quantum Theory of Solids*, (Wiley, New York, 1963), p.340.

[14]K. Terakura, T. Oguchi, T. Mohri and K. Watanabe, Phys. Rev. B. **35**, 2169 (1987).

[15]R.C. Kittler and L.M. Falicov, Phys. Rev. B. **18**, 2506 (1978) and **19**, 291 (1979).

[16]M.O. Robbins and L.M. Falicov, Phys. Rev. B. **25**, 2343 (1982).

[17]A.A. Abrikosov, L.P. Gor'kov and I.E. Dzyaloshinsky, *Methods of the quantum field theory of fields in statistical physics*, (Prentice-Hall, Englewood N.J., 1963).

[18]N.E. Bickers, Rev. Mod. Phys. **59**, 845 (1987).

[19]P. Coleman, Phys. Rev. B. **29**, 3035 (1984).

[20]M.C. Gutzwiller, Phys. Rev. A. **137**, 1726 (1965).

[21]D. J. Scalapino and R.L. Sugar, Phys. Rev. Lett. **46**, 519 (1981); Phys. Rev. B. **24**, 4295 (1981).

[22]R. Blankenbecker, D.J. Scalapino and R.L. Sugar, Phys. Rev. D. **24**, 2278 (1981).

[23]N. Metropolis, A.W. Rosenbluth, A.H. Teller and E. Teller, J. Chem. Phys. **21**, 1087 (1953).

[24]J. E. Hirsch, Phys. Rev. B. **28**, 4059 (1983).

[25]L.M. Falicov and R.A. Harris, J. Chem. Phys. **51**, 3153 (1969).

[26]T-h. Lin and L.M. Falicov, Phys. Rev. B. **22**, 857 (1980).

[27]L.M. Falicov and R.H. Victora, Phys. Rev. B. **30**, 1695 (1984).

[28]See references in L.M. Falicov, *Recent Progress in Many-Body Theories*, Vol. I, edited by E. Pajanne and R. Bishop, (Plenum, New York, 1988), p. 275.

[29]L.M. Falicov, *Group Theory and its Physical Applications*, (U. of Chicago Press, Chicago, 1966).

[30]M. Tinkham, *Group Theory and Quantum Mechanics*, (McGraw-Hill, New York, 1964).

[31]C. Cohen-Tannoudji, B. Diu and F. Laloe, *Quantum Mechanics*, (Wiley, New York, 1970), Vol. 2, pp. 1027-34.

Chapter II. Calculation of Fluctuations and Photoemission Properties in a Tetrahedral-Cluster Model for an Intermediate-Valence System

I. Introduction

The lanthanides present an interesting physical situation in which the *f* orbitals, lying close to the Fermi level, can interact strongly with the conduction bands, the phenomenon being known in the literature as Intermediate Valence.[1-4] This situation arises when two electron configurations, $(4f)^n$ and $(4f)^{n+1}$, are very close in energy, but differ greatly from any other due to strong Coulomb electron-electron repulsion. These *f*-orbitals can, however, hybridize with completely delocalized conduction states.

The many-body aspects of the electronic structure of cerium have been investigated by many groups[3,5,6]. In its fullest sense, these effects cannot be derived in a Local-Density Approximation (LDA), although calculations incorporating various screening effects on the *4f* electrons have been published[7]. It is therefore a challenge to include more throroughly the many-body effects. The approach taken here is the exact solution of a limited-size crystal with all many-body interactions.

The crystal under consideration here is a tetrahedral grouping of only four atoms with periodic boundary conditions, which is the smallest non-trivial fcc crystal, the structure[8] of α- and γ-cerium. This small-cluster approach, used successfully before to explore photoemission behavior[9] in the transition-metal nickel, was applied by Parlebas *et. al.*[10] to the present problem. The extent of their investigation was only to map out the rather large phase space offered by the choice of coupling parameters, and the results indicated a model dominated by one-electron effects.

The calculation on this small cluster is exact, but the Brillouin Zone is restricted to four points[11], the center of the zone, Γ, and the centers of the three square faces, X. This approach yields good results for uniform and very short-range correlation behavior, and is therefore meaningful for photoemission and inverse-photoemission processes. The bandwidth is one of the adjustable parameters, and can be chosen to fit best the experimental data.

The model is inadequate, however, in its treatment of the conduction band, since it yields a series of distinct and disconnected levels, whereas cerium is known to have a wide s - d band, with $4f$ electrons located near the Fermi level[12]. With only nearest neighbor interactions coming into play, phenomena depending on intermediate and long-range forces are poorly mimicked. Thus, one would not expect to see phase transitions, although one might see indications of how they might occur.

In this chapter, the behavior of the tetrahedral cluster with total populations of three, four and five electrons is analyzed. Four electrons in the crystal correspond to one electron per atom, a situation similar in some sense to cerium, which has one of its four outer electrons participating in hybridization. In this approach, one can study the value of the intermediate-valence, photoemission spectra, and thermal properties.

II. The Hamiltonian

The tetrahedral cluster has four sites labeled i=1,2,3,4. Two types of orbitals are proposed, each being either spin up or down, denoted with subscript σ. The creation (destruction) operator for an extended conduction-like state is written as $c^{\dagger}_{i\sigma}$($c_{i\sigma}$) and that for a single f-like state, denoted by $f^{\dagger}_{i\sigma}$($f_{i\sigma}$). The latter is a localized state, but is not a true f-state, since it has positive parity and a degeneracy of one. This feature makes the problem tractable. The Hamiltonian is composed of five parts:

$$H = H_c + H_f + H_{hyb} + H_{f\text{-}f} + H_{c\text{-}f} \qquad (2.1)$$

where

$$H_c = -t \sum_{\substack{i,j;\sigma \\ i \neq j}} c^{\dagger}_{i\sigma} c_{j\sigma} \qquad (2.2)$$

$$H_f = E_0 \sum_{i,\sigma} f^{\dagger}_{i\sigma} f_{i\sigma} \qquad (2.3)$$

$$H_{hyb} = v \sum_{\substack{i,j;\sigma \\ i \neq j}} (c^{\dagger}_{i\sigma} f_{j\sigma} + f^{\dagger}_{i\sigma} c_{j\sigma}) \qquad (2.4)$$

$$H_{f-f} = U \sum_i f^{\dagger}_{i\uparrow} f_{i\uparrow} f^{\dagger}_{i\downarrow} f_{i\downarrow} \qquad (2.5)$$

$$H_{c-f} = G \sum_{i;\sigma\sigma'} c^{\dagger}_{i\sigma} c_{i\sigma} f^{\dagger}_{i\sigma} f_{i\sigma} \qquad (2.6)$$

These terms are:

(a) a "hopping" interaction (2.2) between conduction states on adjacent sites, with transfer integral t;

(b) an occupation energy (2.3) for the f-orbital, whose strength E_0 is measured with respect to the center of gravity of the conduction band states;

(c) a hybridization interaction (2.4) between the conduction and f-states on adjacent sites (crystal symmetry usually forbids on-site mixing[13]), with strength dependent only on $|v|$, as shall be shown;

(d) an f - f on-site (intra-atomic) Coulomb repulsion (2.5), with $U > 0$;

(e) the c - f on-site Coulomb repulsion (2.6), with $G > 0$. The model presents some limiting cases which permit analytic solution. If (2.5) and (2.6) are neglected, the Hamiltonian becomes that of a one-electron problem; (2.2), (2.3) and (2.4) can be diagonalized simultaneously to yield two singlet and two triplet one-electron orbitals with energies:

$$E_{1\pm} = \frac{1}{2}\left[E_0 - 3t \pm \sqrt{(E_0 + 3t)^2 + 36v^2} \right] \qquad (2.7)$$

and

$$E_{3\pm} = \frac{1}{2}\left[E_0 + t \pm \sqrt{(E_0 - t)^2 + 4v^2} \right] \qquad (2.8)$$

respectively. These orbitals can be occupied independently. If (2.4) and (2.6) are neglected, the conduction and *f*-states decouple. The conduction states are extended one-electron orbitals [a singlet at $(-3t)$ and a triplet at t], and the *f*-states produce a collection of atomic configurations of energies 0, E_0, and $2E_0+U$, corresponding to zero, one and two *f*-electrons per site, respectively. If (2.2) and (2.6) are neglected, the problem becomes atomic-like, i.e. is decoupled into four sites, with a straightforward assignment of energies.

The parameters were chosen as follows.

(a) The transfer integral t is set to be positive and equal to 1 *eV* (bandwidth $4|t| = 4$ *eV*); because t is positive the singlet lies below the triplet, and the conduction-band states "pile up" at the top of the band;

(b) The *f*-orbital energy is set at $E_0 = 0.75$ *eV*, so that it lies close to the conduction band triplet, allowing sizeable hybridization to take place;

(c) The strong f - f repulsion, which is effectively infinite for ground state configurations[8], turns out to be at least an order of magnitude greater than the bandwidth, and so was taken arbitrarily to be $U = 25$ *eV*.

(d) The choice for the hybridization and the c - f Coulomb repulsion is a much more subtle question; both parameters have been left as varying.

III. Method of Calculation

The Hamiltonian presented above (2.1)-(2.6) has many symmetries to exploit, thus permitting group-theoretical techniques to reduce greatly the size of the problem.

First of all, the number of electrons, N, is a good quantum number. There are sixteen orbitals to be occupied, with simple combinatorial arguments predicting $16!\,/\,(16\text{–}N)!\,N!$ states for N electrons. In the absence of spin-orbit coupling, the total angular momentum and its z-projection, (J, J_z), are good quantum numbers as well.

The fcc structure with four sites (four lattice translations) spans a space group with 192 operations. This group contains the inversion and has 20 irreducible representations[11] (ten at Γ and ten at X) with the following degeneracies: Γ_1, Γ_1', Γ_2, Γ_2' (d=1); Γ_{12}, Γ_{12}' (d=2); Γ_{15}, Γ_{15}', Γ_{25}, Γ_{25}', X_1, X_1', X_2, X_2', X_3, X_3', X_4, X_4' (d=3); and X_5, X_5' (d=6). For spherically symmetric atomic orbitals (even parity) only five representations remain: Γ_1, Γ_2, Γ_{12}, X_1 and X_2. These representations transform, under the operations of the full tetrahedral group, T_d, *at the center of the tetrahedron*, like the five traditional representations given in Table I.

TABLE I. Character Table of T_d

	1 E	3 C_2	8 C_3	6 σ	6 S_4
Γ_1	1	1	1	1	1
Γ_2	1	1	1	-1	-1
Γ_3	2	2	-1	0	0
Γ_4	3	-1	0	1	-1
Γ_5	3	-1	0	-1	1

The T_d notation is retained, with associations: $\Gamma_1 = \Gamma_1$; $\Gamma_2 = \Gamma_2$; $\Gamma_3 = \Gamma_{12}$; $\Gamma_4 = X_1$ and $\Gamma_5 = X_2$. A left superscript, $2S+1$, as in ${}^{2S+1}\Gamma_j$, refers to the spin degeneracy. For example, the the one-electron energies presented in (2.7) and (2.8) correspond to ${}^2\Gamma_1$, and

$^2\Gamma_4$, respectively. These energies are depicted in Figure 1.

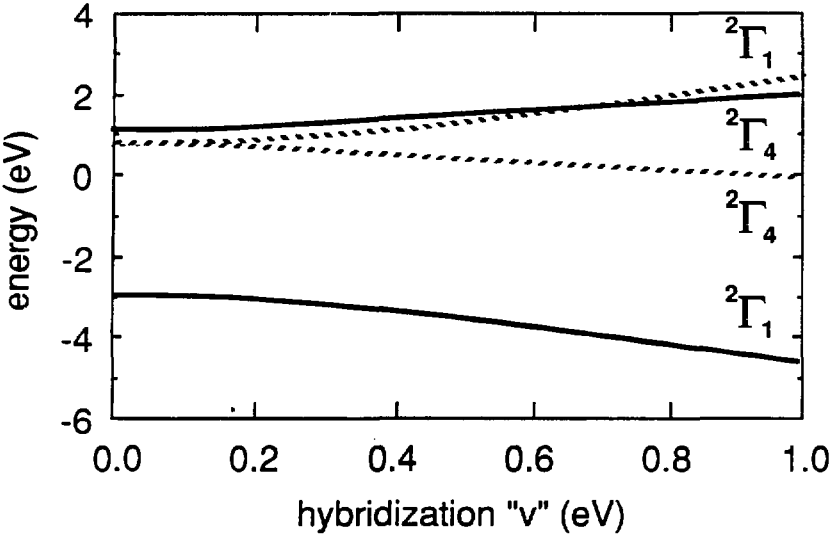

FIG. 1 One-electron energies (without many-body effects) for $t = 1\ eV, E_0 = 0.75\ eV$. The hopping term (2.2) breaks up the four c-states into a lower $^2\Gamma_1$ singlet and an upper $^2\Gamma_4$ triplet.Hybridization (2.4) breaks up the f-states analogously, and mixes them with the c-states.

TABLE II. Size of blocks of the various representations.

N	Spin	Γ_1	Γ_2	Γ_3	Γ_4	Γ_5
3	3/2	2	4	4	6	8
	1/2	12	2	14	26	16
4	2	2	8	6	6	10
	1	14	16	30	46	50
	0	23	7	33	48	32
5	5/2	2	4	4	6	8
	3/2	14	32	40	54	72
	1/2	46	34	86	132	120

The multi-dimensional representations of $T_d - \Gamma_3$, Γ_4 and Γ_5 – yield another quantum number: the index of the function within the representation. With the use of all these symmetries, the problem factorizes into much smaller sets as shown in Table II. Thus, group-theoretical techniques bring the size of the largest block to be diagonalized down to 132 × 132, a considerable reduction from 4368 × 4368 for the five-electron problem. It should be noted that these blocks, when diagonalized, represent exact solutions of the Hamiltonian (2.1).

IV. Results

A. Valence – "f"-occupancy

Intermediate-valence properties of this model were investigated first, as a function of the various parameters. The *f*-occupancy, for *N* electrons, is defined simply as:

$$n_f = \frac{1}{4} < \Psi_{NG} \mid \sum_{i;\sigma} f^{\dagger}_{i\sigma} f_{i\sigma} \mid \Psi_{NG} > \qquad (4.1)$$

where Ψ_{NG} is the *N*-electron ground state. For the sake of comparison, cerium has four electrons per atom in its outer shell; its valence is defined as $4 - n_f$. The experimental values of the valence are somewhat controversial[2,14,15,16], and have been quoted to range from 3.3 to 3.7 (n_f = 0.7 to 0.3) for α-cerium, and between 3.0 and 3.1 (n_f = 1.0 to 0.9) for γ-cerium.

Results for four electrons in the cluster (one electron per site) are presented graphically in Figure 2. In the absence of hybridization, n_f = 0.5 (2 electrons in the low-lying conduction state singlet, two in the *f*-states) for small *G* values. Large values of *G* favor promotion to the higher lying conduction-state triplet, yielding n_f = 0.25 for intermediate values, and n_f = 0 for large *G* values. As hybridization blurs the distinction between the conduction and *f*-states, a smooth variation between the two extreme n_f values, for finite *v*, is not surprising.

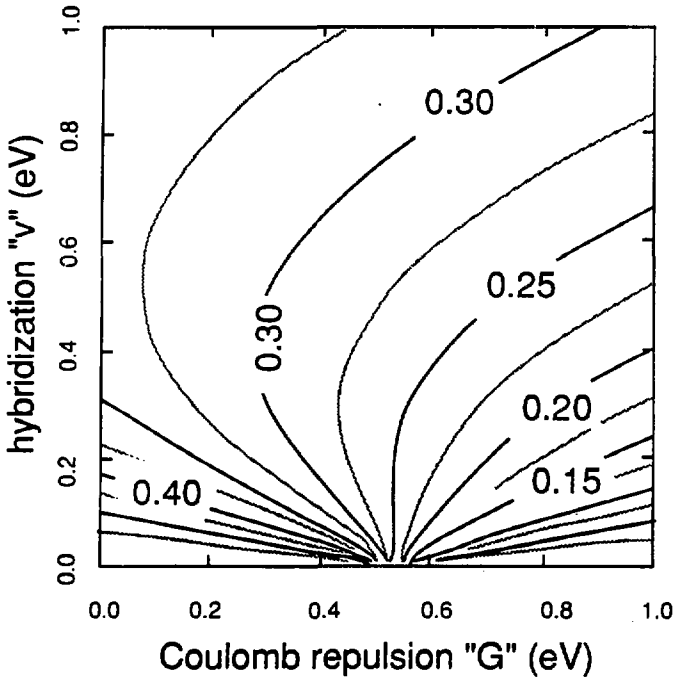

FIG. 2 Contour plot for the *f*-orbital occupancy, for varying values of the on-site Coulomb repulsion G, and hybridization v, with other parameters taken as: $t = 1\ eV$, $E_0 = 0.75\ eV$, $U = 25\ eV$. Singularities occur at $v = 0$, $G = 0.50\ eV$ and $G = 0.55\ eV$, where there are promotions of electrons from the *f*-levels to the conduction-state triplet.

Further inspection shows the contour corresponding to $n_f = 0.33$ passing through $G = 0eV$, $v = 0.5\ eV$. The value of n_f is not a monotonic function of v for small G.

B. Intra-atomic charge fluctuations

With a two-orbital per site and four-electron per cluster configuration, there are finite probabilities for the occupation, at each site, of zero, one, two, three and four electrons. It

can be shown that these probabilities, P_n, are related directly to the one-,two-, three- and four-electron correlation functions by:

$$P_0 = 1 - N_1 + N_2 - N_3 + N_4 \qquad (4.2)$$

$$P_1 = N_1 - 2N_2 + 3N_3 - 4N_4 \qquad (4.3)$$

$$P_2 = N_2 - 3N_3 + 6N_4 \qquad (4.4)$$

$$P_3 = N_3 - 4N_4 \qquad (4.5)$$

$$P_4 = N_4 \qquad (4.6)$$

where

$$N_1 = \sum_{\mu} n_{1\mu} \qquad (4.7)$$

$$N_2 = \sum_{\mu < \nu} n_{1\mu} n_{1\nu} \qquad (4.8)$$

$$N_3 = \sum_{\mu < \nu < \rho} n_{1\mu} n_{1\nu} n_{1\rho} \qquad (4.9)$$

$$N_4 = n_{c1\uparrow} n_{c1\downarrow} n_{f1\uparrow} n_{f1\downarrow} \qquad (4.10)$$

and the number operators $n_{1\mu}$ ($\mu = c\ \uparrow, c$

There is no loss of generality with such a choice since the states are fully symmetrized.

The results for the Γ_3 ground state are plotted in Figures 3 and 4. These plots show, respectively, the cases without and with hybridization. For $v = 0$ *eV*, a double-step function in the *f*-occupancy of Figure 2 is more clearly seen, with two transitions, corresponding to successive *f*-electrons being promoted to the higher conduction-triplet

states. For finite v, the transition is once again smooth.

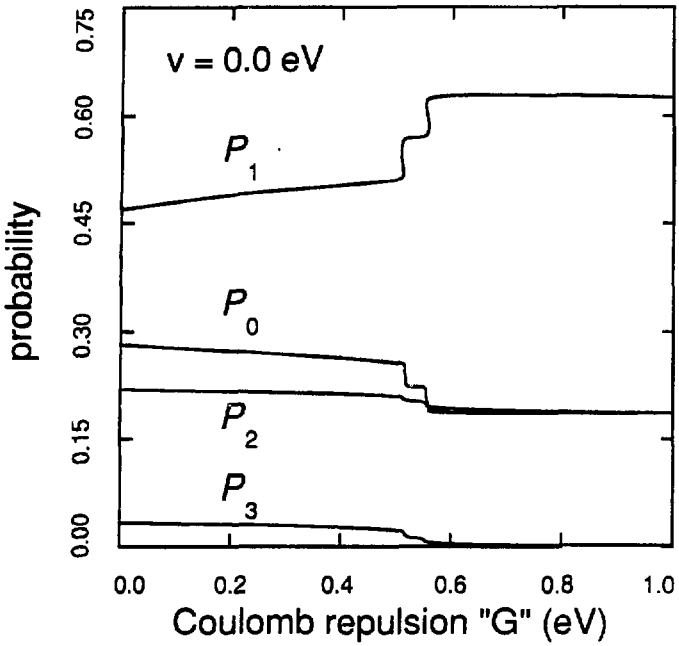

FIG. 3 Plot of the electron-occupation probabilities for 0, 1, 2 and 3 electrons, for t = 1 eV, E_0 = 0.75 eV, v = 0 eV and U = 25 eV as functions of the c - f Coulomb repulsion. Note the successive steps, corresponding to f-electrons being promoted to the conduction states.

Table III shows the values of P_n for various limiting cases ($E_0 << -3t$, $U >> t$, the atomic f-level case; $E_0 >> t$, the pure conduction-band free-electron case; $v = G = 0$, $U >> t$, the unhybridized juxtaposition of free conduction-band and f-electrons; and, a typical intermediate-valence case). It can be seen that the results of Parlebas *et. al.*[10] can now be more easily understood. The structure is dominated by one-electron terms because the main effects of the U and hybridization terms are to reduce P_3 and P_4, which are already small numbers in the free-electron case. In particular, a large U makes $P_4 \equiv 0$.

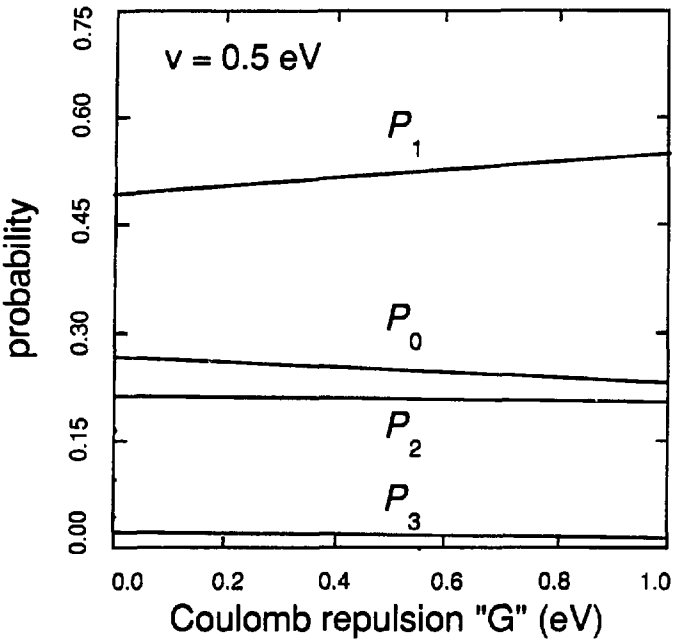

FIG. 4 Plot of the electron-occupation probabilities for 0, 1, 2 and 3 electrons, for $t = 1$ eV, $E_0 = 0.75$ eV, $v = 0.5$ eV and $U = 25$ eV as function of the c - f Coulomb repulsion. The steps of the $v = 0$ eV plot (Figure 3) are here smoothed out.

TABLE III. Electron occupation probabilities.

	Atomic $\begin{bmatrix} E_0 \ll -3t \\ U \gg t \end{bmatrix}$	Free electron $(E_0 \gg t)$	No hybridization strong Coulomb repulsion at the Fermi Level $\begin{bmatrix} v = 0\,eV \\ G = 0 \\ U = 25\,eV \end{bmatrix}$	Intermediate Valence $\begin{bmatrix} v = 0.5eV \\ G = 0 \\ U = 25\,eV \end{bmatrix}$
P_0	0	0.316	0.281	0.267
P_1	1	0.422	0.469	0.492
P_2	0	0.211	0.219	0.215
P_3	0	0.047	0.031	0.026
P_4	0	0.004	0	0

The four-electron probability is identically zero for Γ_3 symmetry, as the states containing terms with electrons in each of the four orbitals of one site must be of $^1\Gamma_3$ or $^1\Gamma_4$ symmetries. The Coulomb repulsion G favors the many-body states being more extended, and thus the decrease of P_0, P_2 and P_3 in favor of that of P_1 is not surprising.

C. Thermodynamic behavior

In order to compensate partially for the small size of the cluster, thermal properties of the system were investigated via a grand canonical ensemble, wherein four-electron states are allowed to come to equilibrium with three- and five-electron states. Having set the average occupancy, $\langle N \rangle$, to four electrons, a straightfoward analysis[17] would show the chemical potential μ to obey:

$$\lambda = e^{\beta \mu} = \sqrt{Z_3 / Z_5} \qquad (4.11)$$

where Z_N is the canonical partition function for N electrons.

The behavior for a typical set of parameters is shown in Figure 5. There are three characteristic temperatures that appear, all arising from transitions that have analogs in atomic physics: configuration, inter-cluster (charge transfer) and term fluctuations.

The highest characteristic temperature, T_E, at about 0.3 eV, is caused by a configuration fluctuation and is a purely one-electron effect. It corresponds to the energy required to excite an electron to the next highest one-electron orbital. As this energy is usually sizeable (see Figure 1), T_E is accordingly large.

At $T_{CF} \approx 2 \times 10^{-3} eV$, there is a rise in the charge fluctuation, $\langle N^2 \rangle - \langle N \rangle^2$, due to many-body effects. It corresponds to the energy to transfer an electron from one tetrahedral-cluster to another[18]. This can be seen from the following argument. The thermodynamic weighting or probability of three and five electrons can be shown to satisfy:

$$p(3) = p(5) = \frac{1}{2}(\langle N^2 \rangle - \langle N \rangle^2) = 1/(2 + \frac{Z_4}{\sqrt{Z_3 Z_5}}) \qquad (4.12)$$

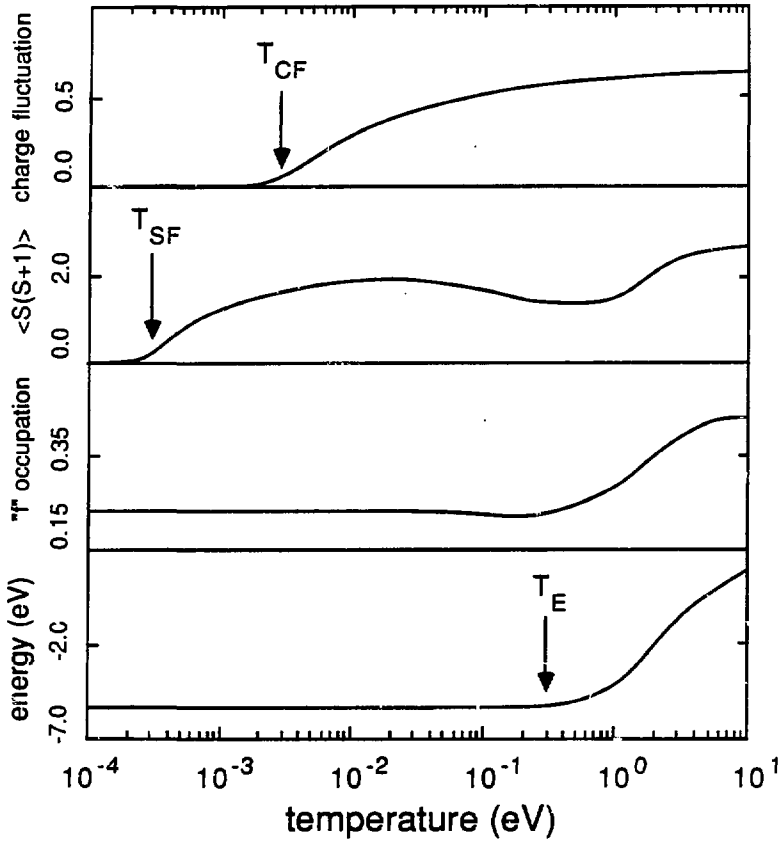

FIG. 5 Grand canonical ensemble average as a function of temperature for: the internal energy; the *f*-occupancy; the mean spin-squared per cluster, $S(S+1)$; and the mean charge fluctuation, $\langle N^2 \rangle - \langle N \rangle^2$. The parameter values are: $t = 1\ eV$, $E_0 = 0.75\ eV$, $v = 0.5\ eV$, $U = 25\ eV$, $G = 1\ eV$. The characteristic fluctuation temperatures, T_E, T_{SF} and T_{CF} are indicated.

The rise is fully consistent with leading term behavior $e^{-\beta T_{CF}}$, where $T_{CF} \approx 1/2\,(\varepsilon_3^0 + \varepsilon_5^0) - \varepsilon_4^0$, and ε_N^0 is the N-electron ground-state energy. In the non-interacting one-electron picture, one should expect T_{CF} to be identically zero, as the four-electron case would truly be an average of the three and the five. The intra-site electron-electron Coulomb repulsions, therefore, cause significant, albeit small, alterations to the ground-state energies.

The lowest temperature rise, $T_{SF} \approx 2\text{x}10^{-4}\ eV$, occurs in the expectation value of the spin squared, $S(S+1)$, for four electrons. It is also a many-body effect, its low temperature caused by the presence a very low-lying excited state, of symmetry $^3\Gamma_5$, relative to the $^1\Gamma_4$ ground state. This close concordance occurs over a wide range in parameter space. It is thus a term fluctuation, the phase space being large enough for four electrons to accomodate the spin-flip without adding a large intra-atomic Coulomb energy from (2.5).

Another question is whether this model can, in any way, address the question of the α to γ-cerium phase transition[8]. As this transition involves a change in lattice constant, from 4.85 Å to 5.16 Å, respectively, one might expect that, as a consequence of the transition, the hybridization, v, might decrease effectively, with a much less marked decrease in t. This is because the overlap between two c-states making up the extended conduction states should be less sensitive to the increased separation than that between a c-state and a more localized f-state. That being the case, then from Figure 2, one can see the parameter values proposed in Section 4.1 are justified. In that parameter region, n_f increases with decreased v, while elsewhere it decreases. It must be stressed that this is not, in any way, being proposed as a mechanism for the transition, but rather a consequence of it.

D. Photoemission and Inverse-Photoemission results

Photoemission (inverse-photoemission) spectra were calculated by the instantaneous removal (addition) of an electron from (to) the four-electron ground state, with the

distribution among the three-electron (five-electron) states then analyzed. These processes involve destruction (creation) operators with the one-electron symmetries $^2\Gamma_1$ and $^2\Gamma_4$. With a four-electron ground state of symmetry $^1\Gamma_3$, group theory predicts that the only possible accessible states, for both three and five electrons, must have symmetries $^2\Gamma_3$, $^2\Gamma_4$, and $^2\Gamma_5$. Examples of the calculated spectra are found in Figures 6 and 7.

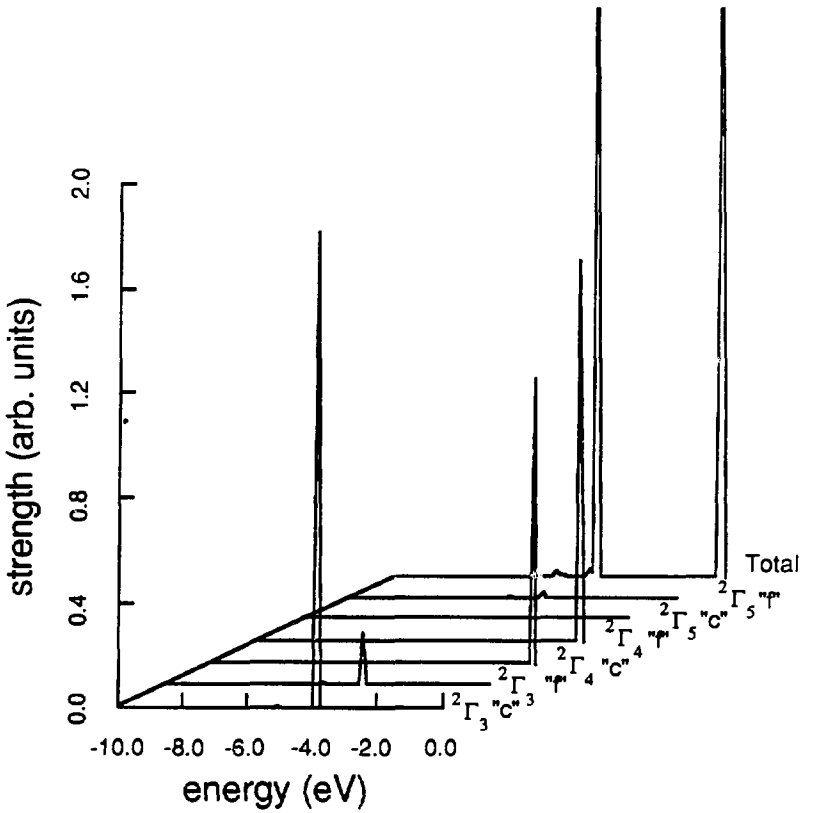

FIG. 6 Spectrally-resolved photoemission distribution, shown for: $t = 1$ *eV*, $E_0 = 0.75$ *eV*, $v = 0.5$ *eV*, $U = 25$ *eV*, $G = 1$ *eV*. For each spectrum the symmetry and band ("*c*" = conduction and "*f*" for *f*-state) of the emitted electron is shown.

An examination of the photoemission and inverse-photoemission results show clear twin-peaked distributions. They are, in some way, reminiscent of the broad two-peaked distribution of real cerium, although they arise for different physical reasons. The

calculated inverse-photoemission spectrum also has a moderately-sized peak, of energy U greater than the other two.

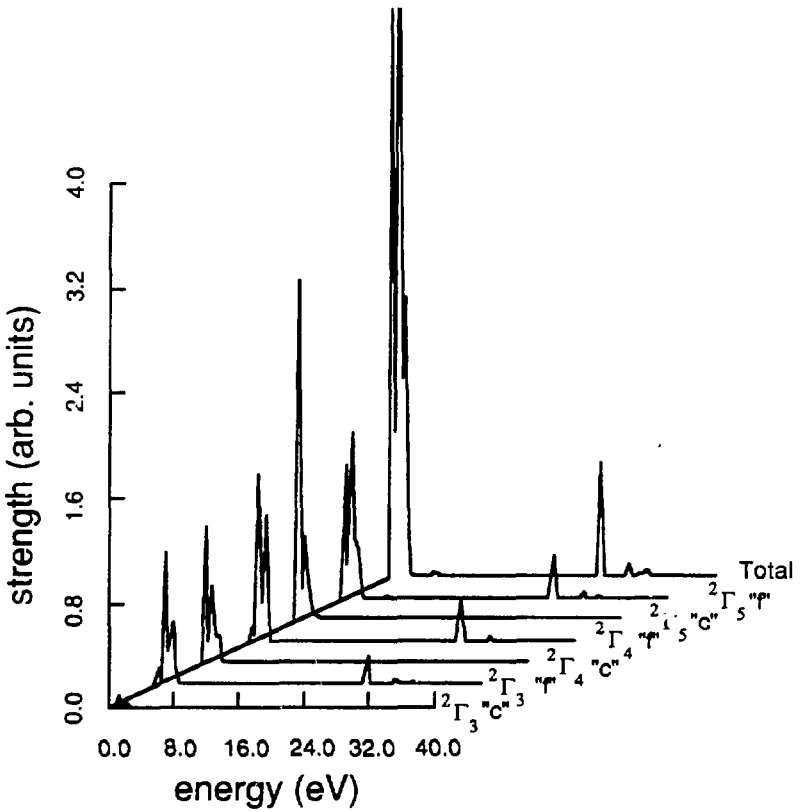

FIG. 7 Spectrally-resolved inverse photoemission distribution for: $t = 1\ eV$, $E_0 = 0.75\ eV$, $v = 0.5\ eV$, $U = 25\ eV$, $G = 1\ eV$. For each spectrum the symmetry and band ("c" = conduction and "f" for f-state) of the absorbed electron is shown. To be noted is the minor peak, of energy U greater than the other two, corresponding to double f-occupancy.

Thus, except for this latter peak being displaced relative to the other two by the f - f

Coulomb repulsion, both distributions are dominated by one-electron effects. The picture, neglecting hybridization, is one of transitions to either a given *f*- or conduction state. It is still very much in evidence with the hybridization, and even the many-body repulsion terms, added. The point to note, however, is that if the distribution is resolved spectrally into the *f* and conduction electron contributions, a clear dependence on the hybridization is seen. With increasing *G*, the height of the second peak decreases, as subsidiary peaks gain in strength. The varying peak composition is presented in Figures 8 and 9.

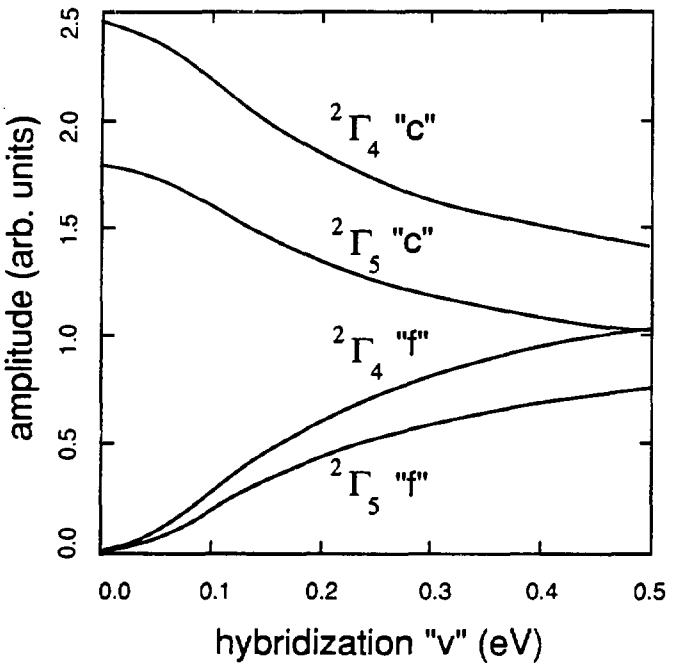

FIG. 8 Spectral composition of the second peak in the inverse-photoemission, as a function of the hybridization *v*, symmetries $^2\Gamma_4$ and $^2\Gamma_5$ (accidentally degenerate) contributing. Here $t = 1$ *eV*, $E_0 = 0.75$ *eV*, $U = 25$ *eV*, $G = 0$ *eV*.

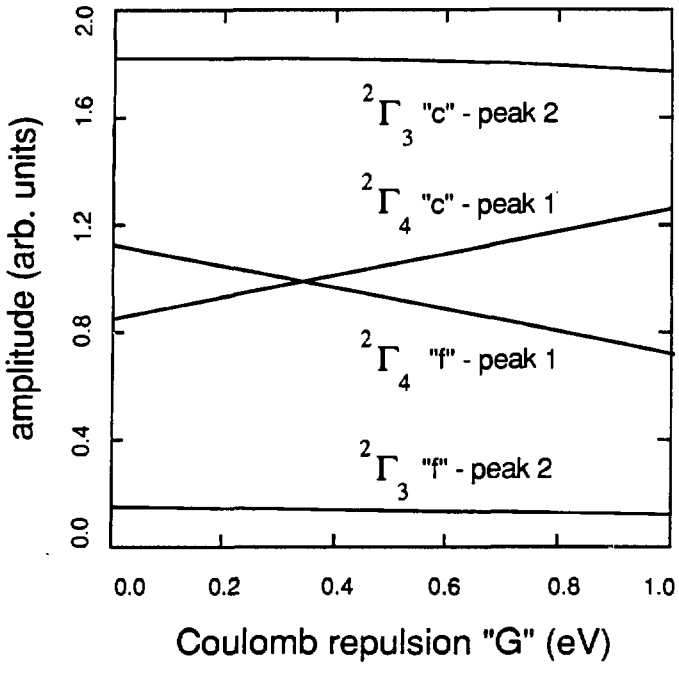

FIG. 9 Spectral composition of both peaks in the photoemission, as a function of the on-site Coulomb repulsion G. Here $t = 1\ eV$, $E_0 = 0.75\ eV$, $v = 0.5\ eV$, $U = 25\ eV$.

V. Conclusions

A model for intermediate valence has been examined, which although too simple to mimic cerium, exhibits many interesting properties in its own right. It shows low-temperature spin and charge fluctuations, which reveal much about the phase space and many-body aspects of the model. The spin fluctuations point to very-low-temperature magnetic behavior, while the charge fluctuations suggest an intermediate-valence system bordering on heavy-fermionic; in other words, the *f*-electrons participate in conduction at modest temperatures. The model also suggests that experimental work should be implemented in intermediate-valence solids to analyze spectrally the photoemission processes, which would reveal the nature of the hybridization and the electron-electron

repulsion contributions.

Although the importance[19] of incorporating an on-site c - f Coulomb repulsion (2.6) in representing real systems has been discussed, it appears that for this mode the addition is not crucial, in view of the evidence from the valence, thermodynamic and photoemission properties.

An extension of this model to represent more accurately metallic cerium obviously suggests itself. Although not suspected as being a relevant improvement alone by the author, the inclusion of seven f-orbitals presents daunting problems. Such action brings the number of one-electron states to consider up to 64 which, which for the four electron problem, offers 64!/60!4! = 635,376 combinations. These states would be either even or odd under inversion, thus bringing in the full set of twenty representations of the space group, rather than the present five.

Of considerably more importance is the broadening of the conduction states into a continuous band[20] responsible for transport effects. This non-negligible feature is not compatible with a small-cluster approach.

VI. References

[1] *Valence Instabilities and Related Narrow-Band Phenomena*, edited by R.D. Parks (Plenum, New York, 1977).

[2] *Valence Fluctuations in Solids*, edited by L.M. Falicov, W. Hanke and M.B. Maple (North Holland, Amsterdam, 1981).

[3] *Valence Instabilities*, edited by P. Wachter and H. Boppart (North Holland, Amsterdam, 1982).

[4] P.W. Anderson, Phys. Rev. **124** , 41 (1961).

[5] S.H. Liu and K.M. Ho, Phys. Rev. B. **28** , 4220 (1983).

[6] O. Gunnarsson and K. Schönhammer, Phys. Rev. Lett. **50** , 604 (1983).

[7] M.R. Norman, D.D. Koelling, A.J. Freeman, H.J.F. Jansen, B.I. Min, T. Oguchi, and L. Ye, Phys. Rev. Lett. **17** , 1673 (1984).

[8]R. Ramirez and L.M. Falicov, Phys. Rev. B. **3** , 2425 (1971).

[9]R.H. Victora and L.M. Falicov, Phys. Rev. Lett. **55** , 1140 (1985).

[10]J.C. Parlebas, R.H. Victora and L.M. Falicov, J. Phys. (Paris) **47**, 1029, (1986) .

[11]L.P. Bouckaert, R. Smoluchowski and E. Wigner, Phys. Rev. **50** , 58 (1936).

[12]S. Hüfner, Z. Phys. B., **58** , 1 (1984).

[13]T.-h. Lin and L.M. Falicov, Phys. Rev. B. **22** , 857 (1980).

[14]J.W. Allen, S.-J. Oh and I. Lindaw, M.B. Maple and J.F. Suassuna, S.B. Hagstrom, Phys. Rev. B. **26** , 445 (1982).

[15]U. Kornstädt, R. Lässer and B. Lengeler, Phys. Rev. B. **21** , 1898 (1980).

[16]M. Croft, J.H. Weaver, D.J. Peterman and A. Franciosi, Phys. Rev. Lett. **46**, 1104 (1981).

[17]C. Kittel, *Thermal Physics* (Wiley, New York, 1969), p.315

[18]It should be emphasized that charge fluctuations were calculated in the thermodynamic sense, and no inter-cluster or inter-atomic Coulomb forces were included. Inclusion of Coulomb terms may make the fluctuations even more easily accessible.

[19]S.H. Liu, private communication

[20]See for example, P.S. Riseborough, Sol. State Commun. **8** , 721 (1986).

Chapter III. Many-Body Tetrahedral-Cluster Model for Binary and Ternary Alloys

I. Introduction

As viewed from the perspective of the constituent elements, the alloy phase diagrams of copper, silver, and gold should be very simple and straightforward. These elements are, after all,[1-5] simple *s* band monovalent metals, with a full *d* band (configuration $(vd)^{10}$ $[(v+1)\,s]^1$), crystallize all in the fcc structure and have topologically identical and quantitatively very similar Fermi surfaces. The question is then, how is it that the alloying behavior between these three metals are completely different: copper-silver alloys show an almost complete tendency to segregate, silver-gold alloys form an almost perfect solid solution throughout the concentration range, whereas gold-copper alloys form intermetallic compounds with only specific ratios – corresponding to the formulas Au_3Cu, AuCu, and $AuCu_3$. Different approaches to study this problem have been taken,[6,7] most notably calculations by the cluster-variation method,[8,9] the cluster-Bethe-lattice[10-12] and local-density-approximation (LDA) methods,[13] but all these methods have their drawbacks. While cluster expansion methods are able to account well for the configurational entropy, they fail to take account of the actual band structure, and while the LDA is much better for electronic calculations, it is only good for ground-state properties. The approach taken here is to obtain exact solutions of a limited-size crystal with all many-body interactions, or equivalently, to solve exactly a many-body problem with limited sampling in **k** space.

The small crystal approach has been used successfully to solve the Hubbard model[14-16], to explain photoemission and thermodynamic properties[17,18] in nickel and iron, and to get insight into the intermediate-valence behavior[19,20] of cerium. It has proved to be very good at determining uniform and short-range properties in crystals. In the

context of alloying, it is felt that the method should also prove useful and informative. Random groupings of atoms do not have long-range order and, because of the short-range order character of the interatomic interactions, a given atom only interacts with a local environment of the surrounding atoms. This is precisely the setting for a small cluster approximation. Thus, one might see the trends of order-disorder transition, though not the actual abrupt changes of phase caused by the long-range-order correlations.

II. The Hamiltonian

The tetrahedral cluster used here has periodic boundary conditions and four sites labeled i=1,2,3,4. There is one s orbital per site, each being either spin up or down, denoted with subscript σ. The creation (destruction) operator is written as $c^{\dagger}_{i\sigma}$ ($c_{i\sigma}$). The Hamiltonian, essentially based on the Hubbard model,[14] is composed of three parts:

$$H = H_{band} + H_{occ} + H_{many} , \qquad (2.1)$$

where

$$H_{band} = -\sum_{\substack{i,j;\sigma \\ i \neq j}} t_{ij} c^{\dagger}_{i\sigma} c_{j\sigma} , \qquad (2.2)$$

$$H_{occ} = \sum_{i;\sigma} E_i c^{\dagger}_{i\sigma} c_{i\sigma} , \qquad (2.3)$$

$$H_{many} = \sum_{i} U_i c^{\dagger}_{i\uparrow} c_{i\uparrow} c^{\dagger}_{i\downarrow} c_{i\downarrow} . \qquad (2.4)$$

These terms are :

(a) a band "hopping" interaction (2.2) between conduction states on adjacent sites, with transfer integral t_{ij}, equal to t_{AA} if both sites i and j are atoms of type A and t_{AB} if one is of type A and the other B;

(b) an "occupation" energy (2.3) for the i-th atom, whose strength E_i is measured as an offset between unlike atoms, equal to E_A for atom A, E_B for atom B;

(c) an on-site (intra-atomic) Coulomb repulsion (2.4) for site i, with $U_i > 0$, which takes value U_A, or U_B, etc., depending on the type of atom.

It is a common, well established and good approximation[12] to assume that the hybrid hopping element t_{AB} is

$$t_{AB} = \sqrt{t_{AA}\, t_{BB}} \qquad (2.5)$$

i.e. the hopping parameter for two different atoms is the geometric mean of the two identical-atom hopping elements. It follows straightforwardly from many physical models and can be seen to be, loosely, the result of the overlap of the exponential tails of the two wave functions. The decay constants average arithmetically and thus the total overlap averages geometrically. This approximation is independent of the size of the atoms and of the spatial extent of the wave functions.

By means of a virial-type argument, the t_{ij}'s being considered as a measure of the electron kinetic energy, and the U_i's as a potential energy, one establishes a proportionality between them:

$$U_i = f\, t_{ii} \qquad (2.6)$$

where f is a scaling factor, of the same order of magnitude as that employed by Robbins and Falicov.[12] The required magnitude of f implies a many-body interaction too strong to be handled perturbatively. The large value is necessary to keep charge fluctuations within the cluster realistically small, yet it must not be so large, in comparison to the bandwidth, to produce metal-insulator transitions, ferromagnetic and antiferromagnetic behavior, and other broken-symmetry effects.

A simple assumption of setting a constant, species-independent U was soon dismissed, because it does not produce the wide range of alloying behavior encountered in nature. A possible consideration of setting the Coulomb repulsion inversely proportional to the atomic size was also abandoned based on the author's previous experience.

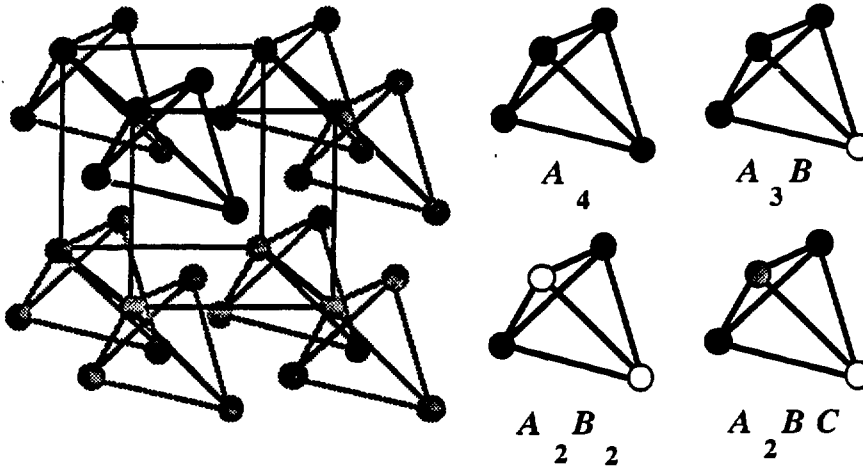

FIG. 1. The tetrahedral-cluster method as employed in the context of alloying. There are, topologically, four different types of clusters, repeated indefinitely throughout the crystal by periodic boundary conditions : A_4, the pure metal; the binary intermediates A_3B and A_2B_2 ; and the ternary intermediate A_2BC.

For a binary alloy A-B in the tetrahedral-cluster approximation the following five compounds must be considered: A_4, A_3B, A_2B_2, AB_3, and B_4. In this case, the Hamiltonian (2.1)–(2.4) has only two relevant parameters, θ and ε, defined by

$$\theta = \sqrt{t_{AA} / t_{BB}} \qquad (2.7)$$

and

$$\varepsilon = (E_A - E_B) / 8 t_{AB} . \qquad (2.8)$$

It should be noted that the substitution $\theta \rightarrow 1/\theta$, $\varepsilon \rightarrow -\varepsilon$, is equivalent to interchanging A and B. For ternary alloys, there are 15 compositions, the five above plus A_3C, A_2BC, A_2C_2, AB_2C, ABC_2, AC_3, B_3C, B_2C_2, BC_3, and finally, C_4 (see Fig. 1). There are also, as discussed below, four independent Hamiltonian parameters.

III. Method of Calculation

The Hamiltonian presented above (2.1)-(2.4), for the four-atom cluster is computationally very simple. With eight orbitals, the number of many-body states for N electrons is $8!\,/\,(8\text{-}N)!\,N!$, which in the case of four electrons (one per site) results in 70 states which separate, according to spin, into 1 quintuplet, 15 triplets, and 20 singlets, regardless of atomic composition.

With the many-body repulsion (2.4) neglected, the remaining one-electron terms can be diagonalized analytically. For A_4, the one-electron energies break up into a singlet of energy

$$E_1(A_4) = E_A - 12t_{AA}, \tag{3.1}$$

and a triplet

$$E_3(A_4) = E_A + 4t_{AA}, \tag{3.2}$$

The bandwidth in this model is therefore $16t_{ii}$ for the pure metals. Furthermore, it should be noted that the A_4 cluster can be solved analytically, with the many-body terms included, by judicious use of group theory.[15] For A_3B, the four one-electron states are a doublet with energy (3.2), and two singlets:

$$E_{1\pm}(A_3B) = \frac{1}{2}(E_A + E_B) - 4t_{AA} \pm \frac{1}{2}\sqrt{(E_A - E_B - 8t_{AA})^2 + 192t_{AA}t_{BB}} \tag{3.3}$$

For A_2B_2, there are four singlets: one with energy (3.2), one (its mirror image) with B replaced by A throughout, and two additional ones with energies:

$$E_{1\pm}(A_2B_2) = \frac{1}{2}(E_A + E_B) - 2(t_{AA} + t_{BB}) \pm \frac{1}{2}\sqrt{(E_A - E_B + 4t_{BB} - 4t_{AA})^2 + 256t_{AA}t_{BB}} \tag{3.4}$$

Finally, for the ternary compound A_2BC there remains a singlet of energy (3.2), plus three

singlets which are the solutions of the cubic equation:

$$E^3 + [\,16t_{AA} - (E_A + E_B + E_C)]E^2 +$$

$$[E_A E_B + E_B E_C + E_C E_A - 4t_{AA}(E_B + E_C) - 32(t_{AA} t_{BB} + \frac{1}{2} t_{BB} t_{CC} + t_{CC} t_{AA})]E$$

$$+ 32(t_{AA} t_{BB} E_C + \frac{1}{2} t_{BB} t_{CC} E_A + t_{CC} t_{AA} E_B)$$

$$+ 192 t_{AA} t_{BB} t_{CC} + 4t_{AA} E_B E_C - E_A E_B E_C = 0. \qquad (3.5)$$

IV. RESULTS

In a θ–ε plane (Figs. 3 and 4), one can establish triplets of points, one each corresponding to the binary alloys A-B, B-C and C-A, subject to the straightforward constraints :

$$\theta_{AB}\ \theta_{BC}\ \theta_{CA} = 1 \qquad (4.1)$$

and

$$\varepsilon_{AB}\left[\frac{\theta_{BC}}{\theta_{CA}}\right]^{1/3} + \varepsilon_{BC}\left[\frac{\theta_{CA}}{\theta_{AB}}\right]^{1/3} + \varepsilon_{CA}\left[\frac{\theta_{AB}}{\theta_{BC}}\right]^{1/3} = 0. \qquad (4.2)$$

Ideally, one would want to be able to input appropriate parameters, either obtained from first-principles band-structure calculations or experimentally derived. In other words, one could take the known bandwidth and ionization energy, say, and associate them with the relevant parameters θ and ε.

Thus, the approach taken here is to determine whether triplets of binaries can exist with the properties of the copper, silver and gold systems.

A. Zero-temperature results – compound stability

The first property that was investigated was the zero-temperature segregation-solubility tendencies. In deciding on the stability of a particular compound at zero temperature, one

must consider all possible decompositions into other compounds which yield the same global concentrations. The lowest-energy decomposition will be the one selected by nature – this is just a restatement of the fact that the free-energy curves as functions of any parameter, e.g. composition, must have non-negative curvature everywhere.

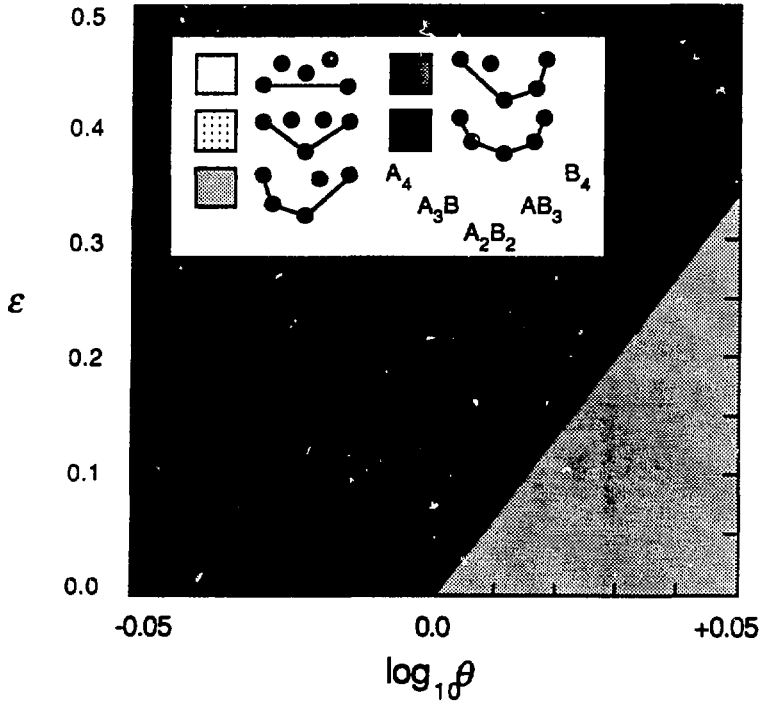

FIG. 2. The independent-electron picture of binary-alloy formation. For modest bandwidth ratios and occupation offsets only three possibilities appear: the fully concave phase (speckled region), the phase with A_3B absent (cross-hatched region), and the phase with AB_3 absent (striped region).

For binary alloys, only the ground-state energies of all five compounds $A_{4-n}B_n$, n = 0,1,2,3,4, are necessary to determine the stability at zero temperature. One must, of course, have the pure metals appearing with 100% probability at the concentration end points, so it is a matter of deciding on the stability of the intermediate compounds at all

other concentrations. It turns out that there are eight different topological possibilities. The first case is that in which no intermediates appear, i.e. there is complete segregation, as in copper-silver alloys. There are three cases of only one intermediate appearing, and three of all but one appearing. Finally, there is the case – here called the fully concave solution – where the three intermetallic intermediate compounds are stable. This is the case for both the complete solid solution, as in silver-gold alloys, and the three truly stable intermetallic compounds – Cu_3Au, CuAu, $CuAu_3$ – of copper-gold. Five of the eight cases – those that occur at reasonable values of the parameters – are illustrated in the inset of Fig. 2.

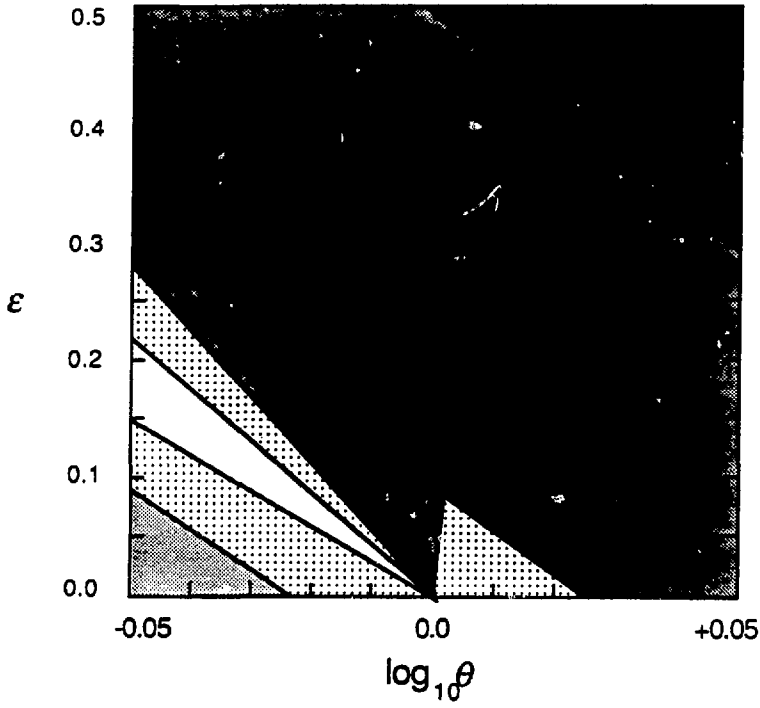

FIG. 3. A many-body picture of binary-alloy formation, Coulomb factor $f = 5.0$. Here, a segregating phase (white region) has opened, bordered by a phase of A_2B_2 stability (thick striped region), and situated amazingly close to a triangular-shaped phase region of fully concave alloys, demonstrating the extreme sensitivity of alloy behavior to one-electron parameters. (For a full explanation of the various shadings, see inset in Fig. 2.)

As mentioned previously, one can reduce the specification of a binary alloy to two parameters, the bandwidth ratio θ and occupancy-energy offset ε, keeping the Coulomb factor f fixed. Three plots of stabiliity regions in the θ–ε plane are presented for various f, i.e. f = 0.0 (the independent-electron picture), 5.0, and 6.0 (in Figs. 2, 3, and 4, respectively).

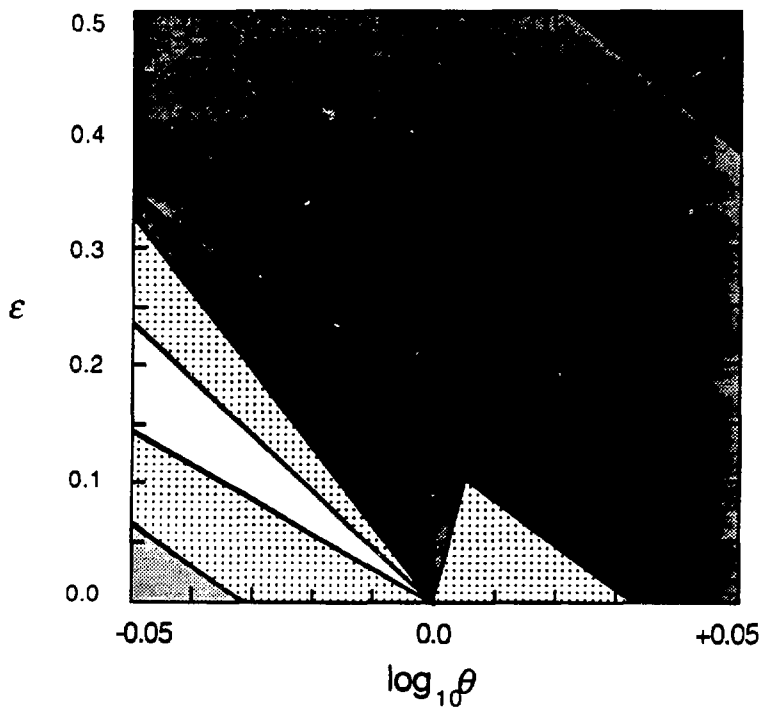

FIG. 4. A many-body picture of binary-alloy formation, Coulomb factor f = 6.0 . Here, the segregating phase is more stable and the fully concave region lying nearby has increased in size. (For a full explanation of the various shadings, see inset in Fig. 2.)

What is most evident from the independent-electron picture (Fig. 2) is its simplicity and lack of structure. Only three of the eight stability regions appear, and none of them is

the fully segregated case. What happens when the Coulomb repulsion is turned on, however, is that a wedge appears between two of the regions, opening up, literally, a solubility gap (Figs. 3 and 4). In addition, a triangular island of fully concave alloys is created, in close proximity to the fully segregated alloys. That leads to the most important conclusion of this work : *when realistic many-body effects are taken into account small changes in the one-electron parameters cause enormous changes in alloying behavior.*

In ternary alloys, the degrees of freedom are many more, with scenarios where the ternary intermediates A_2BC, AB_2C, and ABC_2 may or may not participate. Determining this generalized global stability is a simple problem in linear programming, and it results in the separation of the ternary concentration graph into triangular regions. Within each triangle, a point determining the nominal concentration of the alloy yields a decomposition into three phases with concentrations corresponding to the corners of the triangle and with relative abundance inversely proportional to the distance between the point of nominal concentration and the relevant corner of the triangle.

B. Thermodynamic behavior

With the entire multiple composition, many-body energy spectrum determined, it is straightforward to predict thermodynamic behavior for this model by carrying out the appropriate Boltzmann statistics. With three types of atoms, A, B, and C, there are three corresponding atomic chemical potentials, μ_A , μ_B, μ_C, but as the number of atoms in the cluster is fixed at four, that leaves the potentials overdetermined; thus, one introduces relative potentials:

$$\mu_1 = \mu_A - \mu_B , \quad \mu_2 = \mu_B - \mu_C , \qquad (4.3)$$

and the Gibb's sum, from which all thermodynamic behavior is derived, is defined simply as[21]

$$G = \sum_{\substack{j,k \\ 0 \le j+k \le 4}} e^{\beta (j \mu_1 + k \mu_2)} Z_{jk}(\beta), \qquad (4.4)$$

where β is the inverse temperature, and $Z_{jk}(\beta)$ is the canonical partition of the cluster with j atoms A, k atoms B (and 4-j-k atoms C.)

For a given temperature and concentration, the probability of finding a given cluster j k is given by

$$P_{jk} = e^{\beta (j \mu_1 + k \mu_2)} Z_{jk}(\beta)/G \qquad (4.5)$$

whereas the chemical potentials are determined so that

$$x = \frac{1}{4} \sum_{\substack{j,k \\ 0 \le j+k \le 4}} j P_{jk} \qquad (4.6)$$

and

$$y = \frac{1}{4} \sum_{\substack{j,k \\ 0 \le j+k \le 4}} k P_{jk} \qquad (4.7)$$

where x is the concentration of A, y is the concentration of B (and z = 1-x-y is the concentration of C).

In the infinite-temperature limit, the partition functions tend to the multiplicities of each cluster, which is 4!/j!k! (4-j-k)!, with a resulting trinomial probability distribution of

$$P_{jk}(x,y) = \frac{4!}{j!\,k!\,(4-j-k)!} x^j y^k (1-x-y)^{4-j-k} \qquad (4.8)$$

In the zero-temperature case the problem reduces, as mentioned above, to finding the minimum of a linear function (the weighted energies) on the surface of a polyhedron – formed by connecting the ground-state energy of every one of the 15 clusters to that of every other one. This construction results in phases represented by triangular planar sections, in which a system at a given concentration, (x,y), has the properties of the

weighted average of the sectional end points.

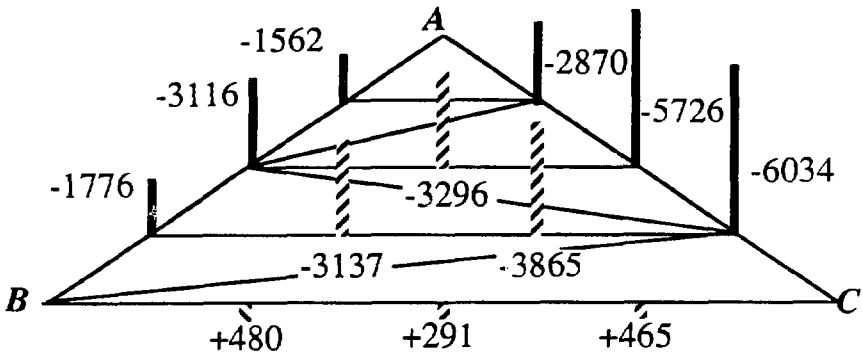

FIG. 6. Graphical representation of the ground-state energies and the zero-temperature triangular segregational regions for the set of parameters labeled 2 in Table I. Energies are in units of $t = (t_{AA}t_{BB}t_{CC})^{1/3}\times 10^{-6}$. The energies represented by stripes do not yield stable configurations at $T = 0$.

Three cases have been selected for the purpose of illustration. The corresponding parameters are displayed in Table I. The first case – labeled number 1 in the Table I and presented in Fig. 5 – demonstrates the extreme behaviors very well. In this situation there exists, for the given set of parameters and in a range of temperatures [$k_BT = 0.0016 (t_{AA}t_{BB}t_{CC})^{1/3}$ in Fig. 5], one binary alloy possessing an intermediate, ordered state (Fig. 5, *C–A*), one rapidly approaching the infinite temperature binomial distribution (Fig. 5, *A-B*), and one almost completely segregated into the pure metals (Fig.5, *B–C*).

TABLE I. The input parameters for the three cases considered.

	θ_{AB}	θ_{BC}	θ_{CA}	ε_{AB}	ε_{BC}	ε_{CA}	f
1	1.000	0.938	1.066	0.025	0.125	-0.148	6.0
2	0.944	0.915	1.099	0.095	0.160	-0.248	5.0
3	1.039	0.929	1.036	-0.217	0.100	0.105	6.0

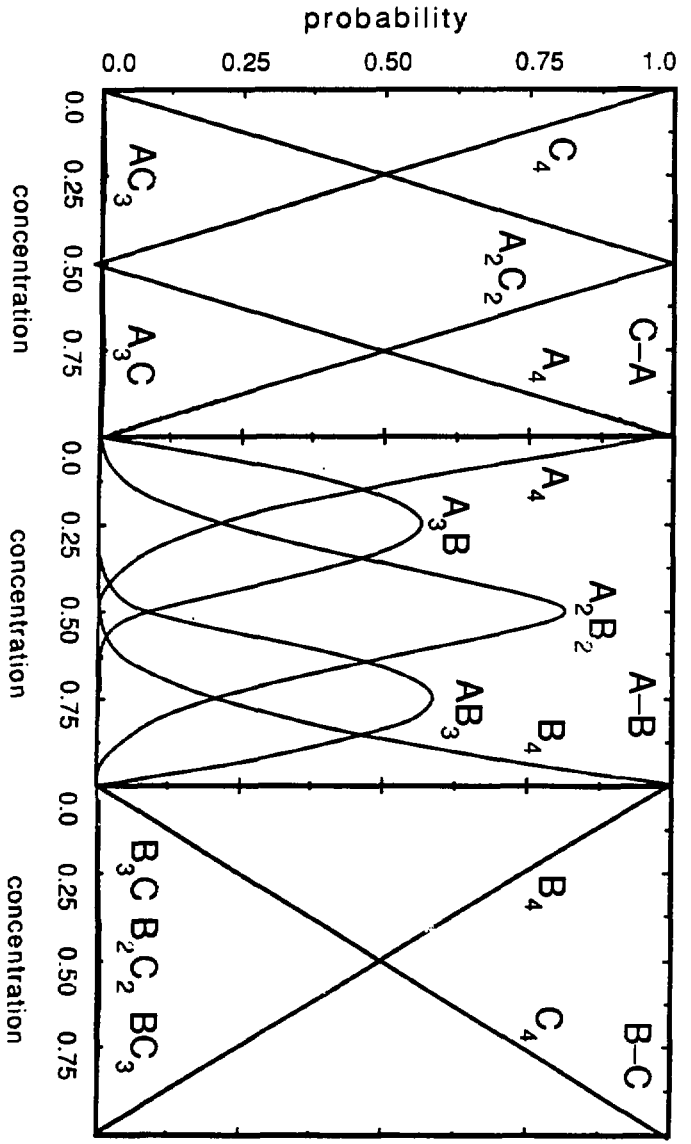

FIG. 5. An example of a ternary-alloy system in which the three binary pairs are such that one has a fully ordered A_2C_2 phase (C–A), another exhibits almost complete random solid solution (A–B), and the third almost completely segregates (B–C). The parameters for this case correspond to those labeled 1 in Table I at a temperature $k_BT = 0.0016\ (t_{AA}t_{BB}t_{CC})^{1/3}$.

For this temperature range one could say that C-A forms the CA intermetallic compound, A–B forms a complete range of solid solutions, and B-C completely segregates into its constituent elements.

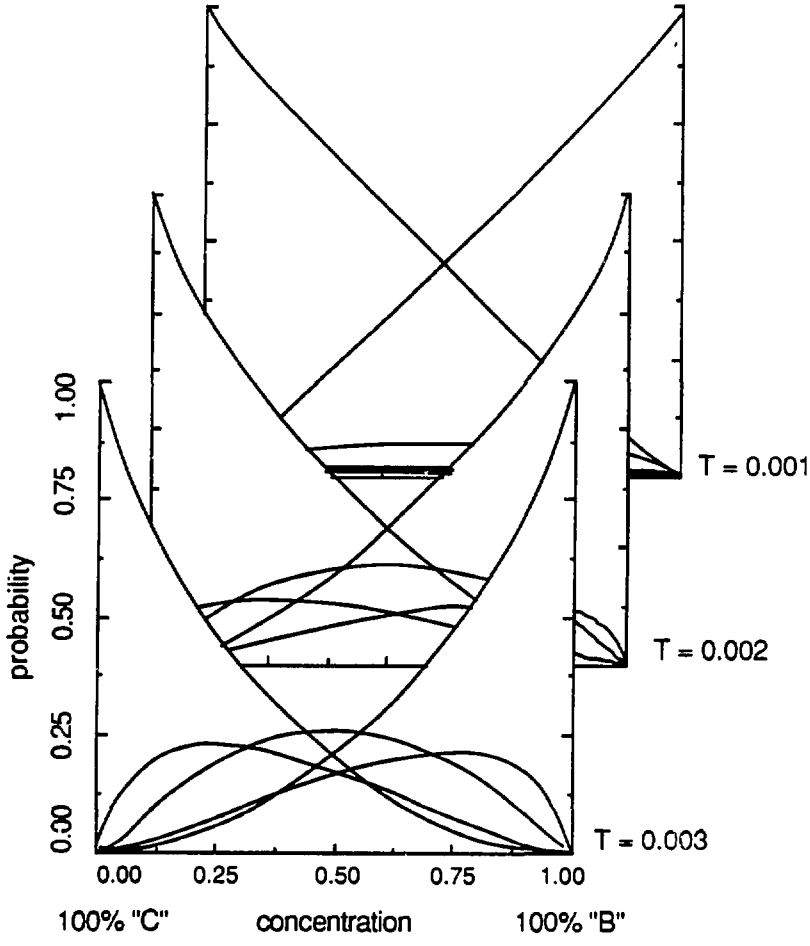

FIG. 7. Depiction of the desegregation of the B–C alloy with temperature, for the sets of parameters labeled 2 in Table I. Energies and temperatures are in units of $t = (t_{AA}t_{BB}t_{CC})^{1/3}$.

The second case, its ground-state energies, and the triangular phase regions are

presented in Fig.6. One can see that two edges, A-B and C-A, have fully concave profiles (the latter has for all compounds larger heats of formation) while the third, B-C has unstable intermediates, i.e. all intermediates have positive energies relative to segregation of the pure metals. Also, the fully intermediate ternaries, A_2BC, AB_2C, and ABC_2 are all unstable.

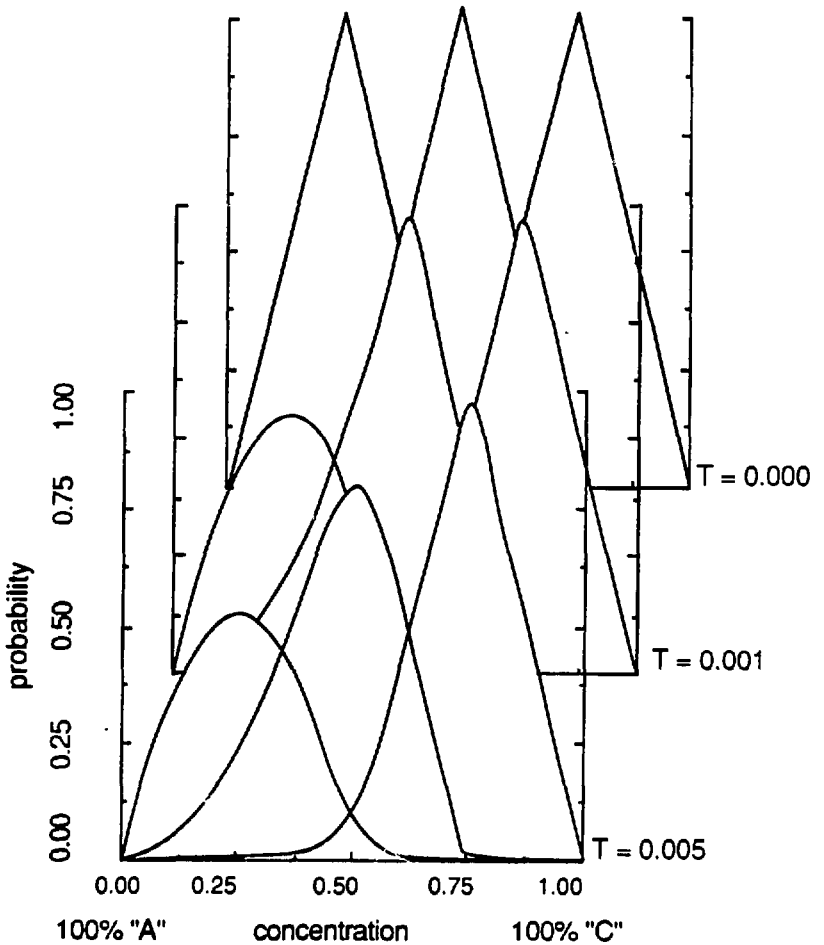

FIG. 8. Depiction of the robustness of the ordering of the intermediate compounds of the C–A alloy for the sets of parameters labeled 2 in Table I. Energies and temperatures are in units of $t = (t_{AA}t_{BB}t_{CC})^{1/3}$.

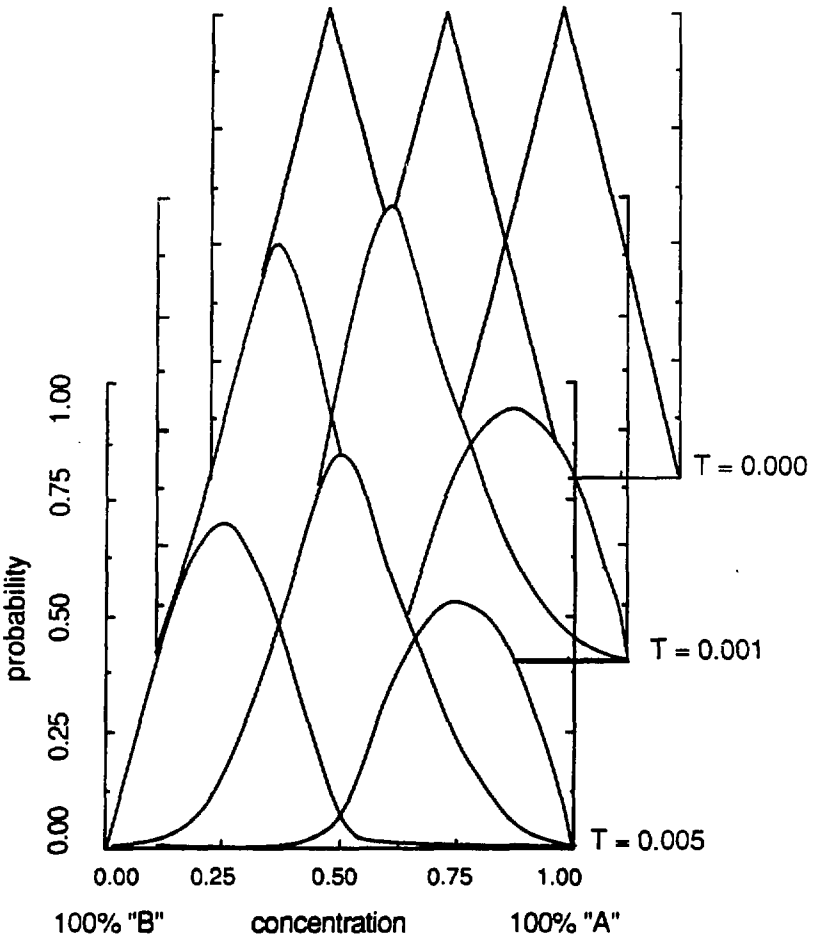

FIG. 9. Depiction of the trend towards randomization of the intermediate compounds of the *A–B* alloy for the sets of parameters labeled 2 in Table I. Energies and temperatures are in units of $t = (t_{AA}t_{BB}t_{CC})^{1/3}$.

This choice of parameters yield properties demonstrated in Figs. 7, 8, and 9. In Fig. 7, one sees the solubility gap of the *B-C* alloy shrinking and vanishing with increasing temperature.

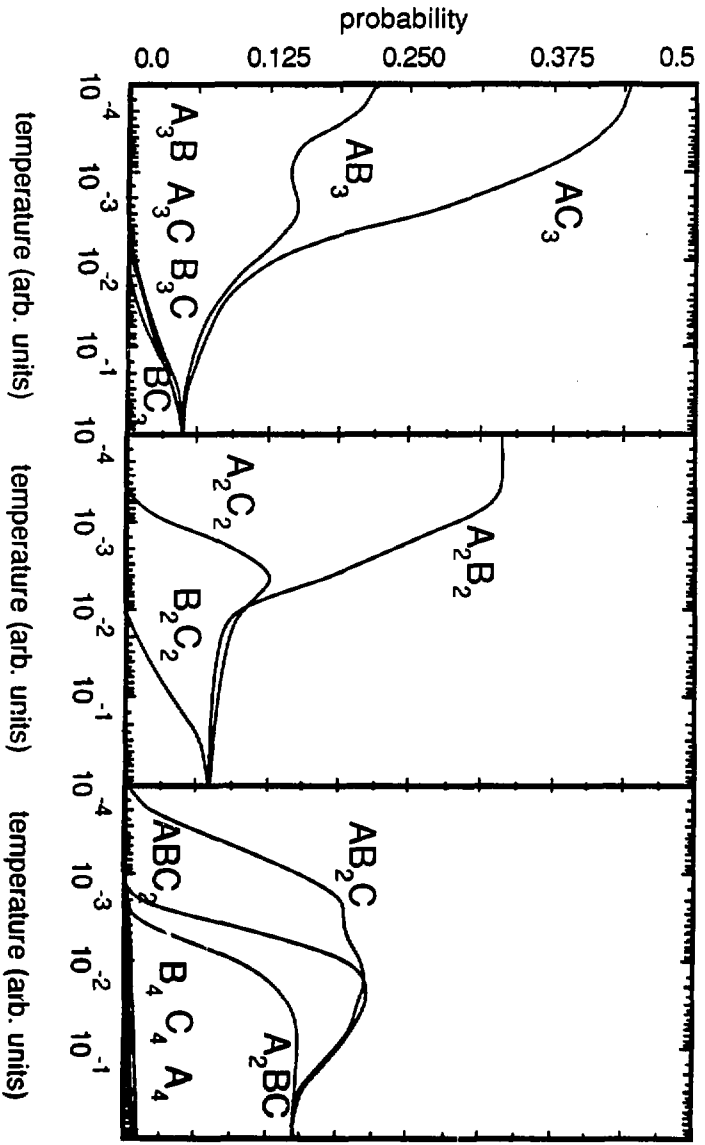

FIG. 13. Representation of all 15 cluster probabilities in the formation of the 1/3 : 1/3 : 1/3 ternary alloy for the sets of parameters labeled 2 in Table I. Energies and temperatures are in units of $t = (t_{AA}t_{BB}t_{CC})^{1/3}$.

In Figs. 8 and 9, one sees fully ordered structures in both C-A and A-B atzero temperature, and both begin to approach random configurations with increasing temperature, the C-A alloy – because of its larger heats of formation – doing so more slowly.

The implications for the full ternary alloy (1/3 : 1/3 : 1/3) are presented if Fig. 10. As one can see, the zero-temperature probabilities are divided among the three compounds AC_3, AB_3, and A_2B_2 in the ratio 4:2:3, respectively. A very low temperature rise in AB_2C is noted, and is attributed to it being only marginally unstable at $T = 0$. The other compounds experience rises in probability distributed over almost two decades of temperature.

The final case, number 3 of Table I, follows Robbins and Falicov[12] in taking the θ's as the tabulated bandwidth ratios[1,2] and fits the ε's as close as possible to those given by the ionization energies. The freedom with which the latter was chosen in this contribution reflects the authors' belief that the ionization energy may not be an adequate measure of the occupation energy. The input values were: $t_{AuAu} = 1.09\ eV$, $t_{AgAg} = 1.01\ eV$, $t_{CuCu} = 1.17\ eV$, $E_{Au} = -9.22\ eV$, $E_{Ag} = -7.40\ eV$, and $E_{Cu} = -8.27\ eV$. Real temperature predictions can now be made. The result is a Cu-Ag analogue which desegregates at $k_BT \approx 10^{-3}\ eV$; a Au-Cu analogue with only Au_2Cu_2 and Au_3Cu stable, which disorders at $k_BT \approx 2.5\times10^{-2}\ eV$, i.e. above room temperature and a Ag-Au analogue, in which the intermediate compound $AuAg_3$ is also missing at $T = 0$ and which randomizes at $k_BT \approx 10^{-3}\ eV$. Although many qualitative features of the real systems are reproduced, the agreement is far from satisfactory.

V. Conclusions

A model for binary and ternary alloy formation has been examined, one which seBks to overcome the difficulties presented by previous methods. It is remarkable that such a simple model should produce such a wide range of alloying behavior, with a very sensitive dependence on input parameters. It also shows the deficiency of an independent-electron

picture; many-body correlations are necessary to allow for such diversity. The widely varied behavior of the copper-silver-gold system is most probably caused by such subtle many-body effects, and the consequent sensitivity of the alloying properties to minute differences of the one-electron parameters.

The model does suffer, as yet, in its ability to translate the experimentally derived parameters of the pure metals into a truly predictive theory of alloy behavior. It is the belief of the author that this is caused partly by the extreme sensitivity to the one-electron parameters and by the too coarse sampling of the electron band structure inherent in a small, four-site cluster approach.[22] Furthermore, it is thought that an eight-atom cluster, otfers many intriguing possibilities. First, it allows a more balanced sampling of the band structure; second, it allows more configurational possibilities, and furthermore, it allows second-nearest neighbor interactions to be included.[23] This larger cluster may produce a true qualitative distinction between silver-gold and copper-gold alloys : the former, with a range of solid solutions, should have all seven intermediate clusters stable, while the latter should have all but the intermetallic structures Au_3Cu, AuCu and $AuCu_3$ unstable.

VI. References

[1]V.L. Moruzzi, J.F. Janak and A.R. Williams, *Calculated Electronic Properties of Metals* (Pergamon Press, New York, 1978).

[2]N.E. Christensen and B.O. Seraphin, Phys. Rev. B 4 , 3321 (1971).

[3]W.B. Pearson, *A Handbook of Lattice Spacings and Structure of Metals and Alloys*, (Pergamon, Oxford, 1967).

[4]M. Hansen and K. Anderko, *Constitution of Binary Alloys* (McGraw-Hill, New York, 1958).

[5]C.S. Barrett and T.B. Massalski, *Structure of Metals*, 3rd ed. (McGraw-Hill, New York, 1966).

[6]Y.Y. Li, J. Chem. Phys. **17** , 447 (1949).

[7]C.M. van Baal, Physica (Utrecht) **64** , 571 (1973).

[8]R. Kikuchi and D. de Fontaine, Natl. Bur. Stand. (U.S.) Spec. Publ. No. 496, (U.S.

GPO, Washington, D.C., 1978) p. 967, and 999.

[9]J.M. Sanchez, D. de Fontaine, and W. Teitler, Phys. Rev. **26** , 1465 (1982).

[10]R.C. Kittler and L.M. Falicov, Phys. Rev. B **18**, 2506 (1978).

[11]R.C. Kittler and L.M. Falicov, Phys. Rev. B **19** , 291 (1979).

[12]M.O. Robbins and L.M. Falicov, Phys. Rev. B **25**, 2343 (1982).

[13]K. Terakura, T. Oguchi, T. Mohri, and K. Watanabe, Phys. Rev. B **35**, 2169 (1987).

[14]J. Hubbard, Proc. R. Soc. London, Ser A **276**, 238 (1963); **277**, 237 (1964); **281**, 401 (1964); **285**, 542 (1965); **296**, 82 (1966); **296** , 100 (1967).

[15]L.M. Falicov and R.H. Victora, Phys. Rev. B **30**, 1695 (1984).

[16]J. Callaway, D.P. Chen and R. Tang, Z. Phys. D **3**, 91 (1986).

[17]R.H. Victora and L.M. Falicov, Phys. Rev. Lett. **55**, 1140 (1985).

[18]E.C. Sowa and L.M. Falicov, Phys. Rev. B **35**, 3765 (1987).

[19]A. Reich and L.M. Falicov, Phys. Rev. B **34**, 6752 (1986).

[20]J.C. Parlebas, R.H. Victora, and L.M. Falicov, J. Phys. (Paris) **47**, 1029 (1986).

[21]C. Kittel and H. Kroemer, *Thermal Physics*, 2nd ed. (Freeman, San Francisco, 1980).

[22]The tetrahedral cluster, with periodic boundary conditions, is equivalent to an infinite crystal, sampled only at specific points in **k** space, the Γ and three X points. These correspond, respectively, to the singlet and triplets of Eqs. (3.1) and (3.2). Introduction of an octahedral cluster, an eight- atom unit cell of the fcc structure, brings in addition the four L points, with energy situated – in this nearest-neighbor-only model – at the center of gravity of the full band, which is also the center of gravity of the Γ- and X-point energies and the position of the Fermi level. The eight-atom cluster would thus produce a more balanced representation of the full band-structure and place correctly the Fermi level.

[23]In the tetrahedral approximation, the second-nearest neighbors are identical to the atom in question, and the interaction only acts as an occupation-energy renormalization.

Chapter IV. Heavy Fermion System: an Exact Many-Body Solution to a Periodic-Cluster Hubbard Model

I. Introduction

Heavy-fermion systems have been of great experimental and theoretical interest over the past few years.[1-5] The narrow-band phenomenon has been found associated with superconductivity, both normal and re-entrant, intermediate valence, large heat capacities, and the Kondo problem of isolated magnetic impurities, with much of the responsible mechanisms still subject to debate. It is thus instructive to investigate models from which one might gain insight into the problem.

The techniques used in solving strongly interacting, and in particular heavy-fermion systems, have included variational, perturbative, diagrammatic and Monte Carlo approaches.[6-11] Typically, Monte Carlo approaches involve approximate solutions of small clusters, with accuracy depending on the statistical sample. As the scope of the problem grows exponentially with the size of the cluster, this approach rapidly becomes the only feasible one. However, the notion of reducing the computational overhead by use of group-theoretical techniques, allowing exact solution of moderate-size clusters, has not, as far as the authors are aware, been otherwise attempted.

This exact small-cluster approach has been used successfully in scenarios where local many-body effects have shown themselves to be important: a four-atom cluster Hubbard model[12], photoemission behavior[13] in Nickel, intermediate-valence behavior[14,15] in Cerium, magnetic behavior[16] in Iron, as well as for thermodynamic properties[17] and valence-bond formation.[18] It has also been used to study alloying in the Copper-Silver-Gold system.[19] The experience has shown that single-site and short-range correlations are

well taken into account, though not longer-range ones. Thus, phase transitions do not occur, though indications of where and how they might occur have been clearly obtained.

This chapter addresses the questions of the nature of the heavy-fermion state as a function of band structure and band filling, and of the interplay of the various one-electron and many-body effects. It also discusses the implications for spin-fluctuation and electron transport.

II. The Hamiltonian

Consider an infinite face-centered-cubic (fcc) lattice of atoms, with one fully symmetric orbital per site, each being either spin up or down, denoted with subscript σ. Using second-quantization notation, one has the creation (destruction) operator on site i written as $c^{\dagger}_{i\sigma}$ ($c_{i\sigma}$). One can write a Hamiltonian for this system, following Hubbard[20], as :

$$H = H_{1nn} + H_{2nn} + H_{C} \qquad (2.1)$$

where

$$H_{1nn} = -t \sum_{\substack{i,j;\sigma \\ <ij>1nn}} c^{\dagger}_{i\sigma} c_{j\sigma} , \qquad (2.2)$$

$$H_{2nn} = -T \sum_{\substack{i,j;\sigma \\ <ij>2nn}} c^{\dagger}_{i\sigma} c_{j\sigma} , \qquad (2.3)$$

$$H_{C} = U \sum_{i} c^{\dagger}_{i\uparrow} c_{i\uparrow} c^{\dagger}_{i\downarrow} c_{i\downarrow} . \qquad (2.4)$$

These terms are:

(a) a band "hopping" interaction (2.2) between conduction states on nearest-neighbor sites, with transfer integral t,

(b) a band "hopping" interaction (2.3) between conduction states on next-nearest-

neighbor sites, with transfer integral T,

(c) an on-site electron-electron Coulomb repulsion, U, (2.4).

In heavy-fermion systems U is considerably larger than the other parameters and could, for all practical purposes, be taken effectively to be infinite. In that case, no on-site double occupation of electrons is allowed and thus the maximum band-filling is one-half, one electron per site. In the half-filled band situation, Anderson[21] pointed out that one could canonically transform (2.1)-(2.4) to a basis of states with sites all singly occupied, with the simultaneous introduction, as a first-order correction in $1/U$, of an antiferromagnetic Heisenberg superexchange mechanism:

$$H_H = \sum_{\substack{i,j \\ i \neq j}} J_{ij} \, S_i \cdot S_j \qquad (2.5)$$

where the coupling parameters J_{ij} are:

$$J_{ij} = \begin{cases} \propto t^2/U & \text{if } i,j \text{ nearest neighbors} \\ \propto T^2/U & \text{if } i,j \text{ next-nearest neighbors} \\ 0 & \text{otherwise} \end{cases} \qquad (2.6)$$

This interaction amounts to a hopping of an electron onto an atom already occupied by a second electron, which costs a virtual energy U, which is then more than repaid in band energy by having this second electron hop into the first electron's original place. Wolff, Schrieffer and others[22,23] went on to show that, in the general filling case, (2.5) would be supplemented by more complicated three-atom hopping processes, which will not be considered here.

The method used in this contribution to solve the model consists of choosing a symmetric small set of points in reciprocal space and, within that set, of treating the many-electron states *exactly*. This approach is equivalent to taking a small crystal, i.e. a small

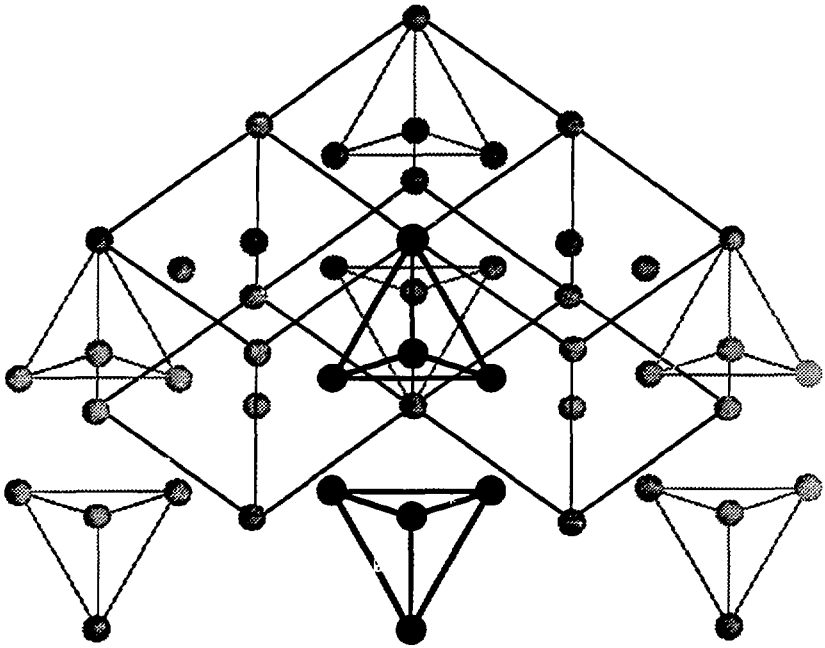

FIG. 1. The eight-atom cluster in the fcc lattice. With periodic boundary conditions this cluster, which fills the entire bulk crystal, is tantamount to sampling the Brillouin zone at the points Γ, X and L. In this scheme, the twelve nearest neighbors of each atom are of six distinct types (each type contributing two neighbors), and the six the second-nearest neighbors are all of the same type.

cluster of sites and periodic boundary conditions. The cluster under consideration here is comprised of eight atoms, and forms a double-length unit cell of the fcc structure. If repeated via periodic boundary conditions with an fcc lattice of twice the original lattice parameter, the original fcc lattice is obtained (see Fig. 1). The eight sites in the cluster are labelled i=0,1,2,...,7. In this case, the Hamiltonian becomes:

$$H = H_{1nn} + H_{2nn} + H_{H1} + H_{H2}, \qquad (2.7)$$

where now

$$H_{1nn} = -2t \sum_{\substack{i,j=0...7;\,\sigma \\ <ij>_{1nn}}} c^{\dagger}_{i\sigma} c_{j\sigma} , \qquad (2.8)$$

$$H_{2nn} = -6T \sum_{\substack{i,j=0...7;\,\sigma \\ <ij>_{2nn}}} c^{\dagger}_{i\sigma} c_{j\sigma} , \qquad (2.9)$$

$$H_{H1} = J \sum_{\substack{i,j=0...7 \\ <ij>_{1nn}}} \mathbf{S}_i \cdot \mathbf{S}_j , \qquad (2.10)$$

$$H_{H2} = J' \sum_{\substack{i,j=0...7 \\ <ij>_{2nn}}} \mathbf{S}_i \cdot \mathbf{S}_j , \qquad (2.11)$$

Several points should be noted here:

(i) the sums on the sites are restricted to the eight-atom cluster;

(ii) the 12 nearest-neighbors of each atom are, in the periodic cluster, two each of six of the other seven atoms (e.g. the twelve nearest neighbors of atom 0 are two each of the atoms 1, 2, 3, 5, 6, and 7); therefore the parameter in H_{1nn} is $2t$ instead of t;

(iii) the 6 second-nearest neighbors of each atom are all the same, and equal to one of the other seven atoms (e.g. the six second-nearest neighbors of atom 0 are all atom 4); as a consequence the parameter in H_{2nn} is $6T$ instead of T;

(iv) in this contribution only the case of seven electrons in the eight-atom cluster will be considered, i.e. only the states which are eigenstates of the number operator

$$N = \sum_{i=0...7;\,\sigma} c^{\dagger}_{i\sigma} c_{i\sigma} , \qquad (2.12)$$

with eigenvalue 7 are included

$$<N> = 7 ; \qquad (2.13)$$

(v) the term H_{H2} can be easily taken into account by subtracting J' from J in H_{H1}, and adding a term similar to H_{H1} with a coefficient J' instead of J; this last term,

added to H_{H2}, can be easily diagonalized by means of a sum rule derived from the expansion of the square of the total spin operator,

$$J' \sum_{\substack{i,j=0...7 \\ i \neq j}} \mathbf{S}_i \cdot \mathbf{S}_j = J' \left[S(S+1) - 21/4 \right], \qquad (2.14)$$

where S is the total spin of the cluster state, and (2.14) is valid for seven electrons which interact via a constant, uniform exchange J' with each other;

(vi) even though it is trivially easy to include second-nearest-neighbor Heisenberg exchange, since J' is proportional to T^2/U, and T is in general much smaller than t, the coefficient J' will be set equal to zero;

(vii) as a consequence of (vi) the Hamiltonian (2.7) is reduced to three terms, and there are in the problem three energy parameters t, T, and J, such that

$$|t| \gg |T|\,; \quad |t| \gg J\,; \qquad (2.15)$$

(viii) the properties of the system are strongly dependent on the sign of t; this is a consequence of the structure of the fcc lattice which, on account of the triangular rings of nearest neighbors, exhibits an asymmetry between top and bottom of the electronic band as well as frustration for states with alternating phases between nearest-neighbor sites.

III. Method of Calculation

The Hamiltonian presented above, for the eight-atom cluster, exhibits many symmetries and constraints which can be exploited to reduce immensely the computational demands of the problem.

With sixteen orbitals, the number of many-body states for N electrons is $16!\,/\,(16-N)!\,N!$, which in the case of seven electrons (nearly-half filled band) amounts to 11440. An infinite on-site repulsion reduces the number of states to only $2^N\,8!\,/\,(8-N)!\,N!$, which is only 1024 for seven electrons, a sizable reduction. Furthermore, these 1024 states separate, according to spin, into 64 octuplets, 288 sextets, 448 quartets and 224 doublets. There is also a space-group decomposition.

TABLE I. The character table of the eight-atom-cluster space group. There are 24 operations in the point group, the identity E, six fourfold rotations, C_4, three associated twofold rotations C_4^2, six other twofold rotations C_2, and eight threefold rotations C_3. There are eight translations, the zero translation 0, the six nearest neighbor translations τ, and the single second-nearest-neighbor translation θ. The τ's are alternatively classified as to whether they are perpendicular ($\tau_\perp$), parallel ($\tau_\parallel$), forming an acute angle ($\tau_<$) or obtuse angle ($\tau_>$), or simply at an angle ($\tau_\angle$) to a given rotation axis.

	1	6	24	12	32	6	6	12	24	24	1	12	32
	E	C_4^2	C_4	C_2	C_3	E	C_4^2	C_4^2	C_4	C_2	E	C_2	C_3
		0θ	$0\theta\tau_\perp$	$0\tau_\parallel$	$0\tau_>$	τ	$\tau_\perp$	$\tau_\angle$	$\tau_\angle$	$\tau_\angle$	θ	$\theta\tau_\perp$	$\theta\tau_<$
Γ_1	1	1	1	1	1	1	1	1	1	1	1	1	1
Γ_2	1	1	-1	-1	1	1	1	1	-1	-1	1	-1	1
Γ_{12}	2	2	0	0	-1	2	2	2	0	0	2	0	-1
Γ_{15}	3	-1	1	-1	0	3	-1	-1	1	-1	3	-1	0
Γ_{25}	3	-1	-1	1	0	3	-1	-1	-1	1	3	1	0
X_1	3	3	1	1	0	-1	-1	-1	-1	-1	3	1	0
X_2	3	3	-1	-1	0	-1	-1	-1	1	1	3	-1	0
X_3	3	-1	-1	1	0	-1	3	-1	1	-1	3	1	0
X_4	3	-1	1	-1	0	-1	3	-1	-1	1	3	-1	0
X_5	6	-2	0	0	0	-2	-2	2	0	0	6	0	0
L_1	4	0	0	2	1	0	0	0	0	0	-4	-2	-1
L_2	4	0	0	-2	1	0	0	0	0	0	-4	2	-1
L_3	8	0	0	0	-1	0	0	0	0	0	-8	0	1

The cubic point group has 24 proper operations (48 if inversion and improper rotations are included, but these yield no additional information for spherically symmetric *s*-orbitals). The eight-atom cluster has 8 translations, which yield a space group of 24 × 8 = 192 operations. This space group possesses 13 irreducible representations with the

following degeneracies : Γ_1 (d=1), Γ_2 (d=1), Γ_{12} (d=2), Γ_{15} ' (d=3), Γ_{25} ' (d=3), X_1 (d=3), X_2 (d=3), X_3 (d=3), X_4 (d=3), X_5 (d=6), L_1 (d=4), L_2 (d=4) and L_3 (d=8). These Γ, X and L representations, labeled by the translation-group **k** vectors,correspond to the eight points of the fcc Brillouin zone[24] (one Γ, three X, and four L) which constitute the finite sampling of reciprocal space inherent in the periodic-cluster approach. The character table of the group[24] is presented in Table I.

With all these symmetries taken into account the largest block to diagonalize is 5×5, a considerable reduction over 11440×11440, or 1024×1024, or even 448×448. These block sizes are presented in Table II. There is, in addition, an extra "hidden" symmetry in the Hubbard model[12,20], which (as seen below) causes additional "accidental" degeneracies. That extra symmetry, in this particular cluster, reduces the 5×5, and all 4×4 and 3×3 blocks to 2×2 and 1×1 blocks, so that the model can be solved in a completely analytical manner.

Table II. Sizes of the blocks of the various representations

	Γ_1	Γ_2	Γ_{12}	Γ_{15}'	Γ_{25}'	X_1	X_2	X_3	X_4	X_5	L_1	L_2	L_3
S = 7/2	1					1					I		
5/2	1		1		1	2	1	1		1	2		2
3/2	1		2	1	2	3	2	2	1	3	3	1	5
1/2	2	1	1	1	2	3	2	2	1	3	4	2	4

It is instructive, at this point, to discuss the band-structure of the infinite crystal, and compare it with the finite sampling considered here. The density of states of an fcc tight-binding, single-band structure, for $t > 0$, starts at its minimum energy value with an *M0* van Hove singularity at Γ, rises to an *M1* singularity at the L energy, and then progresses to a divergent, one-dimensional-type of singularity as the energy reaches its maximum degenerate value all along the X-W line of the Brillouin Zone square face. The situation

is reversed for $t < 0$, with a one-dimensional-type singular minimum along the X-W line, an ordinary $M2$ van Hove singularity at L, and a regular $M3$ van Hove maximum at Γ. In other words, for $t > 0$ there is a "pile-up" of one-electron states at the top of the band which should produce interesting effects for almost full bands; for $t < 0$ the "pile-up" occurs at the bottom of the band and should be of importance only for very low electron occupancies.

In the finite, eight-point sampling of the eight-atom periodic cluster there is one level at Γ (γ_σ), four levels at L ($l_{i\sigma}$); i =1,2,3,4), and three at X ($x_{i\sigma}$; i=1,2,3). One can make the transformation between (Wannier) one-electron localized states $c_{i\sigma}$, and Bloch states (referred to collectively as $a_{i\sigma}$) by:

$$\boldsymbol{a} = \frac{1}{\sqrt{8}} \underline{\boldsymbol{M}} \cdot \boldsymbol{c} \qquad (3.1)$$

where the eight-component column vectors $\boldsymbol{a}$ and $\boldsymbol{c}$ are connected by the 8 ×8 Wannier-Bloch matrix, $\underline{\boldsymbol{M}}$:

$$\begin{bmatrix} 1 & 1 & 1 & 1 & 1 & 1 & 1 & 1 \\ 1 & 1 & -1 & -1 & 1 & 1 & -1 & -1 \\ 1 & -1 & 1 & -1 & 1 & -1 & 1 & -1 \\ 1 & -1 & -1 & 1 & 1 & -1 & -1 & 1 \\ 1 & -1 & -1 & -1 & -1 & 1 & 1 & 1 \\ 1 & -1 & 1 & 1 & -1 & 1 & -1 & -1 \\ 1 & 1 & -1 & 1 & -1 & -1 & 1 & -1 \\ 1 & 1 & 1 & -1 & -1 & -1 & -1 & 1 \end{bmatrix} \qquad (3.2)$$

Table III. Many-body energies for 7 electrons in the non-interacting $U = J = 0$, limit.

Occupation $\gamma l x$	Energy	Degeneracy	Notes
240	$-24t + 18T$	56	ground state ($t > 0$)
241	$-20t + 6T$	420	lowest one-electron excitations, ($t > 0$)
232	$-16t - 6T$	840	
223	$-12t - 18T$	560	
160	$-12t + 30T$	56	one-electron excitations, ($t > 0$)
214	$-8t - 30T$	120	
151	$-8t + 18T$	672	highest one-electron excitations, ($t > 0$)
205	$-4t - 42T$	6	
142	$-4t + 6T$	2100	
133	$-6T$	2240	
070	$+42T$	8	
124	$4t - 18T$	840	
061	$4t + 30T$	168	
115	$8t - 30T$	96	highest one-electron excitations, ($t < 0$)
052	$8t + 18T$	840	
106	$12t - 42T$	2	one-electron excitations, ($t < 0$)
043	$12t + 6T$	1400	
034	$16t - 6T$	840	
025	$20t - 18T$	168	lowest one-electron excitations, ($t < 0$)
016	$24t - 30T$	8	ground state, ($t < 0$)
	total	11440	

These one-electron orbitals γ, x and l, have symmetries ${}^2\Gamma_1$, ${}^2X_1$, and ${}^2L_1$, respectively, and one-electron energies:

$$\varepsilon_{\gamma} = -12t - 6T \,, \qquad (3.3)$$

$$\varepsilon_{t} = 0t + 6T \,, \qquad (3.4)$$

and

$$\varepsilon_{x} = 4t - 6T \,, \qquad (3.5)$$

respectively. Notice that the bandwidth is $(4t - 6T) - (-12t - 6T) = 16t$. With these results, one can easily write down the non-interacting 7-electron energies. These are shown in Table III.

IV. RESULTS

A. Many-body spectrum of states

With nearly-half-filled bands (7/8 electron per site) and infinite interaction U, the two cases $t < 0$ and $t > 0$, represent two entirely different physical situations. A negative t represents a system with one-spin states filled almost to the *M0* van Hove singularity at Γ, while a positive t has the Fermi level falling near the divergent singularity of the X-W line. Their ground states have energies corresponding to the last and first lines, respectively, of the list the many-body 7-electron, $U \rightarrow \infty$, energies presented in Table IV.

One can see that the ground state for $t < 0$ is non-degenerate, with energy $E = (-12|t| + 6T + 9J/2)$, and with spin 7/2. It is thus ferromagnetic and fully saturated. In other words, one-electron, band-structure effects overwhelm the antiferromagnetic-superexchange mechanism and produce ferromagnetic ordering. Neither heavy-fermion behavior nor superconductivity can occur under these circumstances. (A simple Hartree-Fock state, with all electrons with parallel spins, would yield the correct ground state in these conditions).

Table IV. Many-body energies of the various representations for 7 electrons in the infinite U limit.

Energies	States	Symmetries
$-6t + 6T - 3J$	14	${}^2\Gamma_2\ {}^2X_1\ {}^2X_2$
$-6t + 6T - 2J$	16	${}^2L_3$
$-6t + 6T - \frac{3}{2}J$	32	${}^4\Gamma_{12}\ {}^4X_1\ {}^4X_2$
$-6t + 6T - \frac{1}{2}J$	16	${}^4L_2$
$-6t + 6T + J$	18	${}^6X_2$
$-t - \sqrt{(-3t + 6T + J/2)^2 + 8t^2}$	24	${}^4X_5$
$-2t + \frac{3}{2}J - \sqrt{(-2t + 6T + J/2)^2 + 4t^2}$	48	${}^6L_3$
$\frac{3}{2}J - \sqrt{(-2t + 6T + J/2)^2 + 16t^2}$	12	${}^2\Gamma_{25}'\ {}^2X_3$
$2t - \frac{J}{2} - \sqrt{(-2t + 6T + J/2)^2 + 36t^2}$	8	${}^2L_1$
$-4t + 6T + \frac{9}{2}J$	24	${}^8X_1$
$-t - J - \sqrt{(-t + 6T + J/2)^2 + 8t^2}$	48	${}^4L_1\ {}^4L_3$
$2t - \frac{3}{2}J - \sqrt{(6T + J/2)^2 + 32t^2}$	12	${}^2X_5$
$\frac{5}{2}J - \sqrt{(6T + J/2)^2 + 12t^2}$	8	${}^2L_2$
$3t - \sqrt{(t + 6T + J/2)^2 + 40t^2}$	24	${}^4\Gamma_{25}'\ {}^4X_3$
$2t - \frac{5}{2}J - \sqrt{(2t + 6T + J/2)^2 + 20t^2}$	24	${}^2L_1\ {}^2L_3$
$3t - J - \sqrt{(3t + 6T + J/2)^2 + 24t^2}$	32	${}^4L_3$
$4t + \frac{3}{2}J - \sqrt{(4t + 6T + J/2)^2 + 28t^2}$	24	${}^6L_1$
$-2t - 6T - 2J$	24	${}^2\Gamma_{15}'\ {}^2X_4\ {}^2X_5$
$-2t - 6T - J$	16	${}^2L_3$
$-2t - 6T - \frac{1}{2}J$	8	${}^4\Gamma_{15}'\ {}^4X_4\ {}^4X_5$
$-2t - 6T$	6	${}^2X_1$
$-2t - 6T + \frac{1}{2}J$	32	${}^4L_3$
$-2t - 6T + 2J$	36	${}^6X_5$

$-2t + 6T + J$	36	${}^6\Gamma_1\,{}^6\Gamma_{12}\,{}^6X_1$
$-6T + \frac{9}{2}J$	32	${}^8L_1$
$6T - \frac{3}{2}J$	24	${}^4X_1\,{}^4X_2$
$-2t + \frac{3}{2}J + \sqrt{(-2t + 6T + J/2)^2 + 4t^2}$	48	${}^6L_3$
$2t - 6T + 2J$	36	${}^6\Gamma'_{25}\,{}^6X_3$
$-t - J + \sqrt{(-t + 6T + J/2)^2 + 8t^2}$	48	${}^4L_1\,{}^4L_3$
$2t + 6T - 3J$	6	${}^2\Gamma_1\,{}^2\Gamma_{12}$
$-t + \sqrt{(-3t + 6T + J/2)^2 + 8t^2}$	24	${}^4X_5$
$\frac{5}{2}J + \sqrt{(6T + J/2)^2 + 12t^2}$	8	${}^2L_2$
$4t - 6T + \frac{J}{2}$	16	${}^4L_1$
$\frac{3}{2}J + \sqrt{(-2t + 6T + J/2)^2 + 16t^2}$	12	${}^2\Gamma'_{25}\,{}^2X_3$
$6t - 6T$	2	${}^2\Gamma_1$
$6t + 6T - 3J$	12	${}^2X_1\,{}^2X_2$
$2t - \frac{5}{2}J + \sqrt{(2t + 6T + J/2)^2 + 20t^2}$	24	${}^2L_1\,{}^2L_3$
$2t - \frac{3}{2}J + \sqrt{(6T + J/2)^2 + 32t^2}$	12	${}^2X_5$
$8t + 6T - \frac{3}{2}J$	24	${}^4\Gamma_1\,{}^4\Gamma_{12}\,{}^4X_1$
$2t - \frac{J}{2} + \sqrt{(-2t + 6T + J/2)^2 + 36t^2}$	8	${}^2L_1$
$3t - J + \sqrt{(3t + 6T + J/2)^2 + 24t^2}$	32	${}^4L_3$
$3t + \sqrt{(t + 6T + J/2)^2 + 40t^2}$	24	${}^4\Gamma'_{25}\,{}^4X_3$
$10t + 6T + J$	18	${}^6X_1$
$4t + \frac{3}{2}J + \sqrt{(4t + 6T + J/2)^2 + 28t^2}$	24	${}^6L_1$
$12t + 6T + \frac{9}{2}J$	8	${}^8\Gamma_1$
total	1024	69

For $t > 0$ a completely different picture emerges. For $J = 0$ one can see a large number of states present in the ground-state manifold, of energy $E = -6t + 6T$, with symmetries $^2\Gamma_2$, $^2X_1$, $^2X_2$, $^2L_3$, $^2\Gamma_{12}$, $^4X_1$, $^4X_2$, $^4L_2$ and $^6X_2$. Ninety-six of the total 1024 possible states, a surprising 9.375%, are in the ground-state manifold. This huge "pile-up" of many-body states at the lowest energies is, in fact, the single most characteristic property of heavy fermions, the feature responsible for the extremely large electronic specific heats reported in such systems[1]. [It should be noted, for comparison, that the non-interacting, $U = 0$, case for the same cluster contains 56 out of 11440 states in the ground-state manifold, a paltry 0.49% ; the lowest excited states are $(4t - 12T)$ higher in energy]. It can be thus said that, at least for this model, heavy-fermion behavior is a consequence of both, large electron correlations (the infinite U term) *and band structure effects*. It is indeed very surprising that the very simple Hubbard model, for the same crystal structure and the same occupancy, can yield both a simple, fully saturated ferromagnet and a richly structured, complex heavy-fermion system depending only upon the change of sign of a single band-structure parameter.

As one would expect, the introduction of a finite J splits, albeit partially, the ground-state manifold. The spin-doublets retain the lowest energy, followed by the spin-quartets, with the sextet $^6X_2$ having the highest energy. For a given spin, the Γ and X states are lower than the corresponding L states. The manifold has a total superexchange bandwidth of $4J$.

It has been repeatedly suggested[8,10,25] that, at least for heavy-fermion systems, the "true" ground state of the system can be adequately represented by selecting one of the possible ground states of the non-interacting system and projecting out of it all components with two electrons per site, retaining only that part with site occupations of either zero or one. It can be seen from the present calculation that that procedure is, at best, an uncertain one, and at worst, plainly wrong. One should bear in mind that the projection process, because it is applied to *all sites* simultaneously, is a completely symmetric one, and it does not change the space-group symmetry of the state.

In this context, one may first consider the case of $t < 0$. Under such conditions the

non-interacting manifold has a ground state of energy E = -24|t| - 30T (see Table III), which corresponds to a filling of the x-shell (3×2 = 6 electrons) and a lone l-electron, and thus has spin 1/2. The complete x-shell is fully symmetric, and has a global $^1\Gamma_1$ symmetry, whereas the l-electron has, of course, $^2L_1$ symmetry; the resulting seven-electron state must have an overall $^2L_1$ symmetry, i.e. spin 1/2. Consultation of Table IV, however, reveals that the ground state of the strongly interacting case is $^8\Gamma_1$, the saturated ferromagnet (spin 7/2) described previously, which has both the wrong spin and space symmetries. At E = 12t + 6T + 9J/2, the $^8\Gamma_1$ state is considerably lower in energy that the lowest $^2L_1$ state, which has an excitation of the order of (3|t|). It may be argued that the previous procedure is not applicable to the ferromagnetic case because a phase transition (spin-symmetry cross over) has taken place, with a consequent breakdown of the projection technique. But, as seen below, that is also the situation for the heavy-fermion case.

For the case t > 0, one has a non-interacting ground-state manifold of 56 states and energy E = -24t + 18T, as listed in Table III. These 56 states span four representations: $^4L_2$ and $^2L_2$ once, and $^2L_3$ twice. The lowest state of the strongly interacting heavy-fermion system of $^2L_2$ symmetry has an energy of order (2t) greater than the true ground state. The other two symmetries do appear in the ground-state manifold for J = 0, but as the latter symmetry, $^2L_3$ appears twice in the non-interacting case, it is always possible to find at least one combination of the two corresponding wavefunctions guaranteed to be orthogonal to the ground state When antiferromagnetic superexchange is included, the states with the lowest energy, E = -6t + 6T -3J, have symmetry $^2\Gamma_2$, $^2X_1$, and $^2X_2$, and cannot at all be attained by the projection technique. It is therefore obvious that such technique cannot be considered to be a sound one.

It is interesting to note that the ground-state manifold has an echo at E = -2t - 6T, which corresponds in energy to a promotion of one electron from the l-levels to the x-shell, of the non-interacting picture. Moreover, this family and the ground-state manifold are the only accidental degeneracies partially removed by the antiferromagnetic interaction.

B. Fermi Surface behavior

With an eight-atom cluster providing reciprocal-space sampling at the Γ, X and L points of the Brillouin Zone, one may ask: in these heavily correlated systems, is it meaningful to speak of a Fermi surface, and if so, how are the usual notions modified by the many-body effects? The question should be faced with extreme care, since the sampling technique provides information not on the one-electron continuum, as the notion of Fermi surface implies, but *only* on a *small*, *discrete* set of one-electron energy states.

The non-interacting electron picture is one where one-electron energy levels are occupied with unit probability, up to the Fermi level, and higher energy one-electron states are unoccupied. The pioneering work of Luttinger[6,7] and others[8,9,26], has shown that, in the regime governed by perturbatively small electron-electron interactions, even though the occupation probabilities are finite throughout and no longer constrained to be zero or one, there is still a finite jump discontinuity at the Fermi level, i.e. the Fermi Surface still exists. The exact nature of the occupation profile has been shown to be very model dependent.

In the context of the finite-cluster model, one can discuss the occupancy of the one-electron states by finding the following expectation values:

$$< a^{\dagger}_{i\sigma} a_{i\sigma} > = \sum_{j,k=0}^{7} M_{ij} M_{ik} < c^{\dagger}_{j\sigma} c_{k\sigma} > , \qquad (4.1)$$

where the matrix elements M_{ij} are given by (3.2).

Results are shown in Table V for the heavy-fermion ($U = \infty$; $t > 0$), and the ferromagnetic ($U = \infty$; $t < 0$) cases, together with the isolated atom and the non-interacting states. For the various ground states of the heavy-fermion case, ${}^2\Gamma_2$, ${}^2X_1$, ${}^2X_2$, the occupation probabilities are distributed in various ways among the one-electron orbitals of each shell, but the *average* occupation of each shell is the same in all cases. This is easily understood: even though the system is always perfectly correlated and the electrons rigorously avoid each other at each site, the total energy is (except for the small antiferromagnetic superexchange contribution) *exclusively* band energy; therefore two states with the same total energy must have the same band energy, i.e. the same occupation

of the one-electron energy shells.

Table V. Orbital occupation probabilities

State	γ	l	x
isolated-atom ($t = T = 0$)	7/16	7/16	7/16
heavy fermion ($U = \infty; t > 0$)	9/16	1/2	5/16
ferromagnetic ($U = \infty; t < 0$)	0	1/2	1/2
non-interacting ($U = 0; t > 0$)	1	5/8	0
non-interacting ($U = 0; t < 0$)	0	1/8	1

The non-interacting free-electron cases show the usual step-function occupations. The isolated-atom limit has, at most, one electron per atom, with no correlation between the atoms, and thus all **k**-states are occupied with equal probability.

The ferromagnetic case shows an occupation of one half for the lower-energy orbitals, and zero for the highest ones. This is the well known Stoner state, with spin-up and spin-down electron distributions split by the interaction: an ordinary Fermi distribution and Fermi Surface in the "majority" spins, and "minority" spins states completely empty. The extrapolation to larger clusters and the infinite crystal (full Brillouin Zone sampling) is straightforward: the Fermi Surface of the non-interacting case ($U = 0$; $t < 0$) splits into separate sheets for up- and down-spins, with one sheet vanishing (shrinking down to zero), and the other becoming a small closed surface of holes around the point Γ of the Zone.

The heavy-fermion case is much more difficult to interpret and to generalize. What can clearly be seen is that the occupation probabilities for that system have a profile closer to the flat one of the isolated-atom picture, rather than the sharp drop-off of the non-interacting picture. There is, however, a monotonic drop-off from γ, to l, to x, and it is not unlikely that larger clusters may produce the ever sharper decreases which, in the infinite-cluster

limit, could yield the expected Fermi Surface discontinuity. There is no indication however that, in the continuous **k**-space-sampling limit, the discontinuities in the occupation function will or should take place at exactly the same locus of points where it occurs in the corresponding non-interacting limit. In fact experience with many other strongly interacting problems points out to drastic changes in geometry and topology of the Fermi Surface with changes in interaction parameters. Even though the *volume* of the Fermi Surface is a conserved quantity[6,7], similarities between non-interacting or mean-field (calculated[27]) and strongly interacting (measured[28]) heavy-fermion Fermi Surfaces should, at this point, be considered fortuitous.

C. Spin-Wave spectrum

With double-occupancy forbidden on any given site, the consequences for redistribution of energies involved in a spin-flip on a given atom is of great interest. It amounts to exciting all the possible spin waves; in this case waves with the periodicities of Γ, X and L. One can project the spin-flipped state onto the whole manifold of many-body states and obtain thus a spectrum:

$$F_{SW}(\varepsilon;\sigma) = \sum_{\alpha}\sum_{i} |\langle \alpha : S_{\alpha} S_{\alpha z} | c^{\dagger}_{i,-\sigma} c_{i\sigma} | GS : S_{GS} S_{GSz} \rangle|^2 \delta(\varepsilon - (\varepsilon_{\alpha} - \varepsilon_{GS}))$$

(4.2)

where GS represents the ground state, with energy ε_{GS} spin magnitude S_{GS}, spin z-component S_{GSz}, and the index α refers to any given state of the manifold. It is straightforward to show the following sum rule holds in the heavy-fermion limit:

$$\sum_{\sigma}\int_{0}^{+\infty} F_{SW}(\varepsilon;\sigma)\, d\varepsilon = N = 1. \qquad (4.3)$$

Table VI. Spin-wave spectral features for the ferromagnetic ($U = \infty$; $t < 0$) ground state ${}^8\Gamma_1$. The state is spin-maximally aligned (i.e. $S_z = 7/2$). The parameters are $-t = 10T = 100J$. Energies are given in units of $|t|$.

Final State Symmetry	Excitation Energy	Spectral Weight
${}^8\Gamma_1$	0.000	0.875
${}^6L_1$	1.083	3.354
${}^6X_1$	1.965	2.571
${}^8L_1$	10.800	0.071
${}^8L_1$	13.657	0.075
${}^8X_1$	16.000	0.053

The spin-wave spectrum of the ground state of the ferromagnetic case ($U = \infty$; $t < 0$), is presented in Table VI for the specific case of $-t = 10\ T = 100\ J$. A simple *fcc* Heisenberg ferromagnet, should exhibit a spin wave structure with one mode per point in the Brillouin Zone. In particular – and given the normalization of (4.2) – a zero-frequency mode at Γ, with weight 0.875, four modes at L, with symmetry ${}^6L_1$ and weight 3.500, and three modes at X with symmetry ${}^6X_1$ and weight 2.625. The data of Table VI clearly show that the Heisenberg model for this *very itinerant* model works reasonable well, that the first two excited states of this case are indeed almost exclusively spin-wave modes, and that the spin-wave-spin-wave interaction, as well as the itinerant character of the states, impart partial spin-wave characteristics to three other states. The spin-wave character is, however, very small, and each of these additional states has a spin-wave weight smaller than 0.08. From Tables VI and IV it can also be inferred that this itinerant ferromagnet has, for spin one-half, an effective exchange interaction[29] equal to $(-|t|/8 + 7J/16)$, i.e. an interaction whose dominant term is of the order of $|t|$ and not of the order $|t|^2/U$.

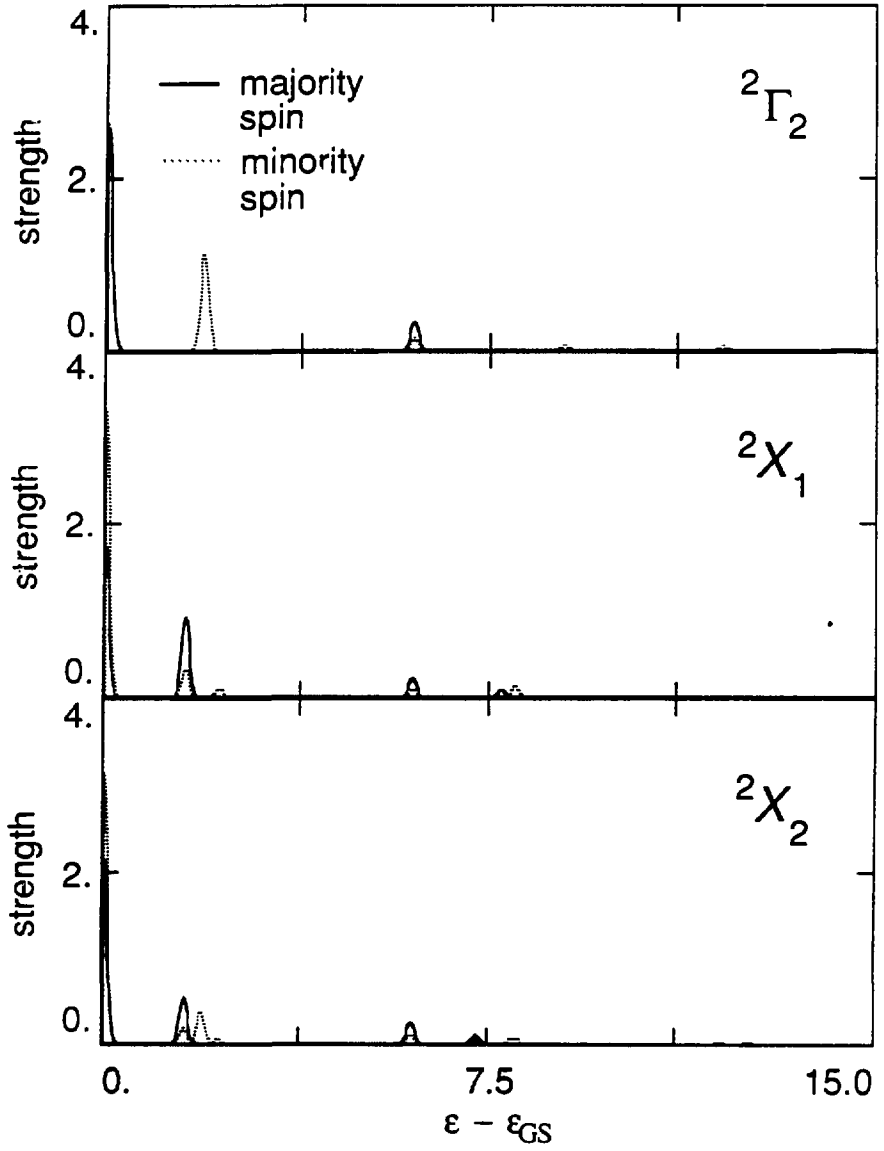

FIG. 2. Spin-excitation spectra for the heavy-fermion ground states $^2\Gamma_2$, $^2X_1$ and $^2X_2$ are shown for parameter values $t = 10T = 100J$, with energies in units of t. Notice the overwhelming weight attached to the zero-energy peaks, indicating great zero- and low-temperature spin fluctuations. The peaks are artificially broadened for clarity.

For the ground-state manifold of the heavy-fermion case ($U = \infty$; $t > 0$), namely the states ${}^2\Gamma_2$, ${}^2X_1$, and ${}^2X_2$, the spin-wave spectrum, as evaluated for $t = 10T = 100J$, is shown in Fig. 2. One can compare this with the structure of the ferromagnetic case discussed above (Table VI), and with the non-interacting spectrum, ($U = 0$; $t > 0$), which is presented in Table VII.

TABLE VII. Spin-wave spectral weights for the non-interacting ($U = 0$; $t > 0$) case. States are spin-maximally aligned (i.e. $S_z = S$).

Spin	Flip	Excitation Energies			
		0	$4t - 12T$	$12t + 12T$	$16t$
3/2	+	3/2	3/2	3/8	3/8
	−	0	3/8	0	3/8
1/2	+	3/4	9/8	1/4	3/8
	−	1/4	3/4	1/8	3/8

The non-interacting case has considerable weights at all band excitation energies. The heavy-fermion system, by contrast, has almost its total weight at zero energy (see Table VIII). Furthermore, the total strength of the spin-wave spectrum is greater in the heavy-fermion case because, as can be shown, the sum rule in (4.3) is diminished by the presence of on-site electron-electron pairing. Thus, one can surmise that the heavy-fermion state is indeed characterized by enormous zero- and low-temperature spin fluctuations; i.e. there is much freedom to flip spins around, and yet remain within the ground-state, or at most reach the low-lying, antiferromagnetically split excited states.

TABLE VIII. Spin-wave spectral weights for the heavy-fermion ($U = \infty$; $t > 0$) case of Figure 2. The parameters are $t = 10T = 100J$. States are spin-up (i.e. $S_z = 1/2$).

Symmetry	Flip	Ground-State Manifold	Low-Energy States *	Total weight
$^2\Gamma_2$	+	0.000	2.667	
	–	1.805	2.693	5.360
$^2\chi_1$	+	0.000	1.778	
	–	1.690	3.350	5.128
$^2\chi_2$	+	0.000	2.185	
	–	1.728	3.167	5.352

* Set of states with excitation energies of the order of J, including the ground-state manifold.

D. Electron transport properties

It is also very instructive to see how the highly correlated electrons, in particular the sluggish heavy-fermions, move about through the lattice. Within the context of this model, it is possible to address the question of the hopping to both nearest and second-nearest neighbors. In analogy with the spin-wave spectrum, one can define electron-hopping spectra as:

$$F_{Eff\ 1nn/2nn}(\varepsilon;\sigma) = \sum_{\alpha}\sum_{<ij>} |< \alpha; S_{\alpha}\ S_{\alpha z}\ | c^{\dagger}_{i\sigma}\, c_{j\sigma}\, (1 - c^{\dagger}_{i,-\sigma}\, c_{i,-\sigma}) | GS; S_{GS}\ S_{GSz} >|^2 \times \delta(\varepsilon - (\varepsilon_{\alpha} - \varepsilon_{GS})) \qquad (4.4)$$

where the additional $(1 - c^{\dagger}_{i,-\sigma} c_{i,-\sigma})$ factor guarantees that all accessible states are, at most, singly occupied. The sum $<ij>$ is on nearest and second-nearest neighbors for the respective distributions. There is also a sum rule in place, in the $U = \infty$ limit:

$$\sum_{\sigma} \int_{0}^{+\infty} [\, F_{EH\ 1nn}(\varepsilon;\sigma) + F_{EH\ 2nn}(\varepsilon;\sigma) \,]\, d\varepsilon = N\ (8-N) = 7\ . \quad (4.5)$$

The electron-hopping spectrum of the ground state of the ferromagnetic case ($U = \infty$; $t < 0$) is presented in Table IX for the specific case of $-t = 10T = 100J$. For the heavy-fermion case ($U = \infty$; $t > 0$) and the specific value $t = 10T = 100J$, the nearest-neighbor electron-hopping spectra are presented in Figure 3.

TABLE IX. Electron-hopping spectral features for the ferromagnetic ($U = \infty$; $t < 0$) ground state ${}^{8}\Gamma_1$. The state is spin-maximally aligned (i.e. $S_z = 7/2$). The parameters are $-t = 10T = 100J$ and the energies are given in units of t.

Final State Symmetry	Excitation Energy	Spectral Weight	
		Nearest-Neighbor	Second-Nearest-Neighbor
${}^{8}\Gamma_1$	0.000	0.750	0.125
${}^{8}L_1$	10.800	3.000	0.500
${}^{8}X_1$	16.000	2.250	0.375

First of all, one may notice that the zero-energy contribution is much smaller than in the spin-wave spectra, with the weights being spread more or less throughout. Thus, since the weight at zero energy is very small but not zero, one would expect these systems to be poor conductors. There appears to be a sizeable contribution to the a.c electron hopping around 2.8 units, corresponding to the $l \rightarrow x$ electron promotion.

The second-nearest-neighbor electron-hopping spectra in Figure 4, display a different situation again. Here the largest weights occurs at energies of 12 units or greater, and thus electrically- and thermally-activated second-nearest-neighbor hops require considerable activation. Also, this magnitude of energy indicates that the transition must have a significant $\gamma \rightarrow l$ character [(0t + 6T) – (-12t - 6T) = 12(t+T)].

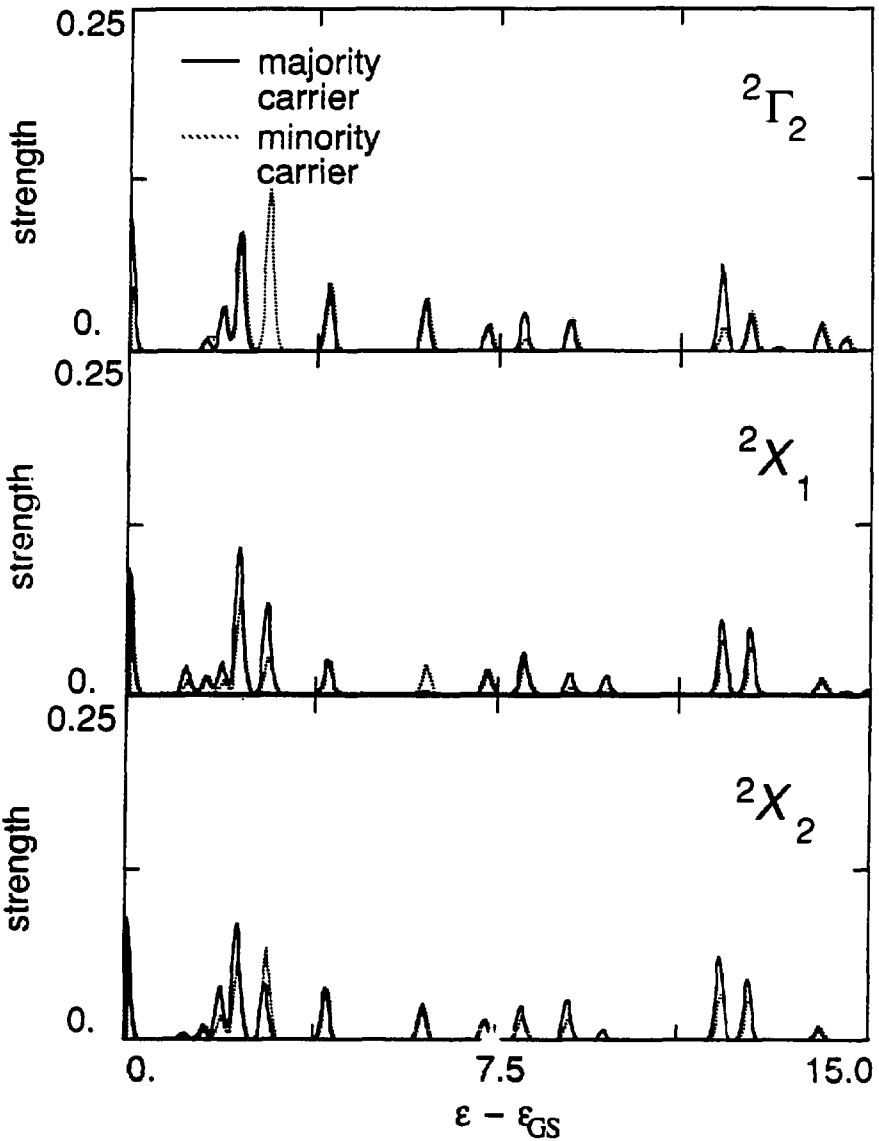

FIG. 3. Nearest-neighbor electron-hopping spectra for the heavy-fermion ground states $^2\Gamma_2$, $^2X_1$ and $^2X_2$ are shown for parameter values $t = 10T = 100J$, with energies in units of t. Notice the distribution of peaks throughout the energy range, and the relatively small weight at zero energy. There is a considerable build-up near 2.81 units, corresponding to an $l \rightarrow x$ electron promotion. The peaks are artificially broadened for clarity.

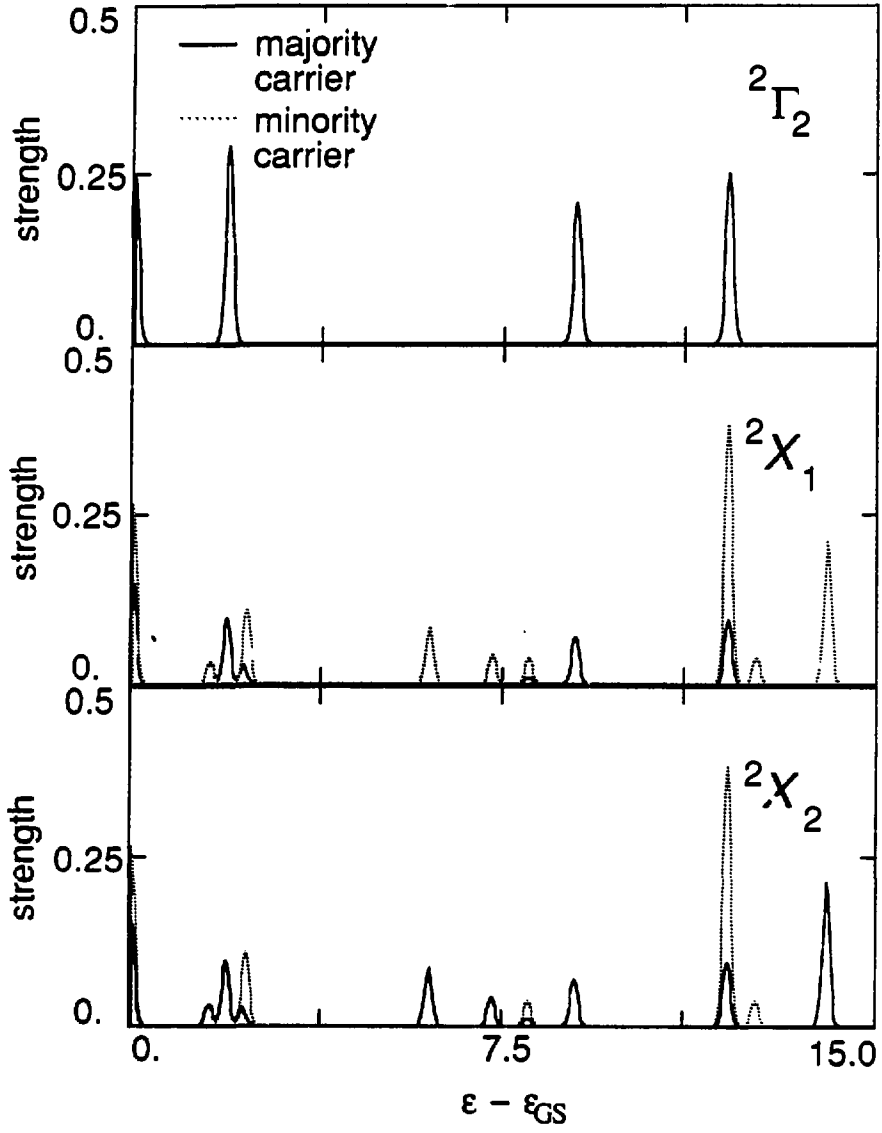

FIG. 4. Second-nearest-neighbor electron-hopping spectra for the heavy-fermion ground states $^2\Gamma_2$, $^2X_1$ and $^2X_2$ are shown for parameter values $t = 10T = 100J$, with energies in units of t. The peak distribution here has weight shifted towards much higher energies than for nearest-neighbor hopping, with a large contribution from the $\gamma \rightarrow l$ electron promotion. The peaks are artificially broadened for clarity.

It should be noted that the structural make-up of all these spectra is rather robust to changes of the parameters, and thus changing T by a factor of two or so with respect to t does not alter any of these conclusions. Also, one can see that the $^2\Gamma_2$ spectrum is devoid of minority-carrier contribution, leading one to conclude that vacancies in adjacent second-nearest neighbors are completely blocked for that state.

V. Conclusions

A Hubbard model for the fcc structure, in the infinite-U limit, and for an occupation of seven-eighths of an electron per site was examined in the periodic small-cluster approximation. Through careful use of inherent symmetries the solution proved to be very simple to obtain, but contained nonetheless some very rich structure reminiscent of real systems. The most important result is that the nature of the ground state and the physical properties of the system are very critically dependent on the details of the one-electron band structure. In particular, if the top of the band is an ordinary van Hove maximum (the negative-t case), the ground state is an itinerant *ferromagnet*, in which the band-structure terms overwhelm the antiferromagnetic superexchange interaction. For a degenerate top of the band (the positive-t case), on the other hand, the ground state is very highly degenerate, with a complex and rich structure that describes well the heavy-fermion behavior.

The ferromagnetic case exhibits properties which are essentially of textbook quality: a non-degenerate ground state (except for spin), well behaved spin-waves, a relatively small spin-wave-spin-wave interaction (less than 8%), and low-energy excitations which can be described in terms of spin waves and of conduction electrons which possess an ordinary, single-spin, single-sheet Fermi Surface.

The heavy-fermion case, by contrast, has an enormously degenerate ground-state manifold: in the eight-atom cluster and in the absence of superexchange interactions over 9% of the available many-body states belong to that manifold. This property yields an unusually large electronic heat capacity, which is the prominent feature of heavy-fermion

systems. An analysis of the low lying states, based on spin-flip and electron-hopping spectra, reveals that they consists many of spin degrees of freedom, but that the inherent conductivity is very poor, once again in agreement with the properties of heavy-fermion solids.

An analysis of the symmetries of the heavy-fermion ground-state manifold and of the non-interacting ($U = 0$) limit clearly indicates that projection methods, based essentially on the Gutzwiller approach[25], and consisting of projecting out states with multiple occupation, must be taken with considerable skepticism, since in general they may provide states considerably different in energy and structure from the true ground state(s).

Even though the analysis of the occupation probabilities and the Fermi Surface discontinuity is very flawed in the small-cluster approach taken here, it was seen that in the heavy-fermion situation the occupation probabilities are more reminiscent of the isolated-atom system than of the step-function, non-interacting case. The Fermi Surface discontinuity, which must exist because the system is metallic, is probably a very small one.

Given the current interest in Hubbard models as related to high-temperature superconductivity[5,30-33], it will be of great interest to study the superconducting-fluctuation properties of the system described in this paper, and to add to it the effect of the electron-electron interaction mediated by phonons. Some of the results are the subject of the following chapter.

The eight-atom periodic cluster was just large enough for the first few tantalizing pieces of information about bulk heavy-fermion materials to emerge: the Fermi surface structure, the spin correlations and the electron transport. By way of improving the model, the question could be asked: as the burden of computation in this case was lowered so completely as to reduce it to analytic solution, could not the size of the cluster be scaled up, with matrix sizes still within the range of present-day computers? The penalty of scaling is enormous. As it turns out, the next larger size in the hierarchy of fcc cubic-symmetric clusters has 32 atoms, and so the number of states to deal with, for an occupation of 7/8

electron per site, increases from $2^{7}8!/7!1! = 1024$ to $2^{28}\ 32!/28!4! = 9.653 \times 10^{12}$, which even after heroic efforts to factorize by the 15 different spin multiplicities and the relevant 768 element space-group, faces daunting prospects for anything but statistical approaches.

As is, only the non-interacting and heavy-fermion limits of the system were studied here. The model can, however, be readily extended to take into account finite U, and reveal, for example, the nature of any intermediate symmetry cross-overs which must by necessity occur.[18]

VI. References

[1]G.R. Stewart, Rev. Mod. Phys. **56**, 755 (1984).

[2]F. Steglich, in *Theory of Heavy Fermions and Valence Fluctuations*, edited by K. Kasuya and T.Saso, Springer Series in Solid State Sciences, Vol. 62 (Springer, New York, 1985), p.23.

[3]W. Buckel and W. Weber, *Superconductivity in d- and f-Band Metals 1982*, (Kenforschungzentrum Karlsruhe GmbH, Karslruhe, 1982).

[4]H. Suhl and M.B. Maple, *Superconductivity in d- and f-Band Metals*, (Academic Press, New York, 1980).

[5]T.M. Rice, Z. Phys. B. **67**, 141 (1987).

[6]J.M. Luttinger, Phys. Rev. **121**, 1251 (1961).

[7]P. Nozières and J.M. Luttinger, Phys. Rev. **127**, 1423 (1962).

[8]M.C. Gutzwiller, Phys. Rev. A. **137**, 1726 (1965).

[9]M. Weger and D. Fay, Phys. Rev. B. **34**, 5939 (1986).

[10]P. Coleman, Phys. Rev. B. **29**, 3035 (1984).

[11]J.E. Hirsch, Phys. Rev. Lett. **54**, 1317 (1985).

[12]R.H. Victora and L.M. Falicov, Phys. Rev. B **30**, 1695 (1984).

[13]R.H. Victora and L.M. Falicov, Phys. Rev. Lett. **55**, 1140 (1985).

[14]A. Reich and L.M. Falicov, Phys. Rev. B **34**, 6752 (1986).

[15]J.C. Parlebas, R.H. Victora, and L.M. Falicov, J. Phys. (Paris) **47**, 1029 (1986).

[16]E.C. Sowa and L.M. Falicov, Phys. Rev. B **35**, 3765 (1987).

[17]J. Callaway, D.P. Chen and R. Tang, Z. Phys. D **3**, 91 (1986); Phys. Rev. B. **35**, 3705 (1987).

[18]J. Callaway, Phys. Rev. B. **35**, 8723 (1987).

[19]A. Reich and L.M. Falicov, Phys. Rev. B. **36**, 3117 (1987).

[20]J. Hubbard, Proc. R. Soc. London, Ser A **276**, 238 (1963); **277**, 237 (1964); **281**, 401 (1964); **285**, 542 (1965); **296**, 82 (1966); **296**, 100 (1967).

[21]P.W. Anderson, in *Solid State Physics*, edited by F.Seitz and D. Turnbull, (Academic Press, New York, 1963) Vol. 14, p.99.

[22]A.B. Harris and R.V. Lange, Phys. Rev. **157**, 295 (1967).

[23]J.R. Schrieffer and P.A. Wolff, Phys. Rev. **149**, 491 (1966).

[24]L. P. Bouckaert, R. Smoluchowsky and E. Wigner, Phys. Rev. **50**, 58 (1936).

[25]T. M. Rice and K. Ueda, Phys. Rev. B **34**, 6420 (1986).

[26]E. Daniel and S.H. Vosko, Phys. Rev. **120**, 2041 (1960).

[27]C.S. Wang, M.R. Norman, R.C. Albers, A.M.Boring, W.E. Pickett, H. Krakauer, and N.E. Christensen, Phys. Rev. B. **35**, 7260 (1987).

[28]L. Taillefer, R. Newbury, G.G. Lonzarich, Z. Fisk, and J.L. Smith, J. Magn. Magn. Mater. .B **63-64**, 372 (1987).

[29]C. Kittel, *Quantum Theory of Solids*, (Wiley, New York, 1963), p 52.

[30]M.L. Cohen, in *Proceedings of the International Workshop on Novel Mechanisms of Superconductivity*, edited by W. Kresin and S. Wolf, (Plenum Press, New York, 1987), p. 1095.

[31]D.J. Scalapino, E. Loh, Jr., and J.E. Hirsch, Phys. Rev. B. **34**, 8190 (1986).

[32]K. Miyake, S. Schmitt-Rink, and C.M. Varma, Phys. Rev. B. **34**, 6554 (1986).

[33]P.W. Anderson, Science **235**, 1196 (1987).

Chapter V. Heavy-Fermion System: Superconducting and Magnetic Fluctuations within a Periodic-Cluster Hubbard Model

I. Introduction

Heavy-fermion materials, with their high heat capacities at low temperatures, exhibit sometimes normal and sometimes re-entrant superconductivity. They have been a source of great experimental and theoretical attention[1-4]. This interest has been further fueled by early experimental evidence showing a degree of similarity between these and the new high-temperature superconducting ceramics, with many of the leading ideas for high T_c mechanisms borrowed from heavy-fermion research[5-9].

One direction in the incorporation of the large Coulomb repulsion between the f-electrons of these lanthanide and actinide heavy-fermion materials has been the use of the single-orbital-per-site Hubbard model[10], or the twin-orbital-per-site Anderson model[11], in order to make the non-neglible many-body effects more mathematically tractable.

The current work focuses on the Hubbard model, wherein the computational overhead is further reduced by a small-cluster approach which incorporates periodic boundary conditions. This method[12] has been applied to various problems: photoemission[13,14], intermediate-valence[14,15], magnetic[16], thermodynamic[17], resonating-valence-bond[18] and alloying behavior[19]. These papers have shown the approach to be good for explaining uniform and short-range correlation properties and, although incapable of exhibiting phase transitions, it has shown indications of possible mechanisms involved in them. In the previous chapter[20] the author has explored the Fermi surface, spin-wave and transport properties of the an eight-site, seven electron fcc cluster, which proved to be similar to real heavy-fermion systems. In this chapter the small-cluster model, with various occupations,

is analyzed for the superconducting-fluctuation behavior, to investigate possible mechanisms for superconductivity.

The lattice in the model is face-centered-cubic, a three-dimensional array of triangular rings, which is the classical example of an antiferromagnetically spin-frustrated system. This idea of electrons having to alternate between forming spin-singlet states with all adjacent electrons is the basis for Anderson's concept[21] of Resonating-Valence-Bond (RVB). Thus, one way to address the relevance of the RVB approach, in the context of high-T_c superconductivity, is to examine an extreme case, such as the present one.

Section II reviews the Hamiltonian employed. Section III examines the nature fo the ground and low-lying excited states, as well as the suitability of the Gutzwiller projection approach. Section IV examines the superconducting correlations, in terms of the anisotropy, degree of spontaneous-symmetry breaking, the relative strengths of various spin-coupling mdoes. The relation between the BCS predicted ground-state wavefunctions and the actual ones are also examined, and finally, the magnetic correlation behavior is studied.

II. The Hamiltonian

The Hamiltonian is thoroughly discussed in the previous chapter[20]. The limit of large on-site Coulomb repulsion, $U \rightarrow \infty$, reduces it[22-24] to the form:

$$H = H_{1nn} + H_{2nn} + H_{AF} , \qquad (2.1)$$

where

$$H_{1nn} = -2t \sum_{\substack{i,j=0...7;\,\sigma \\ <ij>_{1nn}}} c^{\dagger}_{i\sigma} c_{j\sigma} , \qquad (2.2)$$

$$H_{2nn} = -6T \sum_{\substack{i,j=0...7;\,\sigma \\ <ij>_{2nn}}} c^{\dagger}_{i\sigma} c_{j\sigma} , \qquad (2.3)$$

represents second-nearest neighbor hopping, with transfer integral T, and

$$H_{AF} = J \sum_{\substack{i,j=0...7 \\ <ij>_{nn}}} S_i \cdot S_j \quad , \qquad (2.4)$$

is a Heisenberg interaction where J is the antiferromagnetic coupling of order (t^2/U).

TABLE I. Many-body of the low-lying states for 6,7 and 8 electrons in the infinitesimal and infinite-U limits.

Energy	States	Symmetries
6 electrons - small U		
$-24t + 12T + 5U/8$	16	${}^1\Gamma_1\,{}^3X_1\,{}^5\Gamma_2$
$-24t + 12T + 9U/8$	57	${}^1\Gamma_{12}\,{}^1X_2\,{}^1X_5\,{}^3\Gamma_{15}\,{}^3X_2\,{}^3X_4\,{}^3X_5$
$-24t + 12T + 13U/8$	6	${}^1\Gamma_{25}\,{}^3\Gamma_1\,{}^3\Gamma_{12}\,{}^3X_1$
large U		
$-12t + 12T - 11J/4$	2	${}^1\Gamma_{12}$
$-12t + 12T - 7J/4$	9	${}^3X_2$
$-12t + 12T + J/4$	5	${}^5\Gamma_2$
7 electrons - small U		
$-24t + 18T + 5U/4$	32	${}^2L_3\,{}^4L_2$
$-24t + 18T + 7U/4$	24	${}^2L_2\,{}^2L_3$
large U		
$-6t + 6T - 3J$	14	${}^2\Gamma_2\,{}^2X_1\,{}^2X_2$
$-6t + 6T - 2J$	16	${}^2L_3$
$-6t + 6T - 3J/2$	32	${}^4\Gamma_{12}\,{}^4X_1\,{}^4X_2$
$-6t + 6T - J/2$	16	${}^4L_2$
$-6t + 6T + J$	18	${}^6X_2$
8 electrons - small U		
$-24t + 24T + 15U/8$	24	${}^1\Gamma_{25}\,{}^1X_3\,{}^3X_5$
$-24t + 24T + 19U/8$	4	${}^1\Gamma_1\,{}^1X_1$
large U		
$-4J$	3	${}^1\Gamma_1\,{}^1\Gamma_{12}$
$-3J$	22	${}^1L_2\,{}^3X_1\,{}^3X_2$
$-2J$	42	${}^1\Gamma_{25}\,{}^1X_3\,{}^3L_2\,{}^3L_3$
$-J$	48	${}^3X_5\,{}^5\Gamma_1\,{}^5\Gamma_{12}\,{}^5X_1$
0	53	${}^1\Gamma_1\,{}^3L_2\,{}^3L_3$

The eight-atom cluster in the fcc structure has the symmetry of a space group with 192 operations and 13 representations. These representations are: five at the Γ point of the Brillouin zone (referred to as Γ_1, Γ_2, Γ_{12}, Γ_{15}, and Γ_{25}, with degeneracies 1, 1, 2, 3, and 3, respectively), five at X (X_1, X_2, X_3, X_4, X_5; degeneracies 3, 3, 3, 3, and 6, respectively) and three at L (L_1, L_2, L_3; degeneracies 4, 4, and 8, respectively); the labels Γ, X and L refer to the overall **k**-vector of the many-body wavefunction. The notation is the standard one of Bouckaert *et al* [25].

This model has been solved exactly for occupations of 6, 7 and 8 electrons (corresponding to 0.75, 0.875 and 1.0 electrons per site), and the relevant ground and low-lying states are presented in Table I. In addition the non-interacting ground and low-lying states are presented, separated according to their first-order correction in Coulomb energy, which is obtained by diagonalizing, in the $U = 0$ ground-state manifold, the operator :

$$H_C = U \sum_{i=0\ldots7} c^{\dagger}_{i\uparrow} c_{i\uparrow} c^{\dagger}_{i\downarrow} c_{i\downarrow} . \qquad (2.5)$$

III. The Gutzwiller-projected state

It is interesting at this point to examine the so-called Gutzwiller method[9,26-29]. The approach approximates the interacting ground state by projecting out of the non-interacting ground-state wave function any part that contains doubly occupied sites:

$$|\Psi_G\rangle = \prod_i (1 - c^{\dagger}_{i\uparrow} c_{i\uparrow} c^{\dagger}_{i\downarrow} c_{i\downarrow}) |\Psi_0\rangle , \qquad (2.6)$$

where the product index i runs over all sites. The appeal of the approach is obvious from its aesthetics to its relative ease of implementation. However, as shown before[20] and here, the pitfalls of such an approach become evident.

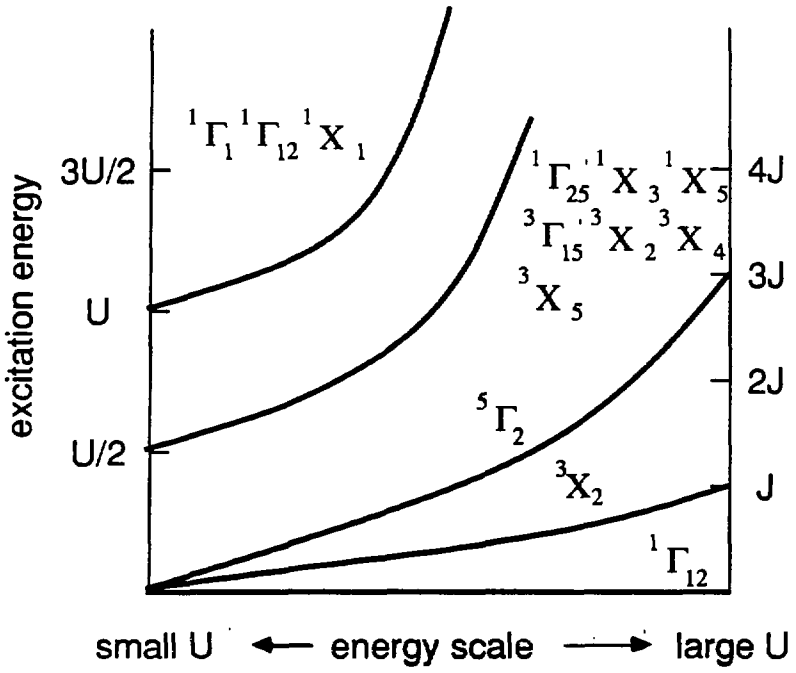

FIG. 1. Schematic representation of the ground- and low-lying states for 6 electrons. The situation is rather straightforward: the symmetries at low-U carry over to the high-U regime, with no cross-overs.

One sees the situation schematically in Figs. 1-3, depicting the ground- and low-lying excited states for occupations of 6, 7 and 8 electrons, respectively. For 6 electrons, if one follows the $^1\Gamma_{12}$ non-interacting ground state of minimal Coulomb energy, and performs the Gutzwiller projection (2.6), one arrives, at infinite U, at the proper ground state.

For 7 electrons, however, the small-U ground state, if projected, yields an excited state of the heavy-fermion manifold, i.e. it is superseded by states of completely different symmetry which correspond to highly-excited states for small U.

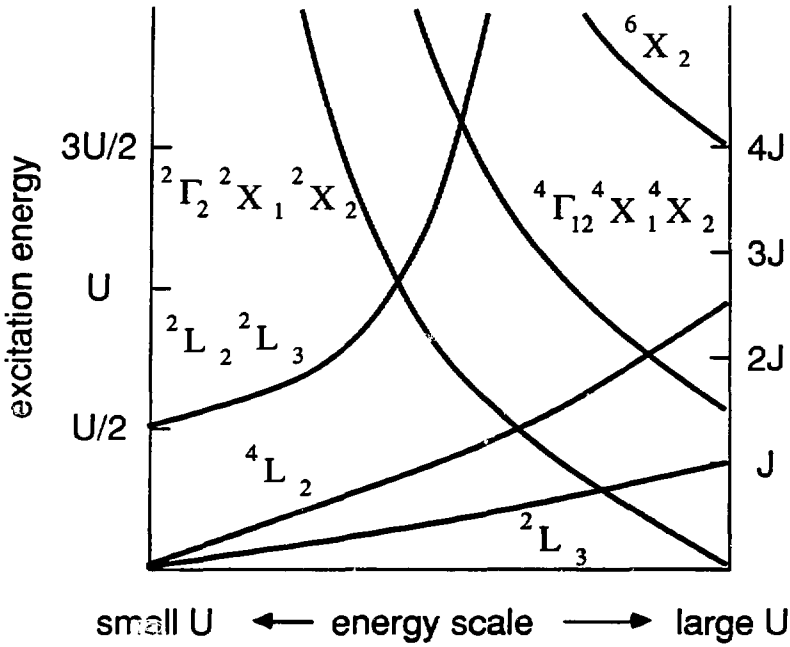

FIG. 2. Schematic representation of the ground- and low-lying states for 7 electrons. Here, the low-U ground states form high-U excited states, with completely different symmetries crossing over.

The situation becomes even more involved for 8 electrons, with small-U ground states becoming large-U excited states, and small-U low-lying excited states mixing with highly excited ones (the $^1\Gamma_1$ symmetry) to contribute to the large-U ground-state manifold.

Figure 4 shows the temperature dependence of the contribution of the various symmetries to the thermodynamic equilibrium state. It is seen there that even though the $^2L_3$ symmetry – the one obtained from the Gutzwiller projection – increases it contribution as temperature$T$ increases, the total spin of the cluster $\langle S(S+1)\rangle$ also increases, making the system more magnetic and therefore less well represented by a projection of a paramagnetic state.

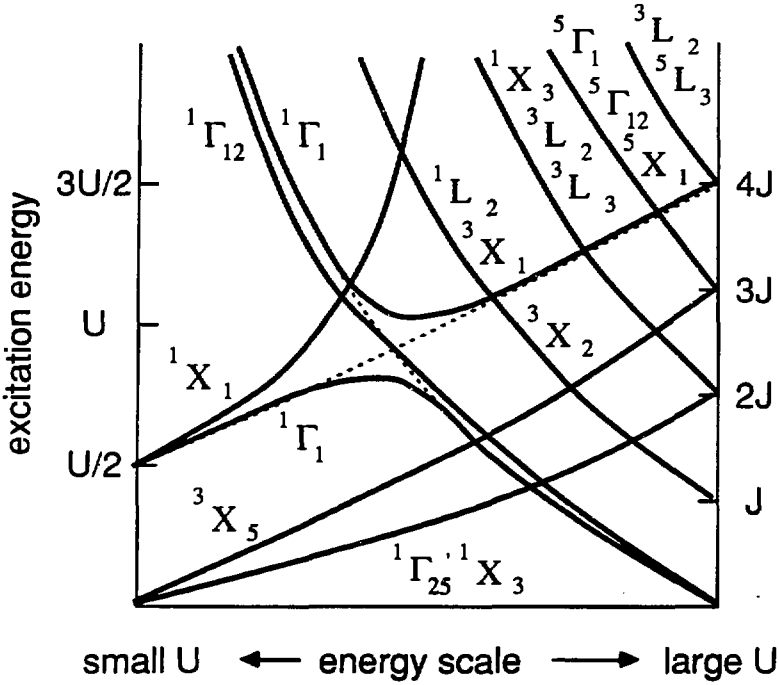

FIG. 3. Schematic representation of the ground- and low-lying states for 8 electrons. The trend as for 7 electrons continues, with many cross-overs, showing the Gutzwiller-projected states to be an inadequate description of the spectrum.

These observations lead one to conclude that the Gutzwiller projection technique alone is inadequate, that one requires in addition the minimization of the Coulomb expectation (2.5), but even so the description of the manifold of ground- and low-lying states is inadequate with the projected states alone.

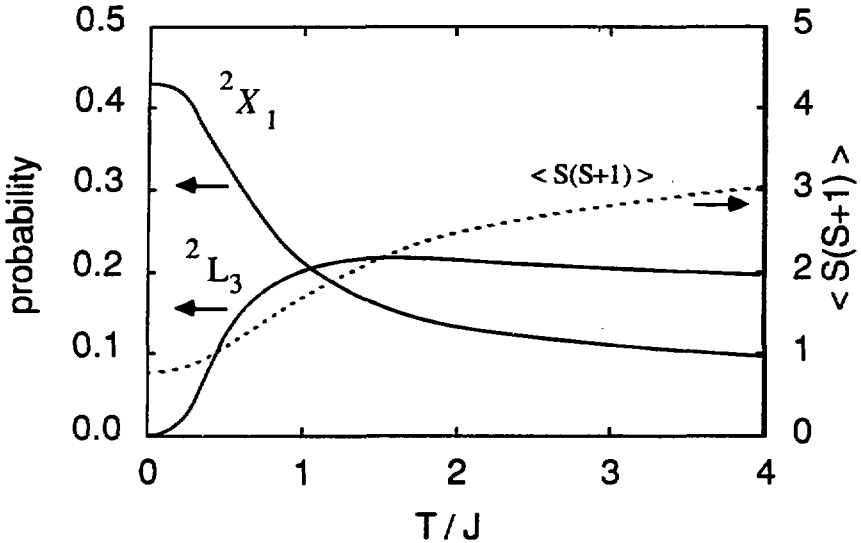

FIG. 4. The competing effects of superconductivity and magnetism are most aptly demonstrated by comparing the thermal probability behavior of the seven-electron superconducting candidate, $^2X_1$, with the Gutzwiller-projected state $^2L_3$, and the mean-spin-squared $<S(S+1)>$. The two states do not mix to form a broken-symmetry superconducting complex, the $^2X_1$ has a stronger correlation than the $^2L_3$, and the latter is washed out by an increasing ferromagnetic tendency.

IV. Results

A. Superconducting correlations

The eight-atom cluster, a finite system, is unable to exhibit the infinite-range correlation behavior of a superconducting transition, i.e. the important region in reciprocal space, the small **k** region, is inaccessible in this treatment, and it is possible that the finiteness might introduce artificial correlations[30]. However, it has been the belief of the present authors and others[9], that the study of the fluctuations towards superconductivity in these small systems could yield clues to the real phenomenon. Along those lines, and following the BCS formalism, one has an order parameter $\Delta(\mathbf{R},\mathbf{r})$, which corresponds to

the system forming Cooper pairs, of the form

$$\Delta(\mathbf{R},\mathbf{r}) = < \hat{\Delta}(\mathbf{R},\mathbf{r}) > = < \Psi(\mathbf{R} + \mathbf{r}/2)\, \Psi(\mathbf{R} - \mathbf{r}/2) > . \qquad (4.1)$$

where the system has a pair of normal electrons destroyed, with center of mass **R** and separation **r**. Following Hirsch[31], one may describe the correlation between the two electrons taking place by one of several modes, the usual on-site ($\mathbf{r} = 0$) spin-singlet coupling (SP) of the form :

$$c_{i\uparrow}\, c_{i\downarrow} , \qquad (4.2)$$

an extended-singlet pairing (SPX) :

$$c_{i\uparrow}\, c_{i+r\downarrow} - c_{i\downarrow}\, c_{i+r\downarrow} , \qquad (4.3)$$

and a (necessarily) extended spin-triplet pairing, as in liquid He^3, with components referred to as TP↑ (triplet parallel, $S_z = 1$), TP0 (antiparallel, $S_z = 0$), and TP↓ ($S_z = -1$) of forms :

$$c_{i\uparrow}\, c_{i+r\uparrow} , \qquad (4.4)$$

$$c_{i\uparrow}\, c_{i+r\downarrow} + c_{i\downarrow}\, c_{i+r\downarrow} , \qquad (4.5)$$

$$c_{i\downarrow}\, c_{i+r\downarrow} , \qquad (4.6)$$

respectively. In uniform systems the position **R** within the crystal has no intrinsic importance[32]. One may proceed directly to reciprocal **k**-space via Fourier transform:

$$\Delta(\mathbf{k}, \mathbf{r}) = \frac{1}{\Omega} \int e^{i\,\mathbf{k}\cdot\mathbf{R}}\, \Delta(\mathbf{R}, \mathbf{r})\, d^3R \; ; \qquad (4.7)$$

In finite systems, one may study the order parameter fluctuation,

$$S(\mathbf{k}, \mathbf{r}) = < \hat{\Delta}(\mathbf{k}, \mathbf{r})\, \hat{\Delta}^{\dagger}(\mathbf{k}, \mathbf{r}) > , \qquad (4.8)$$

which may be considered as a susceptibility to Cooper pair formation, i.e. the amount of phase space available to such a possible condensation process. The dependence on **r** yields

information on the spatial distribution of the correlation; the **k**-dependence yields the transport and coherence properties. As the object $S(\mathbf{k},\mathbf{r})$ is related quadratically to the order parameter, one may not speak of the spatial distribution of superconducting correlations, but only of the square. Thus triplet-spin pairings, which necessitate odd-parity (p,f, etc.) spatial wavefunctions, would have (s,d, etc.) even-parity $S(\mathbf{k},\mathbf{r})$ distributions, as do singlet pairings.

The quantity $S(\mathbf{k},\mathbf{r})$ is in fact the pair susceptibility defined by Lin *et al*[39,40], reformulated for the zero-temperature case when the ground-state is degenerate. The results reported here are the eigenvalues of the pair susceptibility within the ground-state manifold[41].

In the present context, with an eight-atom crystal, there are correspondingly 8 **k**-vectors in the Brillouin Zone, one at Γ (written as γ), three at X (x_1, x_2, x_3), and four at L (l_1, l_2, l_3, l_4). It can be shown then that the SPX and TP0 correlations, written in the **k** basis $a_{\mathbf{k}\sigma}$, take the form:

$$\hat{S}_{SPX/TP0}(\mathbf{k},\mathbf{r}) = \frac{2}{N}\left(1 \pm e^{i\,\mathbf{k}\cdot\mathbf{r}}\right)\left[N - n + \sum_{\kappa_1\kappa_2} e^{i(\kappa_1-\kappa_2)\cdot\mathbf{r}}\, a^{\dagger}_{\kappa_2\uparrow} a_{\kappa_1\uparrow} a^{\dagger}_{\kappa_2+\mathbf{k}\downarrow} a_{\kappa_1+\mathbf{k}\downarrow}\right] \tag{4.9}$$

One can immediately see that the pre-factor $(1 \pm e^{i\,\mathbf{k}\cdot\mathbf{r}})$ forces the correlations of these two forms to take on non-zero values in complementary parts of **k**-space, as the exponential term for this cluster takes on only values ± 1. Similarly, one can establish the expressions for the parallel triplet forms :

$$\hat{S}_{TP\sigma}(\mathbf{k},\mathbf{r}) = \frac{1}{2N}\left(1 - e^{i\,\mathbf{k}\cdot\mathbf{r}}\right)\left[2N - 3n_{\sigma} + \sum_{\kappa_1\kappa_2} e^{i(\kappa_1-\kappa_2)\cdot\mathbf{r}}\, a^{\dagger}_{\kappa_2\sigma} a_{\kappa_1\sigma} a^{\dagger}_{\kappa_2+\mathbf{k}\sigma} a_{\kappa_1+\mathbf{k}\sigma}\right] \tag{4.10}$$

where n_{σ} refers to the number of electrons aligned with σ.

There are six distinct first-nearest neighbors in this model (each represented twice, to give the 12 nearest neighbors of the fcc structure) and thus the information provided by

the six $S(\mathbf{k}, \mathbf{r} = \tau_1, \tau_2, \tau_3, \tau_5, \tau_6, \tau_7)$, where the τ_i's represent the associated displacement vectors, is just sufficient to expand unambiguously the spatial dependence in terms of the s and the five d functions zx, yz, xy, $x^2 - y^2$ and $3z^2 - r^2$. Within a normalization factor of $[(2l+1)/4\pi]^{1/2}$, the expansion coefficients can be given as :

$$A_s(\mathbf{k}) = \frac{1}{6}[S(\mathbf{k},\tau_1) + S(\mathbf{k},\tau_2) + S(\mathbf{k},\tau_3) + S(\mathbf{k},\tau_5) + S(\mathbf{k},\tau_6) + S(\mathbf{k},\tau_7)] \tag{4.11}$$

$$A_{zx}(\mathbf{k}) = \frac{1}{\sqrt{3}}[S(\mathbf{k},\tau_1) - S(\mathbf{k},\tau_5)] \tag{4.12}$$

$$A_{yz}(\mathbf{k}) = \frac{1}{\sqrt{3}}[S(\mathbf{k},\tau_2) - S(\mathbf{k},\tau_6)] \tag{4.13}$$

$$A_{xy}(\mathbf{k}) = \frac{1}{\sqrt{3}}[S(\mathbf{k},\tau_3) - S(\mathbf{k},\tau_7)] \tag{4.14}$$

$$A'_{x^2-y^2}(\mathbf{k}) = \frac{1}{\sqrt{3}}\{[S(\mathbf{k},\tau_1) + S(\mathbf{k},\tau_5)] - [S(\mathbf{k},\tau_2) + S(\mathbf{k},\tau_6)]\} \tag{4.15}$$

$$A_{3z^2-r^2}(\mathbf{k}) = \frac{1}{3}[S(\mathbf{k},\tau_1) + S(\mathbf{k},\tau_2) - 2S(\mathbf{k},\tau_3) + S(\mathbf{k},\tau_5) + S(\mathbf{k},\tau_6) - 2S(\mathbf{k},\tau_7)] \tag{4.16}$$

For an occupation of 7 electrons the true heavy-fermion ground-state manifold – comprising the symmetries ${}^2\Gamma_2$, ${}^2X_1$ and ${}^2X_2$ – and the low-lying excited states of symmetry ${}^2L_3$, are allowed to mix by (4.9) or (4.10), and the patterns of mixing are presented in Tables II and IV, with the actual values of the correlation matrices presented in Tables III and V, respectively. Thus, any trends towards the symmetry-breaking of a superconducting transition can be detected.

Qualitatively, the first thing to note is that the excited ${}^2L_3$ states do not mix with any of the ground-state symmetries for any of the spin-coupling modes. The only mixing occurs between the three pairs of ${}^2X_1$ and ${}^2X_2$.

TABLE II. Correlation mixing pattern for the 7-electron heavy-fermion ground-state manifold

	singlet pairing							triplet pairing						
	γ	x_1	x_2	x_3	l_1	l_2	l_3	l_4	x_1	x_2	x_3	l_1	l_2	l_3	l_4
τ_1 $\vert^2T_2>$	r	r					r	r		r	r		r	r	
$\vert^2X_1$ (a)$>\vert^2X_2$ (a)$>$	A_0	A_0					A_0	A_0		A_0	A_0		A_0	A_0	
$\vert^2X_1$ (b)$>\vert^2X_2$ (b)$>$	B_+	B_+					B_+	B_+		B_+	B_+		B_+	B_+	
$\vert^2X_1$ (c)$>\vert^2X_2$ (c)$>$	B_-	B_-					B_-	B_-		B_-	B_-		B_-	B_-	
τ_2 $\vert^2T_2>$	r		r			r		r	r		r	r		r	
$\vert^2X_1$ (a)$>\vert^2X_2$ (a)$>$	B_-		B_-			B_-		B_-	B_-		B_-	B_-		B_-	
$\vert^2X_1$ (b)$>\vert^2X_2$ (b)$>$	A_0		A_0			A_0		A_0	A_0		A_0	A_0		A_0	
$\vert^2X_1$ (c)$>\vert^2X_2$ (c)$>$	B_+		B_+			B_+		B_+	B_+		B_+	B_+		B_+	
τ_3 $\vert^2T_2>$	r			r		r	r		r	r		r			r
$\vert^2X_1$ (a)$>\vert^2X_2$ (a)$>$	B_+			B_+		B_+	B_+		B_+	B_+		B_+			B_+
$\vert^2X_1$ (b)$>\vert^2X_2$ (b)$>$	B_-			B_-		B_-	B_-		B_-	B_-		B_-			B_-
$\vert^2X_1$ (c)$>\vert^2X_2$ (c)$>$	A_0			A_0		A_0	A_0		A_0	A_0		A_0			A_0
τ_5 $\vert^2T_2>$	r	r			r	r				r	r			r	r
$\vert^2X_1$ (a)$>\vert^2X_2$ (a)$>$	A_0	A_0			A_0	A_0				A_0	A_0			A_0	A_0
$\vert^2X_1$ (b)$>\vert^2X_2$ (b)$>$	B_+	B_+			B_+	B_+				B_+	B_+			B_+	B_+
$\vert^2X_1$ (c)$>\vert^2X_2$ (c)$>$	B_-	B_-			B_-	B_-				B_-	B_-			B_-	B_-
τ_6 $\vert^2T_2>$	r		r		r		r		r		r		r		r
$\vert^2X_1$ (a)$>\vert^2X_2$ (a)$>$	B_-		B_-		B_-		B_-		B_-		B_-		B_-		B_-
$\vert^2X_1$ (b)$>\vert^2X_2$ (b)$>$	A_0		A_0		A_0		A_0		A_0		A_0		A_0		A_0
$\vert^2X_1$ (c)$>\vert^2X_2$ (c)$>$	B_+		B_+		B_+		B_+		B_+		B_+		B_+		B_+
τ_7 $\vert^2T_2>$	r			r	r			r	r	r			r	r	
$\vert^2X_1$ (a)$>\vert^2X_2$ (a)$>$	B_+			B_+	B_+			B_+	B_+	B_+			B_+	B_+	
$\vert^2X_1$ (b)$>\vert^2X_2$ (b)$>$	B_-			B_-	B_-			B_-	B_-	B_-			B_-	B_-	
$\vert^2X_1$ (c)$>\vert^2X_2$ (c)$>$	A_0			A_0	A_0			A_0	A_0	A_0			A_0	A_0	

TABLE III. Values for the couplings of the heavy-fermion ground-state manifold for 7 electrons.

coupling	r	A_0	$B_\pm$
SPX	$\frac{7}{4}$	$\begin{bmatrix} \frac{11}{4} & 0 \\ 0 & \frac{19}{12} \end{bmatrix}$	$\begin{bmatrix} \frac{5}{4} & \pm\frac{7\sqrt{2}}{12} \\ \pm\frac{7\sqrt{2}}{12} & \frac{11}{6} \end{bmatrix}$
TP0	$\frac{13}{12}$	$\begin{bmatrix} \frac{3}{4} & 0 \\ 0 & \frac{41}{36} \end{bmatrix}$	$\begin{bmatrix} \frac{5}{4} & \pm\frac{7\sqrt{2}}{36} \\ \pm\frac{7\sqrt{2}}{36} & \frac{19}{18} \end{bmatrix}$
TP↑	$\frac{1}{6}$	$\begin{bmatrix} \frac{1}{6} & 0 \\ 0 & \frac{13}{36} \end{bmatrix}$	$\begin{bmatrix} \frac{1}{2} & \pm\frac{\sqrt{2}}{9} \\ \pm\frac{\sqrt{2}}{9} & \frac{5}{12} \end{bmatrix}$
TP↓	$\frac{7}{12}$	$\begin{bmatrix} \frac{7}{12} & 0 \\ 0 & \frac{7}{9} \end{bmatrix}$	$\begin{bmatrix} \frac{3}{4} & \pm\frac{\sqrt{2}}{12} \\ \pm\frac{\sqrt{2}}{12} & \frac{23}{36} \end{bmatrix}$

Quantitative results are given in Table VI. Here all correlation strengths are normalized to one, i.e. divided by the maximal eigenvalue over all possible 11440 states. For SPX coupling one notices a considerable enhancement from the almost non-interacting to the Gutzwiller-projected state, but the enhancement from the latter to the true ground state – of different symmetry – is approximately the same; in other words, the difference between the non-interacting and true states is twice as large as the Gutzwiller method would yield. One sees the same trend, albeit more weakly, for the triplet TP0 and TP↑ modes. They both favor a broken-symmetry state. Because these correlations were calculated for the $S_z = +1/2$ states – four electrons with spin up, three electrons with spin down – the TP↓ mode is strongly disfavored, as seen also in Table VI.

TABLE IV. Correlation mixing pattern for the 7-electron Gutzwiller-projected manifold in the large U limit.

		singlet pairing							triplet pairing						
		γ	x_1	x_2	x_3	l_1	l_2	l_3	l_4	x_1	x_2	x_3	l_1	l_2	l_3	l_4
τ_1	$\|^2L_3(1)>\|^2L_3(2)>$	A_0	A_0					A_0	A_0		A_0	A_0		A_0	A_0	
	$\|^2L_3(3)>\|^2L_3(4)>$	A_0	A_0					A_0	A_0		A_0	A_0		A_0	A_0	
	$\|^2L_3(5)>\|^2L_3(6)>$	B_-	B_-					B_-	B_-		B_+	B_+		B_+	B_+	
	$\|^2L_3(7)>\|^2L_3(8)>$	B_-	B_-					B_-	B_-		B_+	B_+		B_+	B_+	
τ_2	$\|^2L_3(1)>\|^2L_3(2)>$	A_+		A_+			A_+		A_+	A_-		A_-		A_-		
	$\|^2L_3(3)>\|^2L_3(4)>$	B_-		B_-			B_-		B_-	B_+		B_+		B_+		
	$\|^2L_3(5)>\|^2L_3(6)>$	A_0		A_0			A_0		A_0	A_0		A_0		A_0		
	$\|^2L_3(7)>\|^2L_3(8)>$	B_+		B_+			B_+		B_+	B_-		B_-		B_-		
τ_3	$\|^2L_3(1)>\|^2L_3(2)>$	A_-			A_-			A_-	A_-	A_+		A_+			A_+	
	$\|^2L_3(3)>\|^2L_3(4)>$	B_+			B_+			B_+	B_+	B_-		B_-			B_-	
	$\|^2L_3(5)>\|^2L_3(6)>$	B_+			B_+			B_+	B_+	B_-		B_-			B_-	
	$\|^2L_3(7)>\|^2L_3(8)>$	A_0			A_0			A_0	A_0	A_0		A_0			A_0	
τ_5	$\|^2L_3(1)>\|^2L_3(2)>$	B_0	B_0			B_0	B_0				B_0	B_0				B_0 B_0
	$\|^2L_3(3)>\|^2L_3(4)>$	B_0	B_0			B_0	B_0				B_0	B_0				B_0 B_0
	$\|^2L_3(5)>\|^2L_3(6)>$	A_-	A_-			A_-	A_-				A_+	A_+				A_+ A_+
	$\|^2L_3(7)>\|^2L_3(8)>$	A_-	A_-			A_-	A_-				A_+	A_+				A_+ A_+
τ_6	$\|^2L_3(1)>\|^2L_3(2)>$	B_+		B_+		B_+		B_+		B_-		B_-		B_-		B_-
	$\|^2L_3(3)>\|^2L_3(4)>$	A_-		A_-		A_-		A_-		A_+		A_+		A_+		A_+
	$\|^2L_3(5)>\|^2L_3(6)>$	B_0		B_0		B_0		B_0		B_0		B_0		B_0		B_0
	$\|^2L_3(7)>\|^2L_3(8)>$	A_+		A_+		A_+		A_+		A_-		A_-		A_-		A_-
τ_7	$\|^2L_3(1)>\|^2L_3(2)>$	B_-			B_-	B_-			B_-	B_+ B_+			B_+ B_+			
	$\|^2L_3(3)>\|^2L_3(4)>$	A_+			A_+	A_+			A_+	A_- A_-			A_- A_-			
	$\|^2L_3(5)>\|^2L_3(6)>$	A_+			A_+	A_+			A_+	A_- A_-			A_- A_-			
	$\|^2L_3(7)>\|^2L_3(8)>$	B_0			B_0	B_0			B_0	B_0 B_0			B_0 B_0			

TABLE V. Values for the couplings of the heavy-fermion Gutzwiller manifold for 7 electrons.

coupling	A_0	$A_\pm$	B_0	$B_\pm$
SPX	$\begin{bmatrix} \frac{9}{4} & 0 \\ 0 & \frac{17}{20} \end{bmatrix}$	$\begin{bmatrix} \frac{6}{5} & \pm\frac{7\sqrt{3}}{20} \\ \pm\frac{7\sqrt{3}}{20} & \frac{19}{10} \end{bmatrix}$	$\begin{bmatrix} \frac{33}{20} & 0 \\ 0 & \frac{19}{12} \end{bmatrix}$	$\begin{bmatrix} \frac{8}{5} & \pm\frac{\sqrt{3}}{60} \\ \pm\frac{\sqrt{3}}{60} & \frac{49}{30} \end{bmatrix}$
TP0	$\begin{bmatrix} \frac{11}{12} & 0 \\ 0 & \frac{83}{60} \end{bmatrix}$	$\begin{bmatrix} \frac{19}{15} & \pm\frac{7\sqrt{3}}{60} \\ \pm\frac{7\sqrt{3}}{60} & \frac{31}{30} \end{bmatrix}$	$\begin{bmatrix} \frac{67}{60} & 0 \\ 0 & \frac{41}{36} \end{bmatrix}$	$\begin{bmatrix} \frac{17}{15} & \pm\frac{\sqrt{3}}{180} \\ \pm\frac{\sqrt{3}}{180} & \frac{101}{90} \end{bmatrix}$
TP↑	$\begin{bmatrix} \frac{7}{20} & 0 \\ 0 & \frac{19}{36} \end{bmatrix}$	$\begin{bmatrix} \frac{29}{60} & \pm\frac{2\sqrt{3}}{45} \\ \pm\frac{2\sqrt{3}}{45} & \frac{71}{180} \end{bmatrix}$	$\begin{bmatrix} \frac{9}{20} & 0 \\ 0 & \frac{73}{180} \end{bmatrix}$	$\begin{bmatrix} \frac{5}{12} & \mp\frac{\sqrt{3}}{90} \\ \mp\frac{\sqrt{3}}{90} & \frac{79}{180} \end{bmatrix}$
TP↓	$\begin{bmatrix} \frac{17}{30} & 0 \\ 0 & \frac{77}{90} \end{bmatrix}$	$\begin{bmatrix} \frac{47}{60} & \pm\frac{13\sqrt{3}}{180} \\ \pm\frac{13\sqrt{3}}{180} & \frac{23}{36} \end{bmatrix}$	$\begin{bmatrix} \frac{2}{3} & 0 \\ 0 & \frac{11}{15} \end{bmatrix}$	$\begin{bmatrix} \frac{43}{60} & \pm\frac{\sqrt{3}}{60} \\ \pm\frac{\sqrt{3}}{60} & \frac{41}{60} \end{bmatrix}$

The evidence appears to favor, in the large-U limit, the extended-singlet over the triplet pairings, a result noted before in the literature[31,33]. However, the critical result here is that *the Gutzwiller-projected state, has neither the correlation strength of the true ground state, nor in any way participates with the ground state to break symmetry and lead towards Cooper pair formation*. Having decided on the ${}^2X_1$ state in the SPX coupling mode as the leading superconducting candidate, one can now apply (4.11-.16) to describe its *s-d*-decomposition, the results of which are presented in Table VII. One can see quite clearly the degree of anisotropy, both in real and in **k**-space.

TABLE VI. Normalized maximal correlation values for 7-electron states at nearest-neighbor separation.

type/# states	SPX	TP0	TP ↑	TP ↓
all states $t, T, U = 0$ 11440	1.000	1.000	1.000	1.000
almost non-interacting $U = 0^+$ 56	0.281 $\|^2L_3>$	0.172 $\|^2L_3>$	0.167 $\|^2L_3>$	0.479 $\|^2L_3>$
Gutzwiller state $U = \infty$ 28	0.313 $\|^2L_3>$	0.173 $\|^2L_3>$	0.176 $\|^2L_3>$	0.428 $\|^2L_3>$
Heavy-fermion state $U = \infty$ 14	0.344 $\|^2X_1>$	0.181 $0.816\|^2X_1> - 0.577\|^2X_2>$	0.207 $0.793\|^2X_1> - 0.610\|^2X_2>$	0.412 $0.845\|^2X_1> - 0.536\|^2X_2>$
Atomic limit $t, T = 0, U = \infty$ 1024	0.438	0.438	0.667	0.500

TABLE VII. Unnormalized s and d expansion of correlations for the maximally-correlated $|^2X_1>$ state, polarized in the x-direction. The degree of anisotropy is quite notable.

	γ	x_1	x_2	x_3	l_1	l_2	l_3	l_4
s	1.750	0.917	0.417	0.417	0.875	0.875	0.875	0.875
zx	0	0	0	0	-1.588	-1.588	1.588	1.588
yz	0	0	0	0	-0.722	0.722	-0.722	0.722
xy	0	0	0	0	-0.722	0.722	0.722	-0.722
$x^2 - y^2$	1.732	3.175	-1.443	0	0.866	0.866	0.866	0.866
$3z^2 - r^2$	1.000	1.833	0.833	-1.667	0.500	0.500	0.500	0.500

B. BCS wavefunction for a finite cluster

In 1957, Bardeen, Cooper and Schrieffer wrote their celebrated paper[34] describing the superconducting-state function:

$$|\Psi_{BCS}> = \prod_{k} (u_k + v_k a^{\dagger}_{k\uparrow} a^{\dagger}_{-k\downarrow}) |0>, \qquad (4.17)$$

where the coefficients u_k and v_k are expressed as[35] :

$$u_k^2 = \frac{1}{2} \left[1 + \frac{\varepsilon_k}{\sqrt{\varepsilon_k^2 + \Delta_k^2}} \right] \qquad (4.18)$$

$$v_k^2 = \frac{1}{2} \left[1 - \frac{\varepsilon_k}{\sqrt{\varepsilon_k^2 + \Delta_k^2}} \right] \qquad (4.19)$$

Here ε_k refers to the one-electron energy of **k**, measured from the Fermi energy, whereas Δ_k represents the corresponding superconducting energy-gap parameter. Historically, the fears that the BCS equation (4.17) (i) did not conserve the number of particles, and (ii) in the thermodynamic limit the predicted wave function was orthogonal to the true ground state, were eventually resolved and the approach has become the cornerstone of the theory of superconductivity.

Recently Gros[36] has examined the consequence of projecting the BCS state onto a fixed number of electrons in a finite cluster, and then applying the Gutzwiller projection to remove any doubly-occupied states. This approach has the advantage of allowing the system in question to reveal its own preferred coupling mode, rather than attempting to match the correlation to those of given models.

In the present situation, given the advantage of considering an even number of electrons, it is convenient to choose the eight-site cluster with six electrons. Thus, the

wavefunction of (4.17) would take on the (unnormalized) form:

$$|\Psi_{BCS}> = \sum_{\kappa_0,\ldots,\kappa_7} v_{\kappa_0} v_{\kappa_1} v_{\kappa_2} u_{\kappa_3} u_{\kappa_4} u_{\kappa_5} u_{\kappa_6} u_{\kappa_7} a^{\dagger}_{\kappa_0\uparrow} a^{\dagger}_{\kappa_0\downarrow} a^{\dagger}_{\kappa_1\uparrow} a^{\dagger}_{\kappa_1\downarrow} a^{\dagger}_{\kappa_2\uparrow} a^{\dagger}_{\kappa_2\downarrow} |0> \tag{4.20}$$

where κ_0, κ_1 and κ_2 are the occupied electron-pair states and κ_3 through κ_7 are the empty one-electron states. Equation (4.20) is considered here in two limits: the almost-non-interacting (small U) and the Gutzwiller-projected strongly-interacting (large U) extremes. For $U = 0$, there are 56 states corresponding to occupied triplets of **k**-pairs (3 chosen from 8), while in the infinite-U limit, the Gutzwiller projection (2.6) reduces these to 28 possible states.

For U vanishingly small, if one restricts the choices for the triplets of occupied **k**-pairs to the γ–pair, and two of the four l -pairs, then one obtains directly a state with energy contributions from (2.3) and (2.4) of $(-24t + 12T)$, which corresponds to the vanishing–U ground state. This is equivalent to setting

$$v_{\gamma} = u_{x_1} = u_{x_2} = u_{x_3} = 1, \quad u_{\gamma} = v_{x_1} = v_{x_2} = v_{x_3} = 0 , \tag{4.21}$$

which amounts to setting the energy-gap parameters, $\Delta_{\gamma} = \Delta_{x_i} = 0$. This leaves the four (u_l, v_l) pairs free to reduce the Coulomb energy (2.5).

Without the constraint of the BCS variational wavefunction, the six functions, denoted by the $(\mathbf{k}\uparrow, \mathbf{k}\downarrow)$ pairings γl_1, γl_2, γl_3, γl_4, $l_2 l_3$, $l_2 l_4$, and $l_3 l_4$, form representations of ${}^1\Gamma_1$, ${}^1\Gamma_{12}$ and ${}^1\Gamma_{15}'$, with expectations, $13U/8$, $7U/8$ and $9U/8$, respectively. It should be noted that the ${}^1\Gamma_1$ and ${}^1\Gamma_{15}'$ states correspond exactly to those listed among the low-lying states in Table I, while the ${}^1\Gamma_{12}$ state overlaps only partially the true ground state.

It can be shown that the Coulomb energy expectation value, with the BCS state, is

$$<H_C> = U \{ 1 + \frac{1}{8}[(\sum v_p v_q u_r u_s)^2 - 6 u_{l_1} v_{l_1} u_{l_2} v_{l_2} u_{l_3} v_{l_3} u_{l_4} v_{l_4}] / \sum v_p^2 v_q^2 u_r^2 u_s^2 \} \tag{4.22}$$

where the summations are over the four l-states. This is not a simple problem in

optimization. However, one can argue, by symmetry, that the optimum solutions will lie on loci of high symmetry. If, for example, one sets all the u's and v's constant, which would amount to s-wave pairing, one obtains precisely the ${}^1\Gamma_1$ state. Thus, if one were to use the BCS wavefunction for attractive potentials, where $U < 0$, one would obtain the correct ground state.

To obtain the minimum of (4.22) for $U > 0$, if one calls this minimum yU, sets any two pairs of the (u_i, v_i)'s equal (three such combinations, e.g. $u_{l_1}=u_{l_3}=u_1$, $u_{l_2}=u_{l_4}=u_2$, and similarly for the v's), and introduces a variable $x=u_1v_2/u_2v_1$, one obtains :

$$(1+x^4)(8y-9)-8(x^3+x)+x^2(32y-44)=0. \quad (4.23)$$

Upon minimization with respect to y (4.23) yields an extremum with the unusual value

$$y = \frac{17\sqrt{3}-39}{8\sqrt{3}-24} = 0.941987298 \quad (4.24)$$

which is achieved for

$$x = \pm\sqrt{\frac{\sqrt{3}}{2}-\sqrt{1+\frac{\sqrt{3}}{2}}} = (-2.296630),\ (-0.435420) \quad (4.25)$$

Clearly, this solution is a compromise. Although it minimizes the band energy, it does not reach the minimum $7U/8$ Coulomb energy accessible with the full BCS set (4.20). And in fact it represents only a 59.15% overlap with the true ${}^1\Gamma_{12}$ ground-state, of expection $3U/4$.

For infinite U, the one-electron orbital energies cease to have meaning. However, if one seeks a solution with minimal nearest-neighbor band energy (2.2), then one finds a minimal manifold corresponding to the choices for (u_i, v_i) of (4.21). Without further BCS contraints, this manifold has expectation values for (2.2) of $(-32t/5)$, $(-96t/11)$ and $(-272t/23)$ [equal to $(-6.4t)$, $(-8.727t)$, $(-11.826t)$, respectively] corresponding respectively to the symmetries ${}^1\Gamma_1$, ${}^1\Gamma_{25}$ and ${}^1\Gamma_{12}$. This results compares with the true

ground-state energy of $(-12t)$. The minimization problem becomes somewhat more complicated than for infinitesimal U, of the form :

$$<H_{1nn}> = -8t \frac{23\sum v_p^2 v_q^2 u_r^2 u_s^2 - 5(\sum v_p v_q u_r u_s)^2 + 66 u_{l_1} v_{l_1} u_{l_2} v_{l_2} u_{l_3} v_{l_3} u_{l_4} v_{l_4}}{17\sum v_p^2 v_q^2 u_r^2 u_s^2 - 3(\sum v_p v_q u_r u_s)^2 + 36 u_{l_1} v_{l_1} u_{l_2} v_{l_2} u_{l_3} v_{l_3} u_{l_4} v_{l_4}} \tag{4.26}$$

Again, as in the infinitesimal–U limit, the maximum ${}^1\Gamma_1$ value may be achieved in an s-wave pairing. The minimal value possible, however, achieved for $x = u_1 v_2 / u_2 v_1 = -1$, is $(-736t/63)$ [equal to $(-11.683t)$].

To study the superconducting energy-gap parameters, one may expand their distributions, as a function of **k**, in terms of functions following the symmetries *s*, *d*, etc. [even parity only is considered with the singlet-spin mode of (4.17)]. With eight **k**-vectors in this small cluster, one has a basis of 8 **k**-functions to work with, and one can obtain, as Sigrist and Rice do[37] for the high-T_c square lattice, the functions compatible with the lattice. For the energy-gap parameters among the l's, this amounts to the following contributions of *d*-functions:

$$d_{xy} = \Delta_{l_1} - \Delta_{l_2} - \Delta_{l_3} + \Delta_{l_4} \tag{4.27}$$

$$d_{yz} = \Delta_{l_1} + \Delta_{l_2} - \Delta_{l_3} - \Delta_{l_4} \tag{4.28}$$

$$d_{zx} = \Delta_{l_1} - \Delta_{l_2} + \Delta_{l_3} - \Delta_{l_4} \tag{4.29}$$

and in addition the *s*-like function

$$s = \Delta_{l_1} + \Delta_{l_2} + \Delta_{l_3} + \Delta_{l_4} \tag{4.30}$$

Thus, one sees a definite *d*-character for the BCS state. However, it is an unsatisfactory approximation, in both low- and high-U limits: the expectation values of the total energy are not close to the true ground-state energy.

C. Magnetic correlations

As the fcc structure is composed of triangular rings of bonds, the antiferromagnetic

coupling (2.4) is frustrated in its attempt to saturate the system. Thus the interaction of the band structure with the spin geometry, a possible resolution of the RVB proposal, is of great interest. In this cluster, there are three reasonable spin-spin correlations to examine – on-site, first and second neighbors – of forms

$$L_0 = \frac{1}{N} \sum_i S_{iz}^2 \qquad (4.31)$$

$$L_1 = \frac{1}{N} \sum_{<ij>_{1nn}} S_{iz} S_{jz} \qquad (4.32)$$

$$L_2 = \frac{1}{N} \sum_{<ij>_{2nn}} S_{iz} S_{jz} \qquad (4.33)$$

respectively, N being the number of sites. It should be pointed out that, within the eight-atom cluster, a sum rule exists,

$$L_0 + 2L_1 + 2L_2 = S_z^2 / 16, \qquad (4.34)$$

where S_z is the z-projection of the spin. Furthermore, in the infinite-U limit, one has L_0 tending upwardly to $n/4N$, where n is the number of electrons

The results for the ground- and low-lying states for 6,7 and 8 electrons in the small and high U limits are presented in Table VIII, along with the extreme values possible for each configuration.

Very clear trends can be gathered from the table. First, at both the low- and high-U limits, the ground state is most strongly nearest-neighbor antiferromagnetic, with L_1 increasing monotonically with excitation energy. The exact opposite can be said of the second-nearest-neighbor behavior. Also, as a function of U, one sees that L_0 and L_2 increase, and L_1 decreases.

Thus, the tendencies at both extremes is towards antiferromagnetism, and states which at low-U may be the ground states, may find themselves overtaken, at high-U, by completely different electronic configurations which are more antiferromagnetic.

TABLE VIII. Magnetic correlations for 6,7 and 8-electron ground and low-lying minimal-spin states in the low and high U limits.

	small U				large U		
state(s)	L_0	L_1	L_2	state(s)	L_0	L_1	L_2
6 electrons							
maxima	0.0000	-0.1563	-0.0938				
minima	0.1875	0.4063	0.0938				
$^1\Gamma_{12}$	0.1484	-0.0859	0.0117	$^1\Gamma_{12}$	0.1875	-0.1146	0.0208
$^1\Gamma_{15}\,^1X_3\,^1X_5$	0.1172	-0.0547	-0.0039				
$^1\Gamma_1\,^1\Gamma_{12}\,^1X_1$	0.0859	0.0234	-0.0195				
7 electrons							
maxima	0.0313	-0.1875	-0.0313				
minima	0.2188	0.5625	0.0938				
$^2L_3$	0.1367	-0.0644	-0.0020	$^2\Gamma_2\,^2X_1\,^2X_2$	0.2188	-0.1250	0.0313
$^2L_2\,^2L_3$	0.1211	-0.0508	-0.0098	$^2L_3$	0.2188	-0.0833	0.0104
8 electrons							
maxima	0.0000	-0.2500	-0.1250				
minima	0.2500	0.7500	0.1250				
$^1\Gamma_{25}\,^1X_3$	0.1328	-0.0547	-0.0117	$^1\Gamma_1\,^1\Gamma_{12}$	0.2500	-0.1667	0.0417
$^1\Gamma_{25}\,^1X_1$	0.1016	-0.0234	-0.0273	$^1L_2$	0.2500	-0.1250	0.0000
				$^1\Gamma_{25}\,^1X_3$	0.2500	-0.0833	-0.0417

IV. Conclusions

A model for superconducting and magnetic behavior in a heavy-fermion system, one comprising an eight-atom cluster in the fcc structure with occupancies of 6,7 and 8 electrons, was examined. A critique of ongoing work is obtained. Although too small a cluster to observe the important long-range correlations present in superconducting transitions, it is the opinion of the authors that this smallness, allowing a full description of

the model system, more than makes up for this liability, while other approaches, such as Monte Carlo[9,36] may be leaving subtle gaps in the true picture.

It was observed that the Gutzwiller projection[26], which obtains a heavy-fermion wavefunction from the non-interacting function by projecting out any part containing any doubly-occupied atoms, is an inadequate description of the ground state and low-lying excitations. This inadequacy becomes more pronounced as one nears the half-filled limit, which is where all the interesting heavy-fermion behavior occurs. The amendment to the projection proposed here, that is, *to take the linear combination of non-interacting ground state wavefunctions which minimizes the Coulomb repulsion*, acts to achieve the optimum state from within that restricted manifold.

The model demonstrates a trend towards superconductivity which is of extended-spin-singlet form and highly anisotropic, with significant s- and d-wave mixing. No significant trends towards symmetry-breaking was noted, indicating possibly that the large-U Hubbard mechanism is not, of itself, responsible for superconductivity; rather, it might be said that, at best, it makes phase space available for another mechanism, such as the standard phonon coupling, to allow superconductivity to proceed. In light of recent evidence denying any magnetic activity in the Yttrium compounds[38], this may be an optimistic assessment.

The BCS trial state, restricted to the small cluster, describes states of considerable d-character, and was shown to be inadequate both in the small and large U regimes, removed considerably from the true ground state. For small attractive U, however, the BCS wavefunction corresponded exactly to the true ground state.

The magnetic correlations showed that this model is remarkably good for antiferromagnetic behavior, with strong antiferromagnetic ordering in both the small and large U limits.

The author recognizes work criticizing the validity of calculations of short-range correlations in small-cluster models, with errors induced by finite-size effects[30] Finite-size effects may also account for a large measure of the discrepancy between the Gutzwiller-

projected and the true ground state. It is possible that the projection process, applied to increasingly larger clusters, may approach a total description of the ground-state behavior, but this is a conjecture which should be scrupulously examined. In the one-dimensional case[29], the results indicate that the approach is not satisfactory in the atomic limit. The present approach, as detailed in previous work[20], does not scale well, so the question may remain open for some time to come.

V. References

[1]G.R. Stewart, Rev. Mod. Phys. **56**, 755 (1984).

[2]F. Steglich, in *Theory of Heavy Fermions and Valence Fluctuations*, edited by K. Kasuya and T. Saso, Springer Series in Solid State Sciences, Vol. 62 (Springer, New York, 1985), p.23.

[3]W. Buckel and W. Weber, *Superconductivity in d- and f-Band Metals 1982*, (Kenforschungzentrum Karlsruhe GmbH, Karslruhe, 1982).

[4]H. Suhl and M.B. Maple, *Superconductivity in d- and f-Band Metals*, (Academic Press, New York, 1980).

[5]T.M. Rice, Z. Phys. B. **67** , 141 (1987).

[6]C. Gros, R. Joynt and T.M. Rice, Phys. Rev. B. **36**, 381 (1987).

[7]P. Fulde, J. Keller and G. Zwicknagl, *Theory of Heavy Fermion Systems*, (Max Planck Inst., Stuttgart), 1987.

[8]J.E. Hirsch, Phys. Rev. Lett. **59**, 228 (1987).

[9]C. Gros, R. Joynt and T.M. Rice, Z. Phys. B. **68**, 425 (1987).

[10]J. Hubbard, Proc. R. Soc. London, Ser A **276**, 238 (1963); **277**, 237 (1964); **281**, 401 (1964); **285**, 542 (1965); **296**, 82 (1966); **296**, 100 (1967).

[11]P.W. Anderson, Phys. Rev., **124**, 41 (1961).

[12]R.H. Victora and L.M. Falicov, Phys. Rev. B **30**, 1695 (1984).

[13]R.H. Victora and L.M. Falicov, Phys. Rev. Lett. **55**, 1140 (1985).

[14]A. Reich and L.M. Falicov, Phys. Rev. B **34**, 6752 (1986).

[15]J.C. Parlebas, R.H. Victora, and L.M. Falicov, J. Phys. (Paris) **47**, 1029 (1986).

[16]E.C. Sowa and L.M. Falicov, Phys. Rev. B **35**, 3765 (1987).

[17]J. Callaway, D.P. Chen and R. Tang, Z. Phys. D **3**, 91 (1986); Phys. Rev. B. **35**, 3705 (1987).

[18]J. Callaway, Phys. Rev. B. **35**, 8723 (1987).

[19]A. Reich and L.M. Falicov, Phys. Rev. B. **36**, 3117 (1987).

[20]A. Reich and L.M. Falicov, Phys. Rev. B **37**, [to appear] (1988).

[21]P.W. Anderson, Science **235**, 1196 (1987).

[22]P.W. Anderson, in *Solid State Physics*, edited by F.Seitz and D. Turnbull, (Academic Press, New York, 1963) Vol. 14, p.99.

[23]A.B. Harris and R.V. Lange, Phys. Rev. **157**, 295 (1967).

[24]J.R. Schrieffer and P.A. Wolff, Phys. Rev. **149**, 491 (1966).

[25]L. P. Bouckaert, R. Smoluchowsky and E. Wigner, Phys. Rev. **50**, 58 (1936).

[26]M.C. Gutzwiller, Phys. Rev. A. **137**, 1726 (1965).

[27]P. Coleman, Phys. Rev. B. **29**, 3035 (1984).

[28]C.S. Wang, M.R. Norman, R.C. Albers, A.M.Boring, W.E. Pickett, H. Krakauer, and N.E. Christensen, Phys. Rev. B. **35**, 7260 (1987).

[29]F. Gebhard and D. Vollhardt, Phys. Rev. Lett. **59**, 1472 (1987).

[30]G. Stollhoff, Z. Phys. B. **69**, 61 (1987).

[31]J.E. Hirsch, Phys. Rev. Lett. **54**, 1317 (1985).

[32]It should be remembered that the **R** dependence, which enters explicitly into the Landau-Ginzburg equations, is used to describe vortices, magnetic impurities, surfaces, interfaces, and other features on the scale of the correlation length, clearly outside the reach of the present treatment.

[33]D.J. Scalapino, E. Loh, Jr. and J.E. Hirsch, Phys. Rev. B. **34**, 8190 (1986).

[34]J. Bardeen, L.N. Cooper and J.R. Schrieffer, Phys. Rev. **108** 1175 (1957).

[35]C. Kittel, *Quantum Theory of Solids*, (Wiley, New York, 1963), p. 166.

[36]C. Gros, Phys. Rev. B. **38**, 931 (1988).

[37]M. Sigrist and T.M. Rice, Z.Phys.B. **68**, 9 (1987).

[38]T. Brückel, H. Capellmann, W. Just, O. Scharpf, S. Kemmler-Sack, R. Kiemel and W. Schaefer, Europhys. Lett. **4**, 1189 (1987).

[39]H.Q.Lin, J.E. Hirsch and D.J. Scalapino, Phys. Rev. B. **37**, 7359 (1988).

[40]J.E. Hirsch and H.Q. Lin, Phys. Rev. B. **37**, 5070 (1988).

[41]The S (**k**,**r**) were also applied between the ground states and the excited Gutzwiller-projected state, but no overlap was found.